Genetics and Regulation of Bacterial Biofilms

Genetics and Regulation of Bacterial Biofilms

A dissertation presented by

Sara Anne Leiman

to

The Department of Molecular and Cellular Biology

in partial fulfillment of the requirements for the degree of

Doctor of Philosophy

in the subject of

Biochemistry

Harvard University

Cambridge, Massachusetts

December 2014

Genetics and Regulation of Bacterial Biofilms

Abstract

Bacterial biofilm formation, the construction of dense, protective, multicellular communities, is a widely conserved behavior. In some bacteria, such as the Gram-positive model organism *Bacillus subtilis*, the genetics controlling biofilm formation are well understood. In other bacteria, however, including the Gram-negative opportunistic pathogen *Pseudomonas aeruginosa*, the identities or roles of many biofilm genes remain unknown. Importantly, many proposed applications of biofilm research, particularly in the medical field, require knowledge not only of biofilm assembly but also of biofilm disassembly, the latter being a recent and underdeveloped area of study.

It was previously reported that *B. subtilis* biofilms disassemble late in their life cycle due to the incorporation of four D-amino acids (D-leucine, D-methionine, D-tryptophan, and D-tyrosine, or D-LMWY) into peptidoglycan. It was further argued that D-LMWY specifically inhibits and disassembles the biofilms of diverse bacterial species, including *B. subtilis* and *P. aeruginosa*. Here I present a contrasting report. I describe how what had been perceived as D-LMWY-mediated biofilm inhibition is actually D-tyrosine-mediated toxicity. *B. subtilis* is sensitive to growth inhibition by D-tyrosine due to the absence of D-tyrosyl $tRNA^{Tyr}$ deacylase (Dtd), an enzyme that prevents the misincorporation of D-tyrosine and other D-amino acids into nascent proteins. By repairing the gene for Dtd, I was able to render *B. subtilis* resistant to both growth inhibition and biofilm inhibition by D-tyrosine and D-LMWY. In parallel, I recovered spontaneous mutants of *B. subtilis* that survive in the presence of D-LMWY. These isolates

harbored mutations in pathways that regulate $tRNA^{Tyr}$ charging. Three of these mutations enhanced the expression of the gene (*tyrS*) for tyrosyl-$tRNA^{Tyr}$ synthetase (TyrRS), while a separate mutation improved the stereoselectivity of TyrRS. I concluded that these spontaneous D-LMWY resistance mutations were compensating for the absence of Dtd.

In addition to my research on *B. subtilis* biofilm regulation, I demonstrated a new, non-destructive screening approach for identifying *P. aeruginosa* biofilm genes. Using this screen, I was able to recover a wide range of known biofilm genes as well as the new biofilm gene candidates *ptsP*, *PA14_16550*, and *PA14_69700*. These three genes are the focus of an ongoing study dedicated to characterizing *P. aeruginosa* biofilm formation, particularly as it relates to the secondary messenger cyclic di-GMP.

In summary, this dissertation covers aspects of biofilm formation and dispersal in two bacterial species. My work offers mechanistic insight into D-amino acid resistance, resolves the relationship between D-amino acids and biofilms, and establishes a new tool for understanding the complexities of biofilm genetics and regulation.

Table of Contents

List of Figures

List of Tables

Acknowledgments

I would like to begin by thanking Rich Losick. Like all others who have had the good fortune to work for Rich, I have benefitted immensely from his insight as a leader in his field and from his talent as an educator. Additionally, Rich has been a wonderful mentor. Needless to say, having Rich's support throughout my (at times controversial) PhD project was invaluable.

Apart from being an excellent PI, Rich has also cultivated a great lab environment. Lucy Foulston and Alicia DeFrancesco, my roommates of BioLabs 3020, make even the most challenging workday a joy. I am also grateful for many stimulating scientific discussions and collaborations, as well as much technical help, courtesy of Matt Cabeen, Tom Norman, Alex Elsholz, Aaron DeLoughery, Bjorn Traag, Niels Bradshaw, and Anna McLoon. Equally important to my PhD experience have been my interactions with the Burton lab, particularly Marina Besprozvannaya, Tanya Sysoeva, and Bijou Bose. Surely, the members of the Losick and Burton labs helped make my graduate school years some of the most rewarding years of my life.

My thesis work began as a collaboration with the Kahne lab, and I am indebted to Janine May and Matt Lebar for their scientific genius and for their friendship. I extend my gratitude to Shugeng Cao, formerly of the Clardy lab, for being a meticulous, honest scientist and a class act. And I would like to thank our lab administrator, Diane Lynch, who does not get thanked nearly enough.

I thank Tina Henkin and Becky Williams-Wagner (Henkin lab, Ohio State University) as well as Eric First and Charles Richardson (First lab, Louisiana State University Health Sciences Center) for offering their advice, data, and time in a marvelous example of open, cooperative

science. Thank you to the Natural Health Research Institute and the Tracie Lawlor Trust for Cystic Fibrosis for funding my research on *Pseudomonas aeruginosa* biofilms.

I thank the faculty and staff at Harvard who have supported me in a variety of ways. In particular, I thank my thesis committee Dan Kahne, Ethan Garner, and Tom Bernhardt for their encouragement and helpful suggestions. Thank you to Catherine Dulac and Mike Lawrence for helping me make a mathematics nanocourse a reality. I also wish to thank the Bauer Core staff for assistance with whole genome sequencing and HPLC.

Attending and organizing the Boston Bacterial Meeting (BBM) truly enriched my PhD experience, and I am grateful to have worked with the dedicated members of the BBM organizing committee. I offer a million thanks to my boyfriend, Tom Iancovici, and to my roommate, Iris Odstrcil, both of whom are heroes for their unending patience, support, and positivity. Thank you to my longtime best friends Risa Navre and Jillian Stark for always being there for me. Of course none of this would be possible without my spectacular family. I especially want to thank my parents, Jill and Mark Leiman, and my sister, Amanda Leiman, for their humor, love, and encouragement.

Lastly, I want to recognize a quote that has guided me through my PhD. Charles Darwin once said, "To kill an error is as good a service as, and sometimes even better than, the establishing of a new truth or fact." It is my hope that, through my dissertation work, I have accomplished both.

Introduction

Much of the research described here has been motivated by work done in the Losick, Clardy, and Kolter labs and published in *Science* in 2010 (heretoafter, Kolodkin-Gal et al., 2010). This work focused on microbial communities ("biofilms") produced by the model bacterium *Bacillus subtilis.* The paper asserted that *B. subtilis* produces metabolites (D-amino acids) capable of inhibiting and disassembling its own biofilms as well as biofilms made by pathogenic bacteria. In the medical field, biofilm formation within a patient is frequently associated with antibiotic resistance and poor prognosis. As such, the discovery that D-amino acids possess potent anti-biofilm activity represented a promising therapeutic advance.

Among other contributions, my thesis work addresses the claims presented in Kolodkin-Gal et al., 2010. Consequently, the evidence and interpretations presented in Kolodkin-Gal et al., 2010 are detailed here and in future chapters. In the interest of putting my work in its proper context, motivations for work done or planned according to the paradigm set by Kolodkin-Gal et al., 2010 are described without the benefit of hindsight. At times, such assumptions are marked and explained using footnotes or appendices.

Dissertation Structure

This dissertation begins with an overview of key concepts that I will address, particularly throughout my first four chapters. I begin by introducing D-amino acids, peptidoglycan (PG) and the presence of D-amino acids in PG structure, and bacterial biofilms, each with a focus on *B. subtilis*. The last topic of the **Introduction** is a review of the findings and implications of

"D-amino acids trigger biofilm disassembly," published by Ilana Kolodkin-Gal and others in 2010 in *Science*.

In **Chapter 1**, I describe my collaboration with members of the Kahne laboratory to characterize the relationship between penicillin binding protein 1, the incorporation of "non-canonical" D-amino acids (NCDAAs) into *B. subtilis* PG, and *B. subtilis* biofilm stability.

In **Chapter 2**, I briefly introduce several mutations that putatively confer resistance to NCDAAs in both a growth-inhibitory and a biofilm-inhibitory context.

The work presented in Chapter 2 raises fundamental questions about how D-amino acids interact with the cell, and brings to light some discrepancies between my results and those in Kolodkin-Gal et al., 2010. Such topics are the focus of **Chapter 3** and **Appendices A**, **B**, and **C**.

In **Chapter 4**, I return to the putative resistance mutations introduced in Chapter 2. I present my investigation into the mechanisms by which these mutations confer resistance to NCDAAs, especially D-Tyr.

In **Chapter 5**, I change gears to introduce biofilms made by another bacterium, *Pseudomonas aeruginosa*.

In **Chapter 6**, I describe an ongoing project – done in collaboration with another member of the Losick laboratory, Matt Cabeen – to identify and characterize novel genes involved in biofilm formation in *P. aeruginosa*.

The main body of the dissertation closes with a **Conclusions** chapter, which summarizes my work and its significance to the fields of *B. subtilis* and *P. aeruginosa* biofilm research. Following my conclusions chapter are my **Materials and Methods**, **References**, and the three aforementioned **Appendices**.

D-amino acids in bacteria: Uses and misuses

D-amino acids are produced and utilized by almost all bacteria, particularly in the bacterial cell wall (Lam et al., 2009, Vollmer et al., 2008). The major cell wall component peptidoglycan (PG) typically contains the D-amino acids D-Ala and D-Glu, while lipoteichoic and wall teichoic acids are modified with D-Ala. Because of their ubiquity, D-Ala and D-Glu are considered canonical D-amino acids. Bacteria can also produce other D-amino acids, and these so-called non-canonical D-amino acids (NCDAAs) are utilized for diverse purposes. For example, D-Met and D-Leu have been shown to regulate PG biosynthesis in *Vibrio cholera* (Lam et al., 2009, Lupoli et al., 2011). NCDAAs may also be incorporated into non-ribosomally synthesized peptides, such as the *Bacillus subtilis* lipopeptides surfactin (containing D-Leu) and iturin A (containing D-Asn and D-Tyr) (Ongena and Jacques, 2008, Perego et al., 1995). For bacteria to exploit D-amino acids effectively, however, they must prevent misincorporation of D-amino acids into proteins, which would cause proteotoxicity (Champney and Jensen, 1969, Champney and Jensen, 1970). Most D-amino acids are eliminated from the translation machinery by L-stereospecific aminoacyl-tRNA synthetases (Nandi, 2012). However, tyrosyl-$tRNA^{Tyr}$ synthetase (TyrRS) cannot effectively distinguish between L-Tyr and D-Tyr, making D-Tyr potentially toxic to cells (Nandi, 2012). In many organisms, D-Tyr toxicity is mitigated by a D-aminoacyl tRNA deacylase, encoded by *dtd*, which prevents D-Tyr from sequestering $tRNA^{Tyr}$ or being subsequently incorporated into protein (Calendar and Berg, 1967, Soutourina et al., 2000, Soutourina et al., 2004).

Bacillus subtilis peptidoglycan

As mentioned above, the *B. subtilis* cell wall largely comprises peptidoglycan (PG). PG, in turn, is made of polymerized and crosslinked units of the precursor Lipid II. Briefly, Lipid II is built stepwise by the enzymes encoded by *mur(AA)BCDEFG* and *mraY*. First, MurAA and MurB convert UDP-GlcNAc to UDP-MurNAc. Next, MurC, MurD, MurE, and MurF successively attach L-Ala, D-Glu, diaminopimelic acid (DAP), and D-Ala-D-Ala to UDP-MurNAc to produce UDP-MurNAc-L-Ala-D-γ-Glu-*m*-DAP-D-Ala-D-Ala (UDP-MurNAc-pentapeptide). The peptide side chain of MurNAc is alternatively called the muropeptide. In the penultimate step of Lipid II biosynthesis, MraY activity couples UDP-MurNAc-pentapeptide to a membrane-anchored lipid carrier and expels UMP. The resultant lipid-linked MurNAc-pentapeptide is known as Lipid I. Finally, MurG activity attaches UDP-GlcNAc to Lipid I to yield Lipid II (van Heijenoort, 2007, VanNieuwenhze et al., 2001).

While Lipid II biosynthesis occurs in the cytosol, PG polymerization, crosslinking, and hydrolysis are all catalyzed by penicillin-binding proteins (PBPs) outside of the cell. *B. subtilis* encodes 16 PBPs, with four PBPs annotated as Class A, six as Class B, one as Class C Type-4, three as Class C Type-5, and two as Class C Type-AmpH. The Class A PBPs are capable of both PG polymerization (transglycosylation, or linking of the MurNAc-GlcNAc disaccharide units) and muropeptide crosslinking (D,D-transpeptidation). Class B PBPs only perform D,D-transpeptidation. Both Class C Type-4 and C Type-5 PBPs hydrolyze uncrosslinked muropeptides to create shortened peptide chains via D,D-carboxylase activity, whereas Class C Type-AmpH PBPs hydrolyze crosslinked muropeptides via D,D-endopeptidase activity. As discussed in later chapters, at least one *B. subtilis* PBP is capable of incorporating NCDAAs into the fifth position of the muropeptide *in vitro*, such that the pentapeptide is altered from L-Ala-D-

γ-Glu-*m*-DAP-D-Ala-D-Ala to L-Ala-D-γ-Glu-*m*-DAP-D-Ala-D-X, wherein X is not D-Ala (Lebar et al., 2014). It has not been established in *B. subtilis* which or how many PBPs are capable of NCDAA incorporation into PG *in vivo*.

Components of the *Bacillus subtilis* biofilm matrix

I offer here a brief review of biofilm matrix components. Typically, biofilm matrices comprise exopolysaccharides, proteins, and eDNA, however the importance or presence of these factors differs from species to species. To further complicate matters, a high degree of variability has been reported for biofilms made by pathogens, such that components required for matrix production in one strain may be unimportant in or absent from another. For example, while eDNA appears to be a conserved biofilm matrix component among *Staphylococcus aureus* strains, some *S. aureus* strains (e.g., ATCC 35556) depend on the exopolysaccharide PIA to build the biofilm matrix while others (e.g., BH1CC) can do away with it completely (Cramton et al., 1999, Fitzpatrick et al., 2005).

The abundance or types of proteins in a biofilm matrix can also be very diverse. On one end of the spectrum are *B. subtilis* biofilms, which not only require the presence of a dedicated matrix protein, TasA, but also require that TasA proteins form amyloid-like fibers (Romero et al., 2010, Romero et al., 2011, Romero et al., 2014). *Escherichia coli* also employs an amyloid matrix protein, curli, although this protein also plays other roles including surface attachment, host cell invasion, and pathogenesis (Barnhart and Chapman, 2006). In stark contrast, a recent report on *S. aureus* biofilms found that their matrices comprise "recycled" or "moonlighting" cytoplasmic proteins, which aggregate to establish a matrix under conditions of low pH (Foulston et al., 2014). To date there is no known dedicated matrix protein for *P. aeruginosa*,

and while some strains require the presence of protein attachment factors for biofilm formation, others employ exopolyssacharide for attachment purposes (Vasseur et al., 2005). *P. aeruginosa* biofilms are introduced in greater detail in Chapter 5. The following paragraph focuses on the biofilm matrix produced by *B. subtilis*, in preparation for the material covered in Chapters 1-4.

B. subtilis biofilms may form on air-exposed surfaces or at air-liquid interfaces. Biofilms that float at the air-liquid interface are often referred to as pellicles. The cells of surface-attached biofilms and pellicles alike are encased by a self-produced matrix comprising exopolysaccharide (EPS), the hydrophobin BslA (formerly YuaB), and the dedicated matrix protein TasA (Vlamakis et al., 2013). The *epsA-O* operon encodes the proteins responsible for EPS biosynthesis, while the gene *bslA* encodes BslA. TasA is encoded by the last gene of the *tapA-sipW-tasA* operon. Importantly, the protein product of *tapA* (TapA) is responsible for anchoring TasA fibers into the cell wall. Furthermore, recent work has shown that the N-terminus of TapA nucleates the formation of amyloid-like TasA fibers, which are required for biofilm formation (Romero et al., 2014). SipW, the protein product of *sipW*, is a signal peptidase responsible for the secretion of TapA and TasA. Knocking out the production of any of these components individually is sufficient to inhibit robust biofilm formation (Hobley et al., 2013, Vlamakis et al., 2013). In contrast to many other bacterial biofilms, *B. subtilis* biofilms do not rely on eDNA to build or maintain the biofilm matrix (Zafra et al., 2012).

"D-amino acids trigger biofilm disassembly"

In 2010, Ilana Kolodkin-Gal, Diego Romero, Shugeng Cao, Jon Clardy, Roberto Kolter, and Richard Losick published a paper in *Science* demonstrating that biofilm disassembly is

mediated by NCDAA incorporation into PG and that, by leveraging this behavior, they could inhibit or destroy a variety of bacterial biofilms (Kolodkin-Gal et al., 2010).

The study focused on the Gram-positive spore-forming model organism *Bacillus subtilis*. The authors discovered that *B. subtilis* pellicles naturally disassembly after six to eight days and that the activating factor for this disassembly is a mixture of four D-amino acids: D-leucine, D-methionine, D-tryptophan, and D-tyrosine (D-LMWY) (Kolodkin-Gal et al., 2010). Production of these NCDAAs was attributed to the predicted amino acid racemaces RacX and YlmE based on evidence that a *racX ylmE* double knockout is blocked in D-Tyr production and impaired in D-Leu production at day six, and that this mutant also exhibits delayed biofilm disassembly (Kolodkin-Gal et al., 2010).

The authors determined that D-Leu inhibits biofilm at 8.5 mM, D-Met at 2 mM, D-Trp at 5 mM, D-Tyr at 3 μM, and that the four NCDAAs at a total of 10 nM work synergistically to inhibit or disassemble biofilms (Kolodkin-Gal et al., 2010). The authors observed that D-LMWY had no effect on the expression of the *epsA-O* or *tapA-sipW-tasA* operons, implying that the role of D-LMWY in biofilm inhibition and disassembly occurs post-transcriptionally (Kolodkin-Gal et al., 2010). Moreover, the authors established that the applied D-amino acids did not elicit a growth defect, thus suggesting a biofilm-specific effect and, ultimately, greater therapeutic potential[1] (Kolodkin-Gal et al., 2010).

How do D-Leu, D-Met, D-Trp, and D-Tyr inhibit and disperse biofilms? Kolodkin-Gal et al. asserted that these NCDAAs are incorporated into PG, replacing D-Ala in the fifth position of the muropeptide, and that the presence of an NCDAA at this position triggers the release of TapA (and thus TasA) from the cell wall (Kolodkin-Gal et al., 2010). They supported this claim

[1] Arguably, bacteria in a clinical setting would be under less selective pressure to quickly overcome an anti-biofilm drug, as opposed to an antibiotic.

with three major pieces of evidence. They found that excess D-Ala rescued pellicle formation when *B. subtilis* was treated with biofilm-inhibitory concentrations of NCDAAs (Kolodkin-Gal et al., 2010). This result suggested that NCDAAs compete with D-Ala for incorporation into PG and that this competition is related to biofilm stability. The authors then grew a *B. subtilis* strain that expresses a fluorescently tagged form of TasA (TasA-mCherry) in the absence or presence of D-Tyr. They noted that the treated cells were no longer in clumps nor were they fluorescent, indicating that D-Tyr interrupts the nucleation or association of the primary biofilm matrix protein component (Kolodkin-Gal et al., 2010). The third piece of evidence was the identification of six frame-shift mutations at the 3' end of *tapA*, all of which conferred resistance to one or more NCDAAs (Kolodkin-Gal et al., 2010). This finding implied that a domain in or near the C-terminus of TapA senses NCDAAs in PG, and that this results in TapA (and TasA) release.

Finally, Kolodkin-Gal et al. demonstrated that their work in *B. subtilis* also holds true for pathogenic bacteria and Gram-negative bacteria. Using a crystal violet assay, the authors found that D-Tyr and D-LMWY prevented biofilm formation in *Staphylococcus aureus* and *Pseudomonas aeruginosa* (Kolodkin-Gal et al., 2010). Moreover, the D-Ala counter-treatment was also effective for these bacteria (Kolodkin-Gal et al., 2010). Therefore, the authors concluded that biofilm inhibition and/or disassembly by NCDAA accumulation in PG is a shared mechanism and a potential therapeutic target.

Chapter 1

Misincorporation of D-amino acids into *Bacillus subtilis* cell wall

In a series of two publications, one in *Science* (2009) and one in *EMBO* (2011), the Waldor group studied the biosynthesis and cell wall incorporation of NCDAAs in several bacterial species. Their work on *B. subtilis* revealed minimal NCDAA production in stationary phase cultures, with a total concentration of 190 μM consisting of 10 μM D-Ile[1], 30 μM D-Leu, 20 μM D-Pro, 60 μM D-Phe, 40 μM D-Val, and 40 μM D-Tyr (Lam et al., 2009). Using physiologic (as well as superphysiologic) concentrations of D-amino acids, the Waldor group concluded that *B. subtilis* can incorporate NCDAAs into the fifth (but not the fourth) position of the PG muropeptide (Cava et al., 2011, Lam et al., 2009). The authors knocked out the two *B. subtilis* L,D-transpeptidases (Ldts), encoded by *yqjB* and *ykuD*, and found no change in NCDAA incorporation (Cava et al., 2011). Similarly, D-cycloserine had no effect on NCDAA incorporation (Cava et al., 2011). D-cycloserine inhibits both D-Ala-D-Ala ligase and the alanine racemace; therefore this finding indicated that NCDAAs are not attached to the muropeptide inside the cell. On the other hand, Penicillin G all but abolished NCDAA incorporation into *B. subtilis* PG, leading the authors to suggest that NCDAA incorporation is performed by a "penicillin-binding D,D-peptidyl transferase" or, more explicitly, a Class A or Class B penicillin-binding protein (PBP) (Cava et al., 2011).

Class A PBPs are bifunctional, possessing both glycosyl transferase and D,D-peptidyl transferase activity. In contrast, Class B PBPs only possess D,D-peptidyl transferase activity. *B.*

[1] Likely D-allo-isoleucine. D-Ile and D-allo-Ile cannot be distinguished by the identification method used in this work. D-allo-Ile is the true enantiomer of L-Ile, whereas the formation of D-Ile would require either novel racemic activity or a separate biosynthetic pathway. To date, no microbial source of D-Ile has been identified.

subtilis has an abundance of both PBP classes, with four Class A PBPs (PBP1, PBP2C, PBP4, and PBP2D) [2] and six Class B PBPs (PBP3, SpoVD, PBP2B, PBP2A, PBPH, and PBP4B). Peptidyl transferase activity by bifunctional PBPs appears to be dependent on active glycosyl transferase activity, such that Class A PBPs are thought to be active primarily at times of cell wall synthesis (e.g., exponential phase) (Lupoli et al., 2014).

In this chapter I discuss my work, in collaboration with Janine May and Matt Lebar in the Kahne laboratory, on PBP1 and its possible relationship to biofilm disassembly. It may seem counterintuitive that we chose to investigate the biofilm-relevant activity of a Class A PBP, given that biofilm formation and disassembly occur well into stationary phase when relatively little cell wall synthesis occurs. However, not only was PBP1 implicated in *B. subtilis* biofilm disassembly by a genetic screen (as detailed in the following section), the Kahne and Walker groups have established *in vitro* that a homologous enzyme, *Escherichia coli* PBP1A, incorporates NCDAAs into PG (Lupoli et al., 2011). Lupoli et al. demonstrated by LC-MS that *E. coli* PBP1A promiscuously incorporates glycine and all classes of D-amino acids, including D-Met, D-Tyr, D-Phe, D-Trp, D-Thr, D-Asp, D-Gln, and D-Pro into the fifth position of the *E. coli* PG muropeptide (Lupoli et al., 2011). They also demonstrated that *E. coli* PBP1A selectively excludes the L-stereocenter of L-amino acids such that L-amino acids are not incorporated into the muropeptide fifth position (Lupoli et al., 2011).

[2] PBP1 is shorthand for two protein products from the same gene (*ponA*): PBP1A and PBP1B. PBP1B is believed to be a C-terminal truncation of PBP1A. In this study, we do not distinguish between the two PBP1 forms.

Preliminary evidence for PBP1 involvement in biofilm disassembly

Penicillin-binding protein 1 (PBP1), encoded by *ponA*, was initially implicated in D-amino acid-mediated biofilm inhibition through a screen performed by Dr. Kolodkin-Gal (unpublished). The screen utilized a strain of *B. subtilis* 3610 that harbors a kanamycin resistance cassette at *yppC*, a gene adjacent to and transcribed divergently from the *recU-ponA* operon. This marked strain was grown on solid MSgg containing a mixture of D-LMWY at 10 μM each. In contrast to the treatment chosen to selectively inhibit or disassemble biofilm[3] (D-LMWY at 2.5 nM each), this stronger treatment was selected to inhibit cell growth. This change was made due to the concern that low levels of D-amino acids might be overcome by mutations that lead to an overexpression of biofilm matrix components, rather than mutations particular to the effects of D-amino acids.

Of the 40 D-LMWY-resistant mutants isolated in this screen, 14 demonstrated linkage[4] to *yppC* (I. Kolodkin-Gal, unpublished). Four of the 14 linked mutants harbored one or more mutations at the 3' end of *ponA*, implying that resistance to D-LMWY-induced biofilm inhibition could be overcome by one or more substitutions in the C-terminus of PBP1[5].

Collectively, the high frequency of *ponA* mutations, the prior evidence that NCDAAs inhibit biofilm through their misincorporation into PG, and the work featured in Lam et al., 2009 suggested that PBP1 is the major source of NCDAA incorporation into *B. subtilis* PG. We hypothesized that *B. subtilis* biofilm inhibition and disassembly is mediated by the transpeptidase activity of PBP1 by the following mechanism: First, PBP1 replaces the D-Ala at the

[3] See Chapter 3.

[4] I was unable to verify the linkage mapping results and ultimately concluded that linkage mapping was a poor method for locating these mutation sites (see Chapter 2).

[5] Later, Janine May and I independently sequenced the four alleged *ponA* mutants at the *ponA* locus. We also sequenced the 1000 base pairs surrounding *ponA* on either side. We detected no mutations.

muropeptide fifth position with D-Leu, D-Met, D-Trp, or D-Tyr. Next, the C-terminus of TapA senses this change in the fifth position, preventing new TapA-PG associations and/or causing previously attached TapA proteins to release from the cell wall. Without cell wall-associated TapA, TasA fibers are not nucleated or become detached from the cell surface. Thus, the incorporation of NCDAA into *B. subtilis* PG by PBP1 renders the protein components of the biofilm matrix unable to build or maintain the biofilm structure.

The role of PBP1 varies among *B. subtilis* strains

Initially, our hypothesis found some support. Janine May succeeded in purifying full-length PBP1 from *B. subtilis* and confirmed that this protein is capable of incorporating NCDAAs such as D-Tyr into the fifth position of the PG muropeptide *in vitro*. This work was performed using the native substrate (Lipid II) for *B. subtilis* PBPs. To determine whether PBP1 is an integral source of NCDAA incorporation *in vivo*, I collaborated with Janine May and Matt Lebar to construct *ponA* deletions and analyze the resulting PG by LC-MS.

In the process of deleting *ponA* in the robust biofilm-forming *B. subtilis* strain 3610, we introduced this deletion into the biofilm-attenuated (but more genetically competent) strain PY79. We observed a striking difference in the colony size between PY79 Δ*ponA* and 3610 Δ*ponA* on solid LB. While the size of wild-type PY79 and PY79 Δ*ponA* colonies were similar, 3610 Δ*ponA* colonies were significantly smaller than were their wild-type counterparts, suggesting that *ponA* is either less important or fulfills a different role in PY79 when compared to 3610. The PY79 Δ*ponA* phenotype was also observed when the gene deletion was created in another biofilm-attenuated strain, *B. subtilis* 168.

I confirmed these observations using growth curves (Fig. 1A). Deletion of *ponA* in a 3610 background resulted in a severe growth defect, whereas PY79 Δ*ponA* and 168 Δ*ponA* exhibited very mild growth defects. Hypothesizing that the importance of *ponA* in *B. subtilis* could be linked to biofilm-forming capability, I deleted *ponA* from *B. subtilis* AM373, a strain of 168 that has been restored for biofilm formation by the repair of the genes *sfp*, *swrA*, *epsC*, and *degQ*, as well as the introduction of a plasmid harboring *rapP* (McLoon et al., 2011). Interestingly, AM373 Δ*ponA* exhibited a growth defect that was intermediate when compared to the growth of 168 Δ*ponA* and 3610 Δ*ponA* (Fig. 1B). I eliminated the plasmid harboring *rapP* as the determining factor for this shift in growth by deleting *ponA* in a plasmidless strain of 3610 (Fig. 1A). It is possible that these findings indicate an inverse relationship between the importance of PBP1 and genetic competence, as *degQ* expression (present in 3610 and AM373 but absent from 168) is associated with lower competence (Amory et al., 1987). However, this notion is somewhat belied by the observation that AM373 is not strongly impaired for

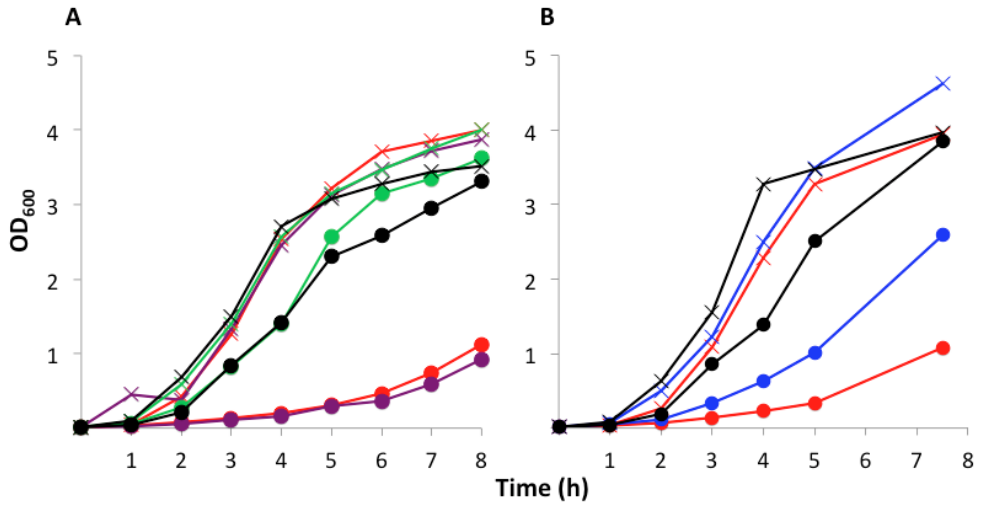

Figure 1. *B. subtilis* reliance on PBP1 for growth correlates with strain background (A) and increases upon repair of biofilm genes (B). Wild-type strains are denoted by Xs and *ponA* nulls are denoted by circles. Growth in shaking LB medium at 37˚C was determined in the following strain backgrounds: 3610 (red), plasmidless 3610 (purple), PY79 (green), 168 (black), and AM373 (blue). Results shown are representative of three (A) and two (B) independent experiments.

competence (A. McLoon, personal communication). That said, *degQ* and *sfp* are pleitropic, and there may be many reasons for the correlation between biofilm-forming capability and heavy reliance on PBP1.

PBP1 is not the main source of NCDAA incorporation into *B. subtilis* peptidoglycan

We isolated PG from pellicles formed by *B. subtilis* 3610 (*ponA*$^{+}$), in the presence or absence of NCDAAs such as D-Trp[6]. LC-MS analysis of the PG fragments confirmed the presence of D-Trp in the fifth position of a subset of muropeptides (Fig. 2). Importantly, we did not observe changes to the overall identity, distribution, or abundance of typical muropeptide fragments when *B. subtilis* 3610 was exposed to D-Trp (Fig. 2).

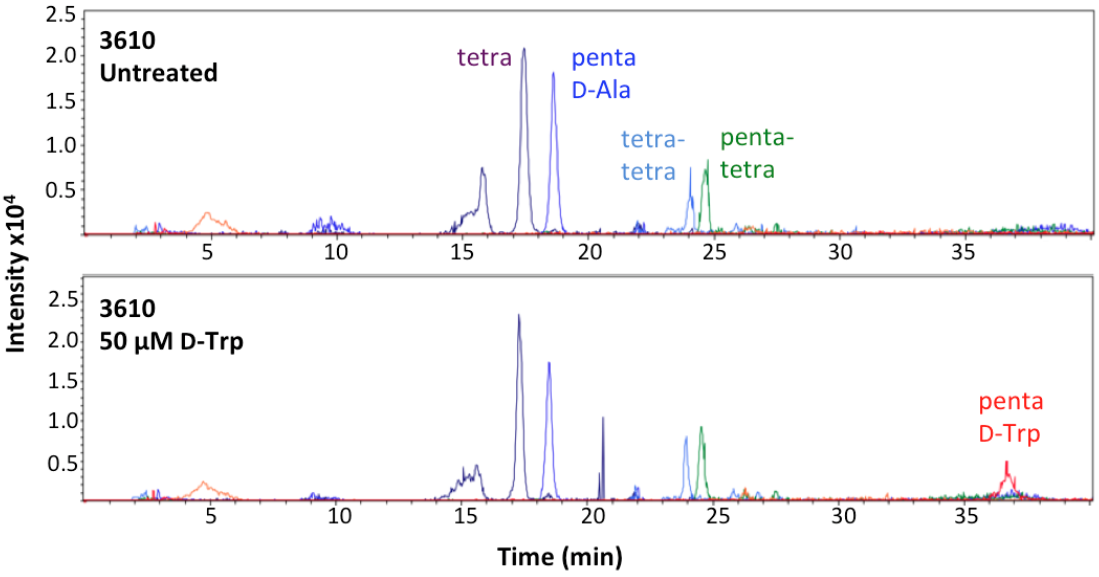

Figure 2. *B. subtilis* 3610 incorporates exogenous NCDAAs into PG. Exogenous D-Trp was detected by LC-MS in the fifth position of the *B. subtilis* 3610 PG muropeptide (penta D-Trp). The other peaks shown represent the pentapeptide (penta D-Ala), tetrapeptide (tetra), unhydrolyzed crosslink (penta-tetra), and hydrolyzed crosslink (tetra-tetra) PG fragments for each sample.

[6] We selected D-Trp as a representative NCDAA because it gives a particularly distinctive signal. The elemental composition and structure of the PG fragments containing D-Trp were confirmed by high-resolution LC-MS/MS (Leiman et al., 2013).

We repeated this work using a *ponA*-null strain of *B. subtilis* 3610. In doing so, we harvested cell wall from wild-type and Δ*ponA* cultures at the same optical density to accommodate for the severe growth defect caused by the deletion of *ponA*. LC-MS of the cell wall fragments revealed no change in NCDAA incorporation into the *B. subtilis* cell wall, suggesting either that PBP1 does not incorporate NCDAAs *in vivo*, or that one or more other proteins can compensate for the loss of PBP1-mediated NCDAA incorporation in the *ponA* null (Fig. 3A). Surprisingly, we instead found that a lack of PBP1 activity is reproducibly associated with an increased abundance of four muropeptide fragments: the unaltered pentapeptide (L-Ala-D-γ-Glu-*m*DAP-D-Ala-D-Ala), the hydrolyzed tetrapeptide (L-Ala-D-γ-Glu-*m*DAP-D-Ala), the crosslink of a pentapeptide and tetrapeptide, and the crosslink of two tetrapeptides (Fig. 3A). No changes in PG structure were detected between wild-type PY79 and PY79 Δ*ponA* (Fig. 3B).

In sum, we determined that *B. subtilis* PBP1 is capable of incorporating NCDAAs *in vitro*, but is not necessary for such incorporation to occur. Also, while the essentiality of PBP1 for cell growth did seem to vary with a strain's biofilm-forming capability, the reason for this phenomenon remains unclear. Regardless, we did not find evidence suggesting that PBP1 plays a direct role in the regulation of *B. subtilis* biofilm.

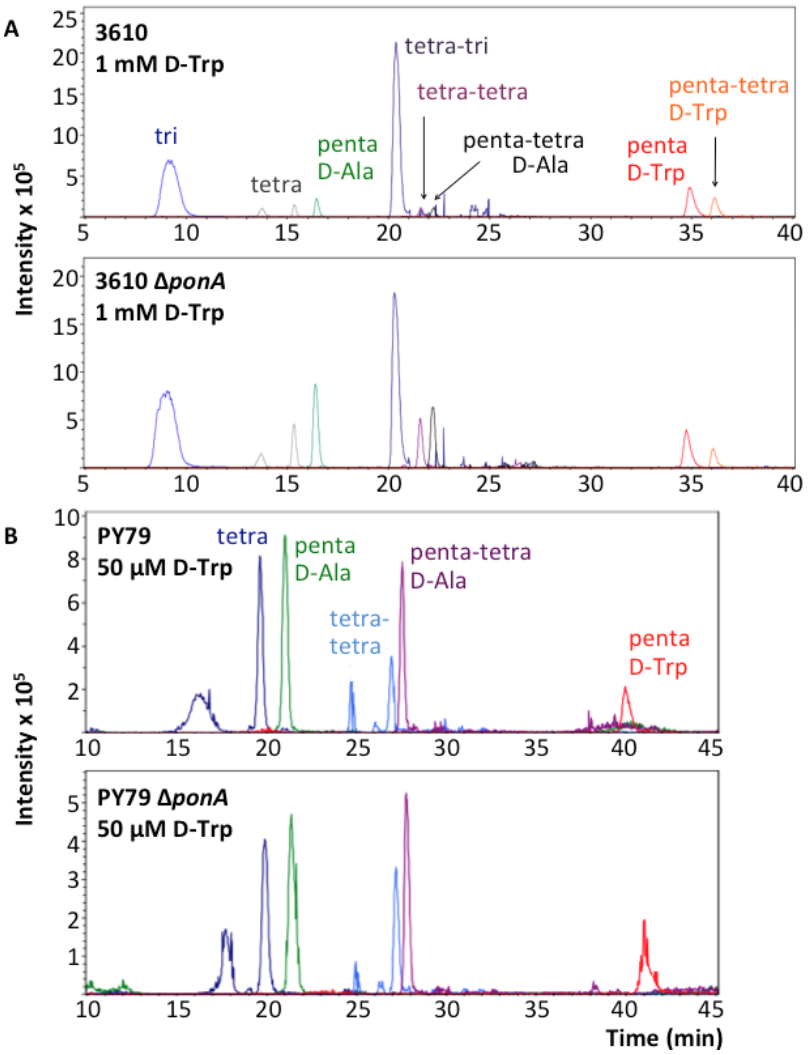

Figure 3. PBP1 is not the main source of NCDAA incorporation into the cell wall. D-Trp was detected in comparable amounts in wild-type and Δ*ponA B. subtilis,* in the fifth position of both uncrosslinked muropeptides (penta D-Trp) and crosslinked muropeptides (penta-tetra D-Trp, not shown in B). The intensities of peaks representing the unmodified pentapeptide (penta D-Ala), its hydrolysis product, tetrapeptide (tetra), the unhydrolyzed crosslinks (penta-tetra D-Ala), and the hydrolyzed crosslinks (tetra-tetra) increased for the deletion mutant in the 3610 background (A) but not in the PY79 background (B).

Chapter 2

Isolation and identification of D-amino acid-resistant mutants

In light of my inability to verify the purported link between *ponA* and biofilm disassembly, I conducted a new screen for NCDAA resistance with a few key changes. I chose to select for D-LMWY-resistant mutants on solid LB rather than on solid MSgg. *B. subtilis* spreads much less rapidly on solid LB than it does on solid MSgg, making the former a better surface on which to grow distinct single colonies and calculate the frequency at which D-LMWY-resistant mutations arise. I quickly learned that in order to conduct this selection on LB, I needed a higher dose of D-LMWY. Whereas 10 µM each of D-LMWY abolished *B. subtilis* growth on MSgg agar, 400-500 µM each of D-LMWY were required to abolish growth on LB agar[1] (Fig. 4). L-LMWY at these high concentrations did not impair *B. subtilis* growth (Fig. 4).

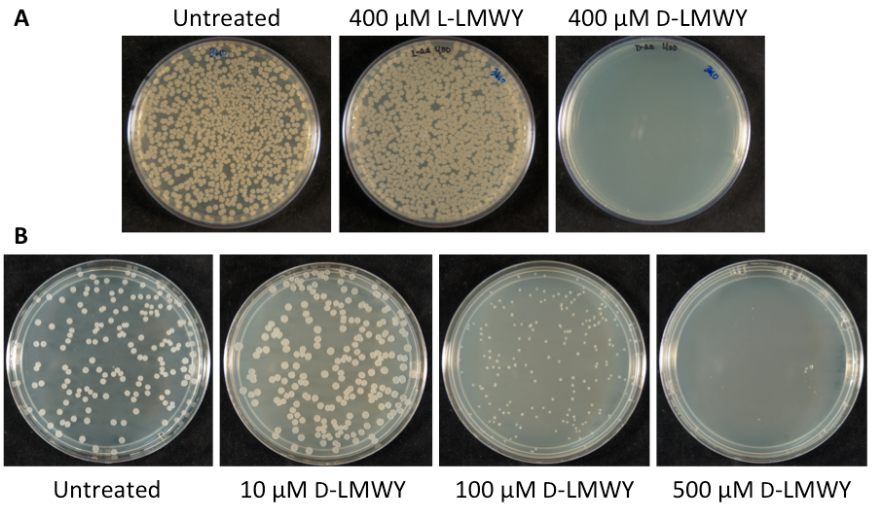

Figure 4. D-amino acids inhibit growth, but L-amino acids do not. Dilutions (10^{-6}) of early stationary phase *B. subtilis* 3610 cultures were plated on LB agar containing the indicated treatments. Plates were incubated at 37˚C and photographed after 15 hours.

[1] That is not to say that lower doses of D-amino acids are harmless in LB. The Waldor group found that D-Tyr at 40 µM (together with comparable or lower concentrations of less potent D-amino acids) reduced the growth rate of *B. subtilis* 3610 (Lam et al., 2009).

Spontaneous resistance to D-amino acids occurs with high frequency

To select for spontaneously arising mutants with resistance to NCDAA toxicity, I plated *B. subtilis* 3610 on solid LB supplemented with D-LMWY at 500 μM each. Using a dilution series, I determined that resistant mutants arose at a high frequency of about one in 10^6, indicating that mutations at multiple loci are able to confer resistance. Such a high frequency of resistance also explained the improper identification of the *ponA* mutants by linkage mapping. Briefly, in linkage mapping, iterative selections for NCDAA resistance would have been performed using concentrated cultures exceeding far more than a million cells. During each round in which a chromosomal marker was moved by phage transduction into a clean background, novel spontaneous resistance mutants would have arisen, leading to artificially high linkage. Effectively, any marker on the genome would have had linkage to the D-amino acid resistance phenotype. Therefore, for my own analyses I turned to whole genome sequencing.

I performed whole genome sequencing for seven spontaneous resistance mutants and uncovered eight distinct mutations: three mutations in the inorganic pyrophosphatase gene *ppaC*, three mutations in or upstream of the tyrosyl-tRNA^{Tyr} synthetase (TyrRS) gene *tyrS*, one mutation in the tRNA^{Phe} encoded by *trnD-Phe*, and one mutation upstream of the protein chaperone repressor gene *hrcA* (Table 1) (Brick et al., 1989, Halonen et al., 2005, Henkin et al., 1992, Homuth et al., 1999). Of the seven mutants analyzed, six harbored only one mutation, while one mutant (SLH15) harbored two mutations (*hrcA*$^{-8A>G}$ and *ppaC*$^{\Delta A166}$).

D-LMWY-resistant mutations are linked to protein synthesis

I was initially surprised by the identities of my putative D-LMWY-resistant mutations. Not one of these mutations had been previously linked to biofilm formation or stability, nor did these mutations have any known role in the construction or maintenance of the cell wall. Rather, all eight mutation loci were related to general metabolism (*ppaC*), tRNA charging (*tyrS*, *trnD-Phe*), or protein folding (*hrcA*). More strikingly, all four tRNA charging mutations ($tyrS^{-38C>T}$, $tyrS^{-38\Omega C}$, $tyrS^{605G>A}$, and $trnD\text{-}Phe^{35A>T}$) appeared to be tyrosine-specific[2]. I discuss these mutations in detail in Chapter 4.

Table 1. Spontaneously arising mutations predicted to confer resistance to D-LMWY. Given positions are relative to the start of the open reading frame**.** n/a = not applicable.

Gene	Nucleotide Change	Amino Acid Change	Strain of Origin
tyrS	-38ΩC	n/a	SLH8
	-38C>T	n/a	SLH9
	605G>A	A202V	SLH16
trnD-Phe	35A>T	n/a	SLH13
hrcA	-8A>G	n/a	SLH15
ppaC	234A>T	E78D	SLH10
	434C>T	A145V	SLH7
	Δ496-498 (GCA)	ΔA166	SLH15

[2] While this claim is fully explained in Chapter 4, it warrants justification here as well. Briefly, *tyrS* encodes TyrRS, which is responsible for charging $tRNA^{Tyr}$ with L-Tyr. The mutation identified in *trnD-Phe* changes the $tRNA^{Phe}$ anticodon to AUG, an L-Tyr anticodon.

Mutants selected on LB agar make pellicles in the presence of D-Tyr

Before addressing the resistance mechanisms of the mutations identified in my screen, I sought to reconcile what I did *not* find: specifically, mutations in *tapA*. Kolodkin-Gal et al. reported six separate C-terminal frame-shifts in TapA (including *yqxM2*, now *tapA2*), and claimed that one such mutation (*yqxM6*, now *tapA6*) was independently recovered three times. Neither my screen nor the screen performed by Dr. Kolodkin-Gal was extensive; we only analyzed a handful of mutants. Yet, we both found different saturating mutations, mine in *ppaC* and *tyrS*, hers in *tapA*.

Why did we not recover similar classes of mutations, let alone the same mutated genes? I considered two possible explanations: first, that the selection pressures for D-LMWY-resistant mutants are inherently different for cells grown on a biofilm-promoting medium (e.g., MSgg) when compared to a non-biofilm-promoting medium (e.g., LB) and, second, that the mutation loci I identified do influence biofilm formation and/or cell wall structure but in some currently unappreciated manner. In a first attempt to resolve this discrepancy, I decided to test how my mutants fare in a pellicle assay. I used the same treatment conditions (6 μM D-Tyr in liquid MSgg) against my mutants that *tapA2* and *tapA6* were known to resist. After 24 hours at 30˚C, I observed that my spontaneous D-LMWY resistant mutants began to form a pellicle, comparable to that formed by the *tapA2* strain, in the presence of D-Tyr at 6 μM (Fig. 5). I attempted this experiment at lower concentrations of D-Tyr but found that the parental strain (3610) either recovered from the treatment or generated suppressors too quickly to reliably judge resistance phenotypes (Fig. 6)[3]. Oddly, I could not reproduce D-Tyr resistance in the *tapA6* strain (Fig. 5). The *tapA* mutant strains are addressed in greater detail in Chapter 3.

[3] In contrast, Kolodkin-Gal et al. claimed that *B. subtilis* 3610 treated with D-Tyr at 3 μM shows no sign of pellicle formation at day 3.

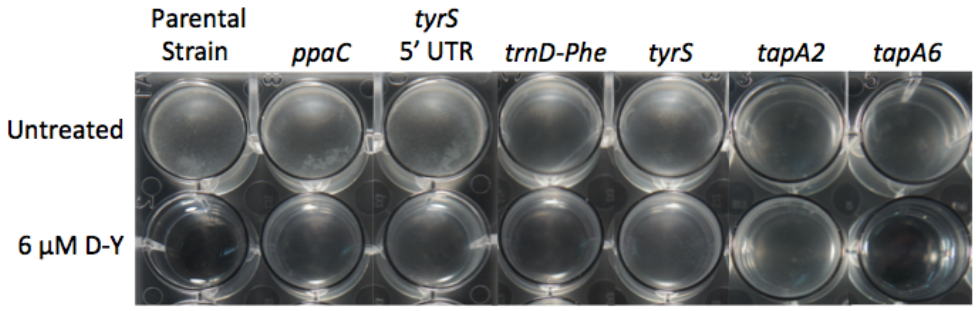

Figure 5. Spontaneous mutants resistant to growth inhibition by D-Tyr are also resistant to biofilm inhibition by D-Tyr. From left to right, the strains are 3610, SLH7, SLH9, SLH13, SLH16, IKG40, and IKG44. Plates were incubated at 30˚C and photographed at 24 hours. The spontaneous mutants that are not shown here (SLH8, SLH10, and SLH15) exhibit resistance to D-Tyr at 6 µM that is comparable to that seen for IKG40 and the shown SLH strains. The *trnD-Phe* mutant has a growth defect and thus makes weaker pellicles at 24 hours.

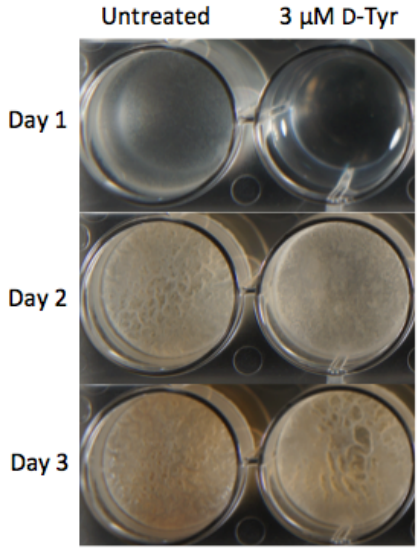

Figure 6. *B. subtilis* 3610 recovers pellicle formation within 24 to 48 hours of treatment with D-Tyr at 3 µM. Cells were grown in MSgg at 30˚C and photographed at 24, 48, and 72 hours.

Can the mechanism by which these mutations act be reconciled with the current biofilm disassembly model of NDCAA incorporation into PG? Mutations affecting tRNA charging imply that NCDAAs are competing with their L-stereoisomers. However, L- and D-amino acids cannot compete for incorporation into the fifth position of the PG muropeptide, as transpeptidation cannot accommodate L-stereocenters.

In the next chapter, I address this issue, starting with the question: can L-amino acids rescue *B. subtilis* biofilm formation in the presence of NCDAAs and, if so, how does this rescue compare to that of the known counter-treatment, D-Ala?

Chapter 3

D-amino acids and biofilm: A corrected story

The work I present in this chapter is a modified and expanded version of my publication Leiman et al., 2013. In addition to the new matter included in the chapter itself, further details and explanations are provided in Appendices A, B, and C.

L-amino acids, but not D-alanine, counteract biofilm inhibition by D-amino acids

As described earlier, Kolodkin-Gal et al. reported that D-Tyr at 3 μM, D-Leu at 8.5 mM, or D-Trp at 5 mM, individually, inhibit pellicle formation by *B. subtilis* (Kolodkin-Gal et al., 2010). These effects were prevented by the addition of D-Ala at 10 mM (Kolodkin-Gal et al., 2010). Since D-Ala is present in the peptide side chain of PG, such results suggested that biofilm inhibition by D-Leu, D-Met, D-Trp, and D-Tyr was due to their incorporation into PG. Due to my whole genome sequencing results (Chapter 2), I became interested in testing L-amino acids as counter-treatments to NCDAA-induced biofilm inhibition and comparing their efficacy to the established counter-treatment D-Ala.

To my surprise, I did not observe that 10 mM D-Ala reversed the biofilm-inhibitory effects of 6 μM D-Tyr (Fig. 7A). Instead, I found that L-Tyr was an effective D-Tyr counter-treatment, even at concentrations far lower than those previously reported for D-Ala. The efficacy of the L-Tyr counter-treatment was proportional to its concentration in the medium (Fig. 7A). Moreover, the effects of L-Tyr were specific. Biofilm inhibition by D-Tyr was unaffected by non-isomeric L-amino acids such as L-Leu, L-Trp, and L-Met (Fig. 8).

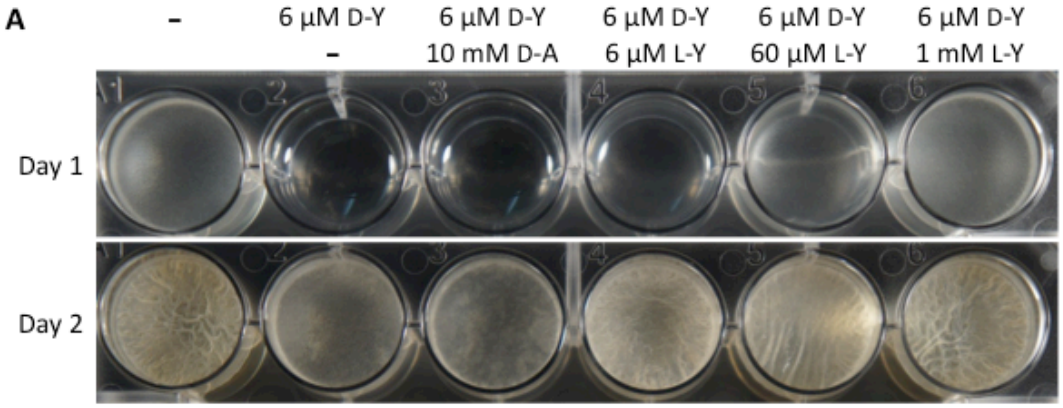

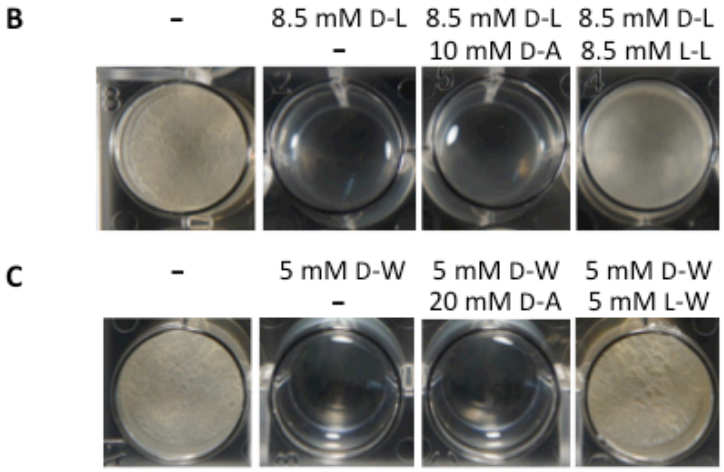

Figure 7. Rescue of biofilm formation by L-stereoisomers of D-amino acids. *B. subtilis* 3610 was treated with D-Tyr alone, D-Tyr plus D-Ala, or D-Tyr plus L-Tyr (A), with D-Leu alone, D-Leu plus D-Ala, or D-Leu plus L-Leu (B), or with D-Trp alone, D-Trp plus D-Ala, or D-Trp plus L-Trp (C). All cultures were grown in MSgg and incubated at 30°C. Photographs of D-Tyr-treated cells were taken at 24 hours and at 48 hours (day 1 and 2 in panel A) after treatment. Images of cells treated with D-Leu or D-Trp were taken at 48 hours post-treatment.

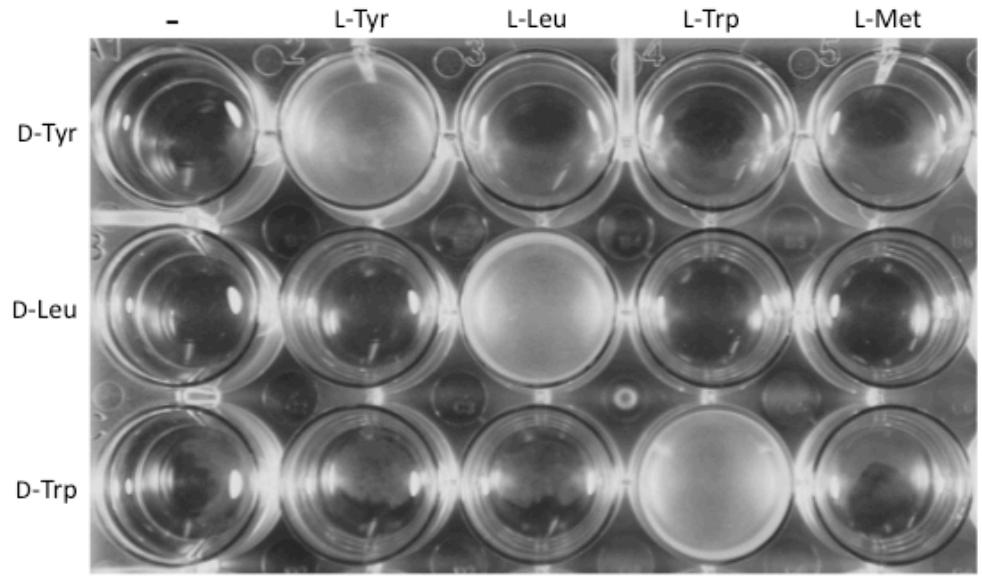

Figure 8. Rescue of pellicle formation by L-amino acids is specific. *B. subtilis* 3610 was treated with a single D-amino acid, a D-amino acid and its cognate L-amino acid, or a D-amino acid and a non-cognate L-amino acid. D-Tyr was applied at 6 µM with L-Tyr, L-Leu, L-Trp, and L-Met each at 600 µM. D-Leu and all four L-amino acid counter-treatments were applied at 8.5 mM. D-Trp and all four L-amino acid counter-treatments were applied at 5 mM. Cultures were incubated at 30˚C in MSgg and photographed at 24 hours.

I obtained similar results with other NCDAAs. I found that D-Ala did not prevent the inhibition of pellicle formation caused by 8.5 mM D-Leu or 5 mM D-Trp, whereas L-Leu and L-Trp effectively counteracted D-Leu and D-Trp, respectively (Fig. 7B,C; Fig. 8). Again, the effects of the L-amino acids were specific. Cells treated with D-Leu or D-Trp and counter-treated with non-cognate L-amino acids did not produce biofilms[1] (Fig. 8).

Biofilm-inhibitory concentrations of D-amino acids inhibit growth

My success in rescuing pellicle formation using L-enantiomers of NCDAAs implied that the NCDAAs were causing a growth defect. I tested this hypothesis by measuring growth rates in the absence or presence of D-Tyr, D-Leu, or D-Trp. D-Tyr, D-Leu, and D-Trp markedly inhibited growth at the concentrations used to inhibit biofilm formation (6 μM, 8.5 mM, and 5 mM, respectively) (Fig. 9). Moreover, growth inhibition was partially or fully reversed by the addition of an equimolar concentration of the corresponding L-enantiomer (Fig. 9). These results indicate that biofilm inhibition by NCDAAs is coupled to growth inhibition. Combined with

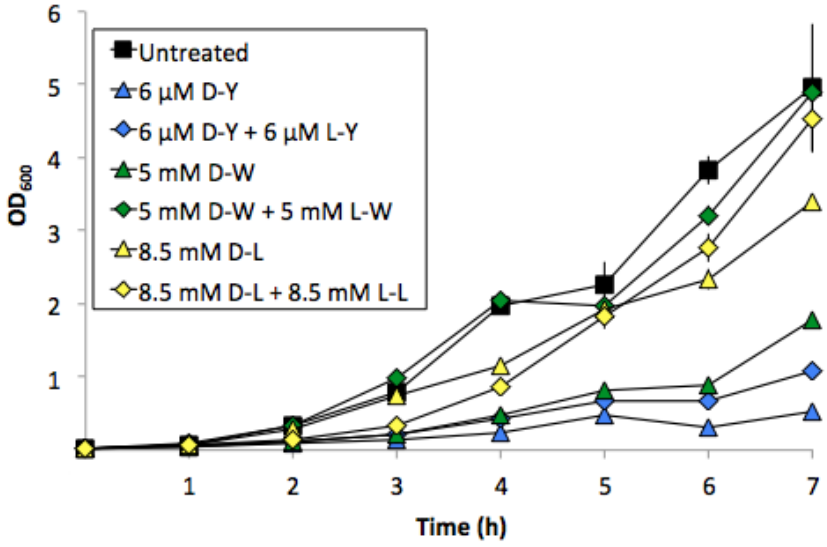

Figure 9. Biofilm-inhibitory concentrations of D-amino acids inhibit growth. *B. subtilis* 3610 was grown in shaking MSgg at 37°C. Optical density was measured at 600 nm every hour. Results represent the average of duplicate experiments, and error bars show the standard deviation.

[1] Studies with D-Met are not included here because I was unable to convincingly reproduce biofilm inhibition by D-Met at 2 mM.

evidence that tRNA charging mutants overcome NCDAA toxicity, a revised model begins to emerge in which the biofilm-inhibitory effects of NCDAAs are mediated by improper tRNA charging and, likely, subsequent protein misincorporation and proteotoxicity.

The Kolter lab has argued that it is possible to uncouple pellicle inhibition from growth inhibition at lower concentrations of D-amino acids (e.g., 700 μM D-Leu) and that, under such conditions, both the corresponding L-enantiomer and D-Ala (albeit less potently than the L-enantiomer) are capable of restoring pellicle formation (H. Vlamakis and R. Kolter, unpublished results). The ability to uncouple biofilm defects from growth defects using low concentrations of NCDAAs could suggest that biofilm formation is more sensitive than is growth to inhibition of protein synthesis. It is worth noting, however, that these results are highly condition-dependent. Thus, this interpretation (which is also presented in Leiman et al., 2013) is oversimplified. I supply a more in-depth analysis of the uncoupling phenomenon in Appendix A.

Biofilm inhibition by a mixture of D-amino acids is reversed by L-amino acids

Kolodkin-Gal et al. reported that a mixture of D-Leu, D-Met, D-Trp, and D-Tyr, each at 2.5 nM, inhibit pellicle formation in *B. subtilis* (Kolodkin-Gal et al., 2010). I was unable to observe biofilm inhibition at this concentration, and higher concentrations sufficient to mildly inhibit pellicle formation (e.g., 500 nM) also inhibited growth (Fig. 10). As a proof of principle, I tried to manipulate growth and treatment conditions such that a biofilm-inhibitory concentration of D-LMWY would not detectably inhibit growth. First, I optimized conditions to allow for biofilm inhibition at low doses of D-LMWY. Biofilm inhibition occurred in the presence of 300 nM D-LMWY when I grew cells in a modified MSgg medium lacking the usual L-amino acid supplements L-phenylalanine, L-threonine, and L-tryptophan (Fig. 11A).

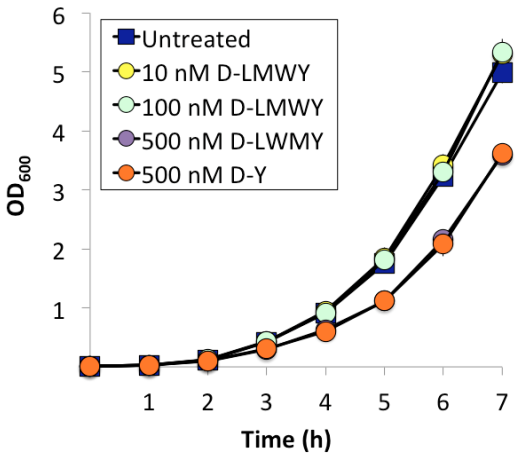

Figure 10. D-Tyr at 500 nM causes a growth defect. *B. subtilis* 3610 was growth in shaking MSgg with treatments as indicated. Results shown represent the average of duplicate experiments and error bars represent the standard deviation. Notably, the growth defect caused by D-LMWY, each at 500 nM, is equivalent to the growth defect caused by D-Tyr alone at 500 nM.

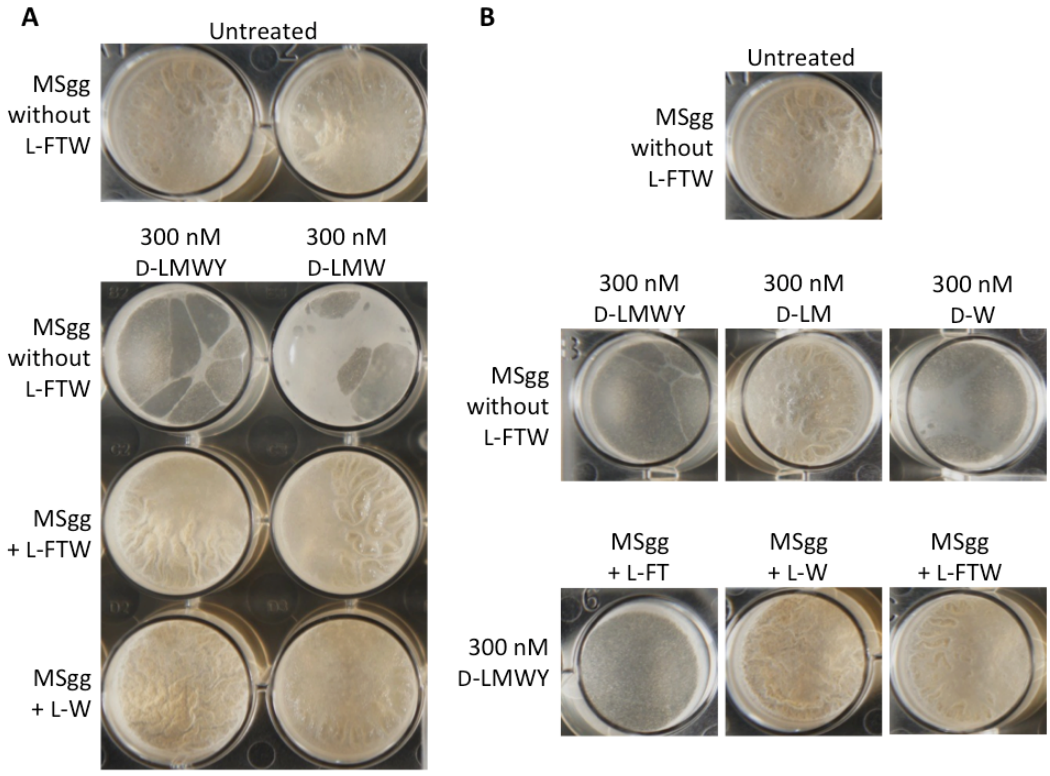

Figure 11. Biofilm inhibition by low concentrations of D-amino acids requires the absence of L-amino acids and is not due to synergy. Unmodified MSgg or MSgg lacking one or more L-amino acids, was inoculated with *B. subtilis* 3610. Cells were treated with a single D-amino acid or combinations of D-amino acids at 300 nM and were incubated at 25˚C. L-amino acids were each applied A) to the final concentration found in unmodified MSgg (L-Phe at 303 µM, L-Thr at 420 µM, L-Trp at 245 µM) or B) at 300 nM. The displayed images were taken 72 hours post-treatment.

Next, I tried growth curves, varying the aeration and inoculum size. I detected little or no growth inhibition at 300 nM D-LMWY in shaking culture when I used a smaller than usual culture volume (3 mL versus 20 mL) and a larger than usual inoculum (OD_{600} 0.05 verses 0.015) (Fig. 12). Importantly, the change from 20 mL to 3 mL in culture volume coincided with a change in glassware size and type as well as a change in shaking apparatus. Growth curves using 20 mL cultures were carried out in 250 mL Erlenmeyer flasks on a flatbed shaker (better aeration), whereas growth curves using 3 mL cultures were carried out in 10 mL test tubes in a roller drum (worse aeration). Thus, while I was able to minimize growth inhibition by 300 nM D-LMWY, I had to do so by optimizing growth curve conditions and could not eliminate the possibility that a subtle growth defect was masked by technical limitations[2].

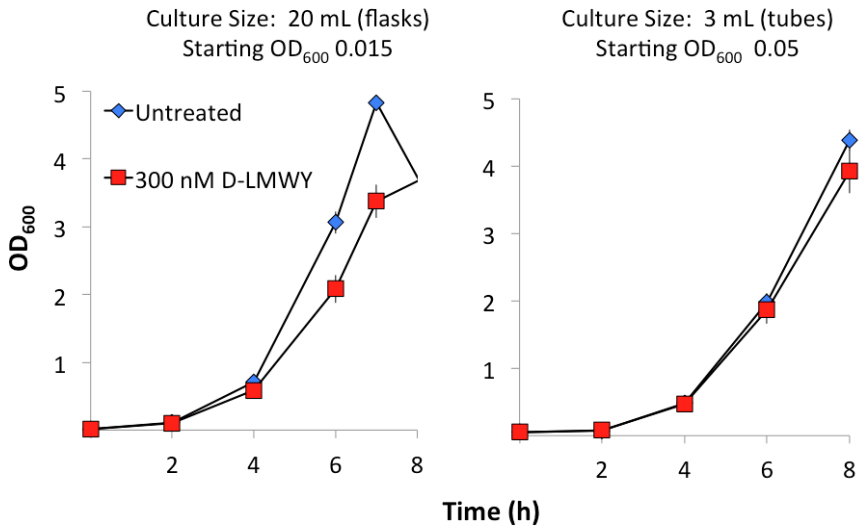

Figure 12. D-LMWY at 300 nM does not inhibit growth under specific growth conditions. *B. subtilis* 3610 was grown as indicated in the text and above each respective growth curve. Both growth curves were performed at 37˚C in MSgg lacking L-FTW. Experiments conducted in flasks (left) were performed in duplicate and experiments conducted in tubes (right) were performed in quadruplet. Results indicate the average optical density at 600 nm and error bars represent the standard deviation.

[2] It is important to note that pellicle assays are carried out in static culture and that *B. subtilis* is an aerobe. It is probable that the challenge (i.e., growth inhibition) that *B. subtilis* faces in a nutrient-poor medium containing a toxic metabolic is exacerbated by a static environment.

Ultimately, whether D-LMWY at 300 nM has no effect or a minimal effect on growth is academic. Even under conditions optimized to uncouple biofilm inhibition and growth inhibition, it was still possible to reverse the biofilm-inhibitory activity of 300 nM D-LMWY with 300 nM L-Trp (Fig. 11B) or 300 nM L-Tyr (data not shown). Moreover, 300 nM D-Trp alone or 300 nM D-Tyr alone was as effective at inhibiting biofilm formation as was the full D-LMWY mixture, each at 300 nM, a finding that is inconsistent with previous results suggesting synergy between the four D-amino acids (Kolodkin-Gal et al., 2010).

In summary, my work using the D-amino acid mixture D-LMWY contradicts several claims in Kolodkin-Gal et al., 2010. Rather than corroborating that D-LMWY at 2.5-10 nM abolishes biofilm in standard MSgg, I found that D-LMWY at 300 nM only partially inhibits biofilm and only in MSgg lacking certain L-amino acids. I determined that even in the nanomolar treatment range, biofilm inhibition and growth inhibition cannot be resolutely uncoupled. Finally, I found further evidence that – regardless of growth inhibition or lack thereof – the palliative affect of L-amino acids is inconsistent with the current model of D-amino acid-mediated biofilm inhibition.

D-Ala does not replace NCDAAs in *B. subtilis* peptidoglycan

While Kolodkin-Gal et al. presented indirect evidence (e.g., reversal of inhibition by excess D-Ala and the D-Tyr-resistant phenotypes of six *tapA* mutants) that NCDAAs inhibit or disassemble biofilms by integrating into the cell wall, the authors did not directly demonstrate competition between D-Ala and NCDAAs. In the interest of conducting a thorough investigation into the mechanism of NCDAAs, I isolated and analyzed PG fragments for *B. subtilis* grown in

MSgg with D-Trp, D-Ala, an equimolar mixture of D-Trp and L-Trp, or a mixture of D-Trp and excess D-Ala. This work was generously facilitated by Janine May in the Kahne laboratory.

I found by LC-MS that D-Trp at 50 μM remained in PG even in the presence of a 200-fold excess of D-Ala (Fig. 13), suggesting that excess D-Ala does not displace NCDAAs from muropeptides. I also found that a treatment of 10 mM D-Ala alone had no measureable effect on the abundance or distribution of PG peaks (Fig. 13). This finding suggests that if excess D-Ala is incorporated into PG, it easily removed by PBPs. Arguably, this result also implies that (unlike D-Ala) NCDAAs are difficult if not impossible to remove by PBPs, and may only be discarded via cell wall turnover. Lastly, I inspected the PG profile of cells treated with a mixture of D-Trp and L-Trp. As expected, L-Trp did not change the *B. subtilis* PG profile, suggesting that the presence of a NCDAA in PG is irrelevant to biofilm formation and stability (Fig. 13). Thus, analyses of the *B. subtilis* cell wall unravels the arguments, made by Kolodkin-Gal et al., that muropeptide incorporation of NCDAAs (1) mediates biofilm inhibition or disassembly and (2) may be corrected by excess D-Ala.

***tapA* mutations do not confer resistance to D-Tyr.**

Kolodkin-Gal et al. claimed that frame shift mutations in the 3' region of the biofilm matrix gene *tapA* confer resistance to D-Tyr during biofilm formation (Kolodkin-Gal et al., 2010). I confirmed D-Tyr resistance for *tapA2*, though not for *tapA6*, in the previous chapter. Regardless, the reported resistance phenotype of the *tapA* mutants is at odds with the growing evidence that NCDAAs do not inhibit biofilm formation through their incorporation into PG but that, instead, they inhibit growth. In light of this evidence, I reexamined the reported effect of the *tapA* mutations *tapA2* and *tapA6.*

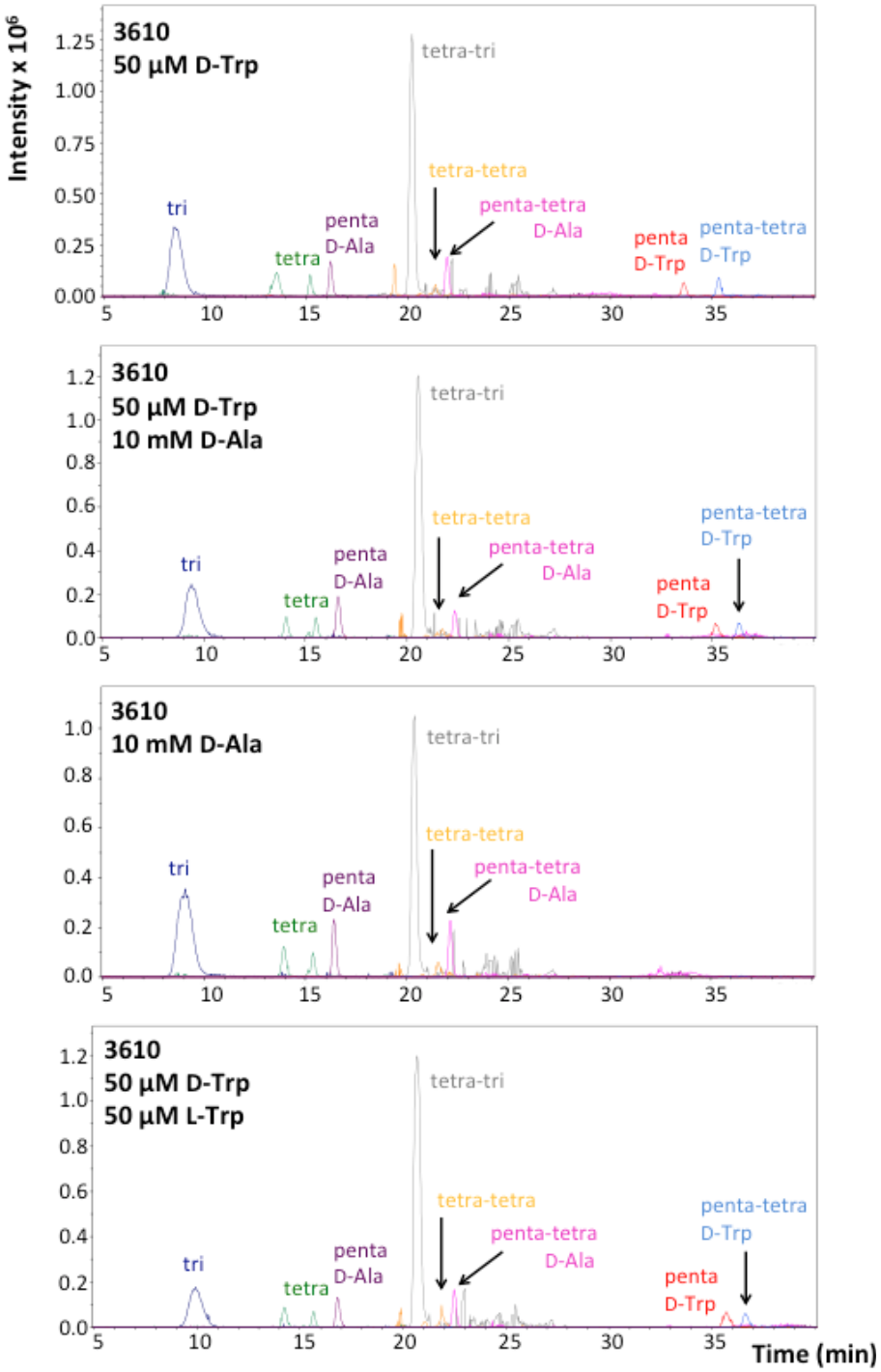

Figure 13. The presence of D-Trp in PG is unrelated to biofilm stability. *B. subtilis* 3610 was grown in MSgg with the indicated treatments. Pellicles were harvested after two days of static growth at 30˚C. PG was isolated, fragmented, and analyzed by LC-MS. The peaks for the tripeptide, tetrapeptide, pentapeptide (with a fifth position D-Ala), tetrapeptide-tripeptide crosslink, tetrapeptide-tetrapeptide crosslink, pentapeptide-tetrapeptide crosslink (with a fifth position D-Ala), pentapeptide (with a fifth position D-Trp), and pentapeptide-tetrapeptide crosslink (with a fifth position D-Trp) were selected by mass for each spectrum.

Unfortunately, I was unable to work with the original mutants. Sequencing revealed that both of the original mutant strains (IKG40 and IKG44) harbored wild-type *tapA*. I concluded that the resistance phenotype of *tapA2* (IKG40) was due to another, unidentified, mutation.

I worked with a post-doctoral fellow in the lab, Alex Elsholz, to reconstruct *tapA2* and *tapA6* using a derivative of the strain 3610 lacking the *tapA-sipW-tasA* operon. The deletion of the native *tapA* operon was complemented with a copy of the operon inserted at the *amyE* locus that was either wild-type for *tapA* or contained the *tapA2* or *tapA6* mutation. Each of the three complementation constructs restored wild-type matrix formation to untreated cells (Fig. 14). However, neither the *tapA2* nor the *tapA6* mutation rescued biofilm formation in the presence of D-Tyr under the conditions of Figure 14 as well as at several other temperatures and nutrient conditions (data not shown). In addition, the visible growth defect of the uncomplemented *tapA*-null strain demonstrates that NCDAAs do not affect *B. subtilis* in a TapA-dependent manner.

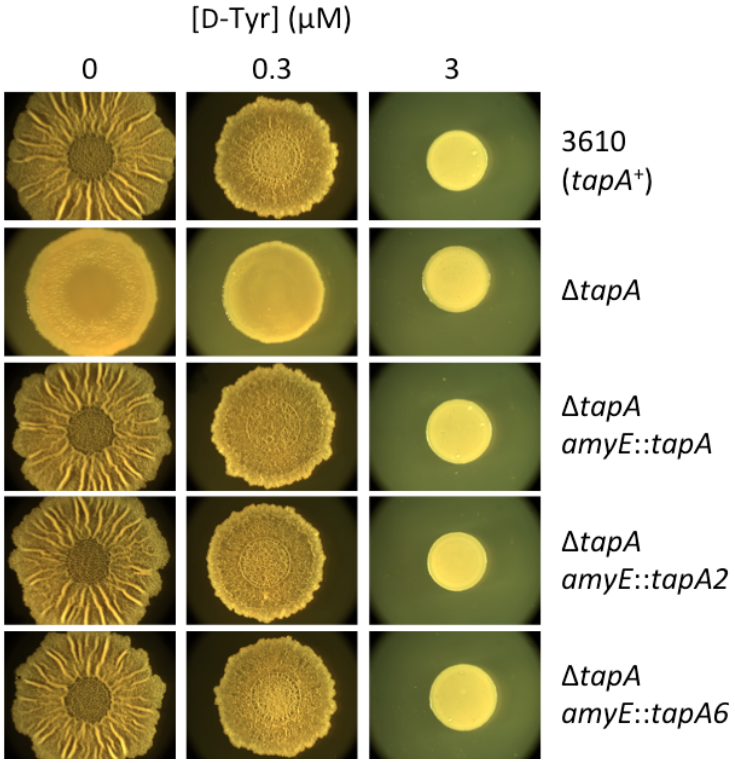

Figure 14. *tapA* mutations do not confer resistance to D-Tyr. A *B. subtilis* strain lacking the *tapA* operon (SLH63) was compared with a *tapA*$^{+}$ strain (3610) as well as with strains complemented at *amyE* for the *tapA* operon containing wild-type (SLH64) *tapA* or mutant *tapA* genes harboring the previously described frameshift mutations *tapA2* (SLH65) or *tapA6* (SLH66). All strains were spotted on solid MSgg lacking L-FTW and containing the indicated concentration of D-Tyr. Images were taken after 72 h incubation at 30˚C.

Repairing *dtd* enhances survival in the presence of D-amino acids

Next, I noticed that in the strain we routinely use (NCIB3610, or 3610) and in its derivative 168, the gene (*dtd*) for D-tyrosyl tRNA deacylase is mutated[3], harboring a lysine codon (AAG) in place of the wild-type initiation codon (AUG). D-tyrosyl tRNA deacylase was originally identified on the basis of its ability to specifically remove D-Tyr from mischarged $tRNA^{Tyr}$ but has since been shown to deacylate tRNAs mischarged with other D-amino acids (Soutourina et al., 2004). Thus, for simplicity, I will henceforth refer to this enzyme as D-aminoacyl tRNA deacylase (Yang et al., 2003). If, as I hypothesized, the effects of NCDAAs are largely due to tRNA mischarging events, then repairing the mutant deacylase gene ought to confer resistance to the inhibitory effects of NCDAAs on growth and biofilm formation. To test this prediction, I repaired the *dtd* gene in 3610 using a protocol that left the chromosome unaltered except for the AAG-to-AUG nucleotide switch. Measurements of growth rates under standard biofilm-promoting conditions revealed that, unlike strain 3610, the dtd^+ strain grew normally in the presence of D-LMWY at 3 μM each (Fig. 15A). Moreover, D-LMWY at 300 μM, which was lethal for the parent strain, merely slowed the growth of the strain repaired for D-aminoacyl-tRNA deacylase activity. Using phase contrast microscopy, I visualized 3610 and dtd^+ cells that had been grown in the absence or presence of 1 μM D-LMWY. Even at this low dose, 3610 cells are clearly lysing (Fig. 15B). I also observed cellular deformations in the treated 3610 sample. These deformations were consistent with those observed by Champney and Jenson upon growing *B. subtilis* ND 40 (a prototrophic derivative of 168) in the presence of D-Tyr (Champney and Jensen, 1970). In contrast, dtd^+ cells treated with D-LMWY were indistinguishable from untreated dtd^+ cells (Fig. 15B).

[3] In the 168 genome, *dtd* is annotated as *yrvI*. PY79 harbors the same mutant copy of *dtd* as do 3610 and 168.

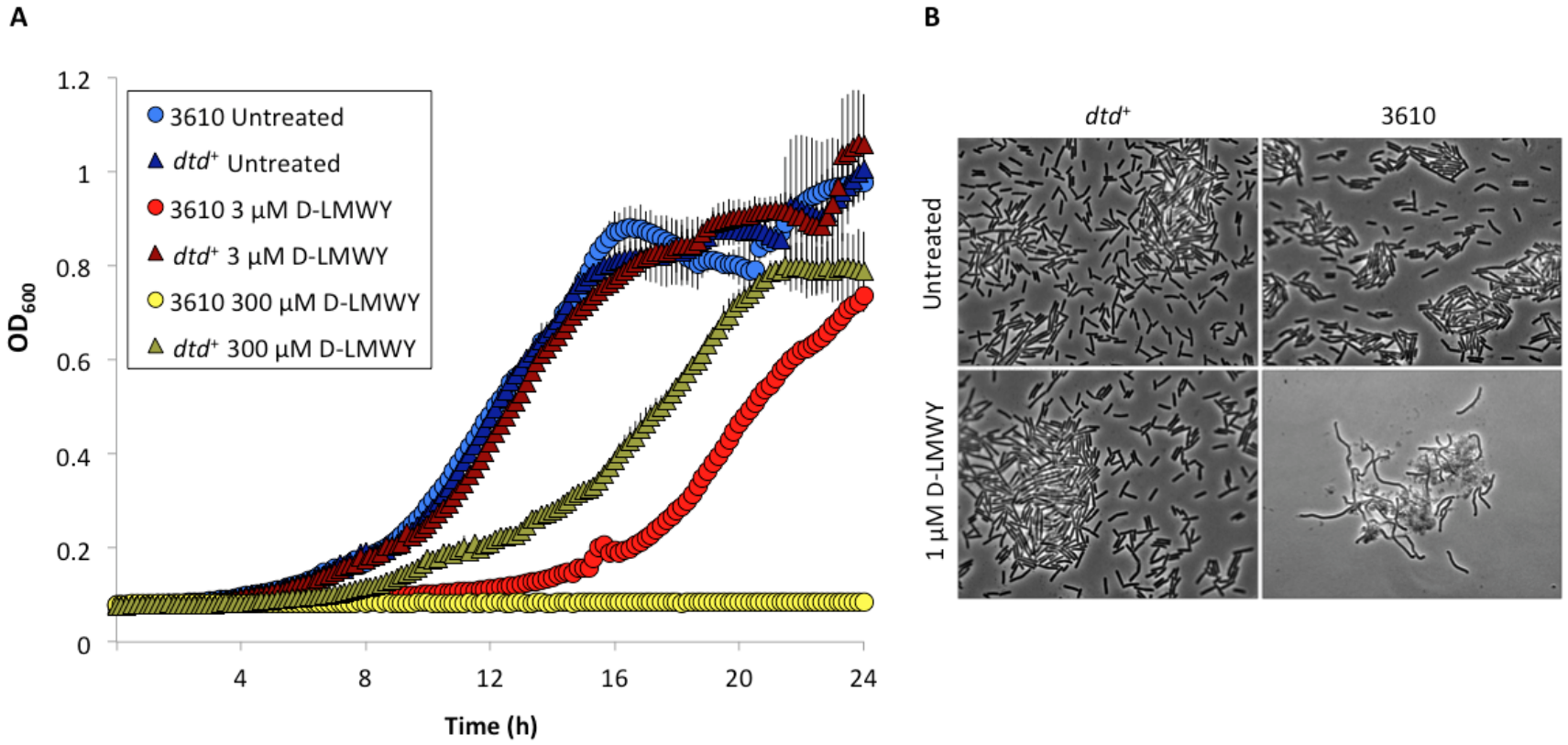

Figure 15. Cells repaired for the D-aminoacyl tRNA deacylase gene exhibit resistance to growth inhibition by D-amino acids. The *dtd* mutant strain (3610) or the *dtd*$^+$ repaired strain (SLH31) was grown in MSgg alone or MSgg containing an equimolar mixture of D-LMWY. (A) Cultures were incubated at 30˚C and continuously shaken in a microplate reader in which optical density was measured at 600 nm every 10 minutes for 24 hours. Results represent the average of three replicates and error bars show the standard deviation. (B) Three-hour-old cultures of untreated SLH31, treated SLH31, or untreated 3610, or six-hour-old cultures of treated 3610, were spotted onto MSgg agar pads. Phase contrast micrographs were taken on an Olympus BX61 microscope at 100x magnification.

Repairing *dtd* restores biofilm formation in the presence of D-amino acids

Repairing *dtd* in *B. subtilis* 3610 also rescued biofilm formation in the presence of NCDAAs. Whereas the parental strain (3610) produced thin biofilms in MSgg containing D-LMWY at 300 nM but lacking the L-amino acids supplements L-FTW, the *dtd*$^{+}$ strain formed robust pellicles under the same medium conditions (Fig. 16). In fact, in the absence of L-FTW, the repaired strain resisted biofilm inhibition when treated with D-LMWY at 300 μM and was partially resistant to D-LMWY at up to 3 mM each[4]. This finding suggests that *B. subtilis* cells expressing *dtd* are at least 10,000 fold more resistant to NCDAA stress than are cells lacking D-aminoacyl-tRNA deacylase activity. These results strongly suggest that the biofilm-inhibitory effects of NCDAAs in *B. subtilis* 3610 are an indirect consequence of their misacylation onto tRNAs, and possibly their subsequent misincorporation into proteins.

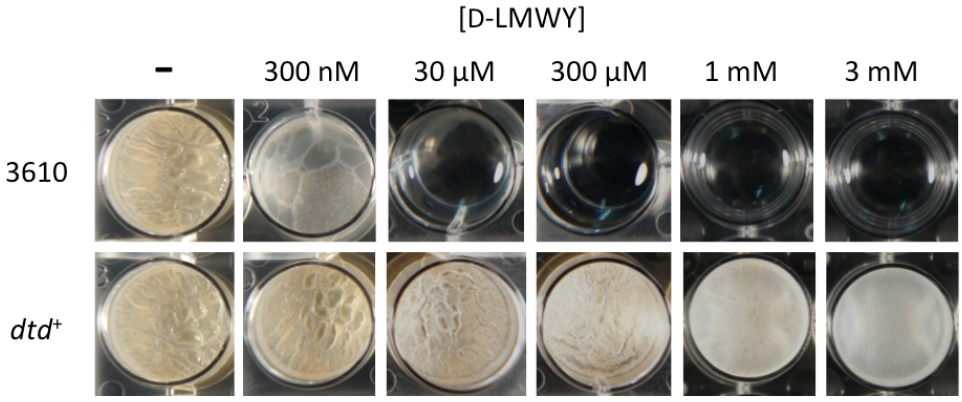

Figure 16. Cells repaired for the D-aminoacyl tRNA deacylase gene exhibit resistance to biofilm inhibition by NCDAAs. The *dtd* mutant strain (3610) or the *dtd*$^{+}$ repaired strain (SLH31) were treated with a range of concentrations of an equimolar mixture of D-LMWY. All cultures were grown in MSgg lacking L-FTW and were incubated at 25˚C. Photographs were taken after 72 hours.

[4] Note that HCl was required to get D-Tyr into solution at millimolar concentrations, and that all four NCDAAs used in this treatment have limited solubility in water (to various degrees). Thus, applying a 1 mM or 3 mM mixture (a total of 4 mM or 12 mM NCDAA, respectively) required both limiting the nutrient or culture density of the sample and exposing the cultures to higher doses of HCl. Such disadvantaging factors should be taken into account when analyzing pellicle formation in strong treatment conditions.

Matrix gene expression decreases in the presence of D-amino acids

In light of the resistance of the *dtd*$^+$ strain to D-LMWY, I revisited the effect of D-LMWY on matrix gene expression using luciferase fusions to the promoters for the *epsA* and *tapA* operons. Untreated 3610 cells, untreated *dtd*$^+$ cells, and *dtd*$^+$ cells treated with D-LMWY at 3 µM all expressed the luciferase fusions at comparable levels (Fig. 17). In contrast, D-LMWY at 3 µM severely inhibited luciferase activity in 3610, consistent with defects in protein synthesis. Excess D-Ala did not change the expression of the luciferase fusions, whereas expression was partially restored by L-LMWY (Fig. 17).

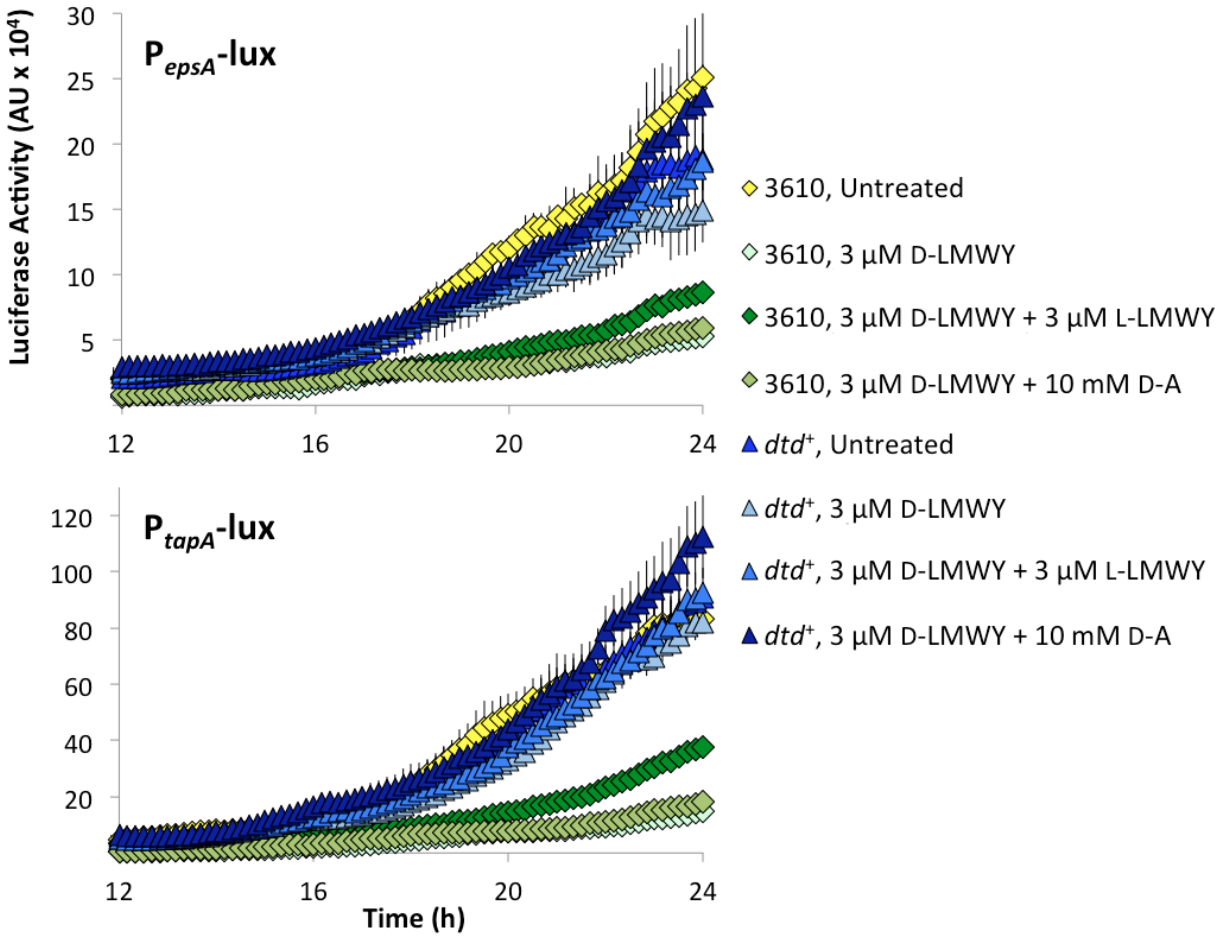

Figure 17. Expression of biofilm matrix genes is sensitive to D-LMWY in 3610 cells, but not in cells repaired for D-aminoacyl-tRNA deacylase activity. 3610 or *dtd*$^+$ cells harboring a luciferase reporter for *epsA* or *tapA* expression were grown in MSgg. Luciferase luminescence was normalized to optical density. Results represent the average of triplicate experiments, and the error bars show the standard deviation.

Repairing *dtd* does not interfere with incorporation of D-amino acids into PG

Finally, I wanted to ensure that the highly NCDAA-resistant phenotypes (e.g., robust growth, gene expression, and biofilm formation in the presence of NCDAAs) of the *dtd*$^+$ *B. subtilis* cells were not attributable to a defect in NCDAA incorporation into PG. Using LC-MS, I analyzed the composition of PG from *dtd*$^+$ cells grown in the presence of D-Trp at 50 μM or 1 mM and compared each of these samples to PG from untreated *dtd*$^+$ cells. Both untreated and treated *dtd*$^+$ cultures produced robust pellicles (data not shown).

LC-MS revealed that D-Trp was incorporated into the fifth position of the PG peptide side chain when *dtd*$^+$ cells were treated with D-Trp at 50 μM or 1 mM (Fig. 18). In contrast, I did not detect D-Trp in PG from untreated *dtd*$^+$ cells. These data indicate that repairing the *dtd* gene did not interfere with NCDAA incorporation into PG. I concluded that *B. subtilis* is capable of incorporating NCDAAs, or at least D-Trp, into PG under conditions in which NCDAAs do not affect biofilm formation or cell growth.

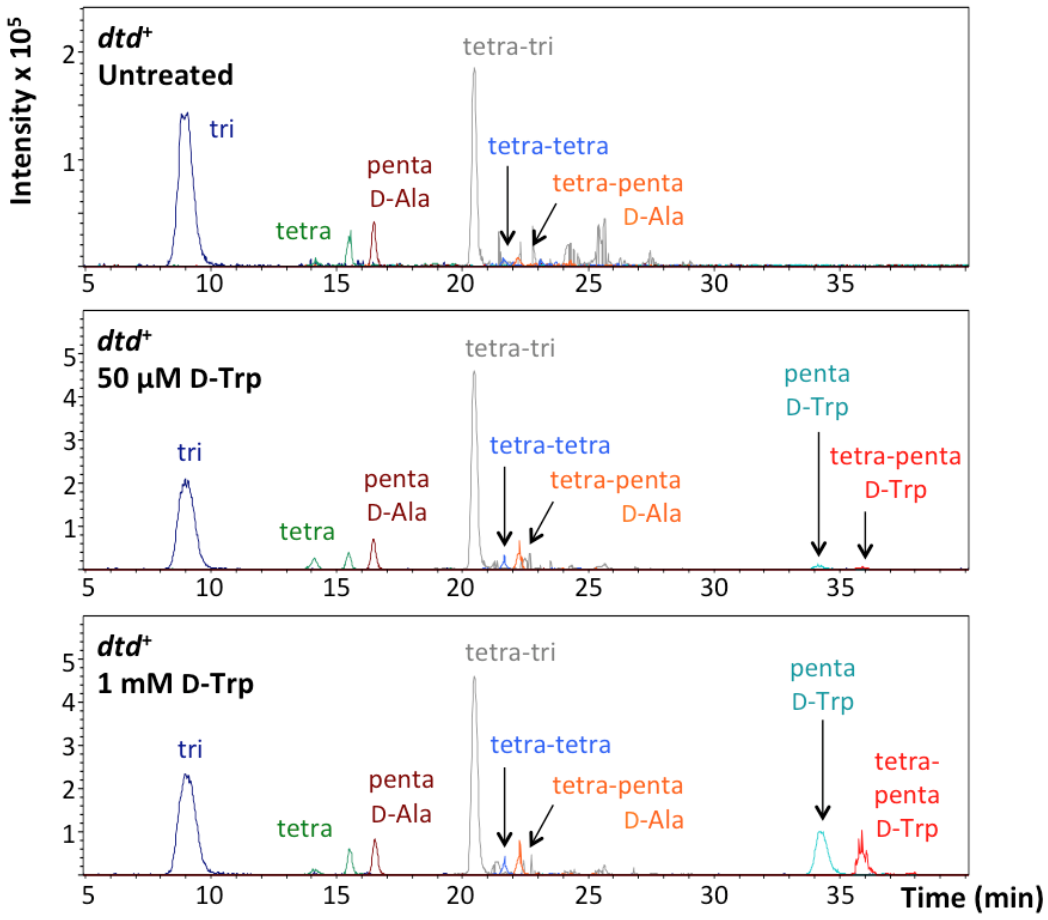

Figure 18. Cells repaired for *dtd* expression incorporate D-Trp into the PG side chain. Pellicles from *dtd*$^+$ cultures left untreated or treated with D-Trp were harvested after incubation for 48 hours at 25˚C. PG from each sample was isolated, digested, and analyzed by LC-MS. Peaks corresponding to PG fragments of interest were selected by mass. All conditions were analyzed for the same eight fragment peaks.

Implications of *dtd* in the genome

It is curious, given the toxic effects of NCDAAs, that certain strains of *B. subtilis* lack D-aminoacyl-tRNA deacylase activity. The absence of deacylase activity in the laboratory strain 168 was discovered by Calendar and Berg in 1966 (Calendar and Berg, 1966a). Interestingly, *B. subtilis* strain 23 is naturally resistant to D-Tyr, and from this observation Champney and Jenson inferred that strain 23 had retained D-aminoacyl tRNA deacylase activity (Champney and Jensen, 1969). Indeed, the presence of a wild-type *dtd* gene in this strain was later confirmed by DNA sequencing. As independent confirmation of the protective effect of *dtd*, I treated three *B. subtilis* strains or relatives, all of which harbor a wild-type copy of *dtd*, with D-Tyr at 10 µM or 100 µM. All three isolates demonstrated resistance to high doses of D-Tyr (Fig. 19).

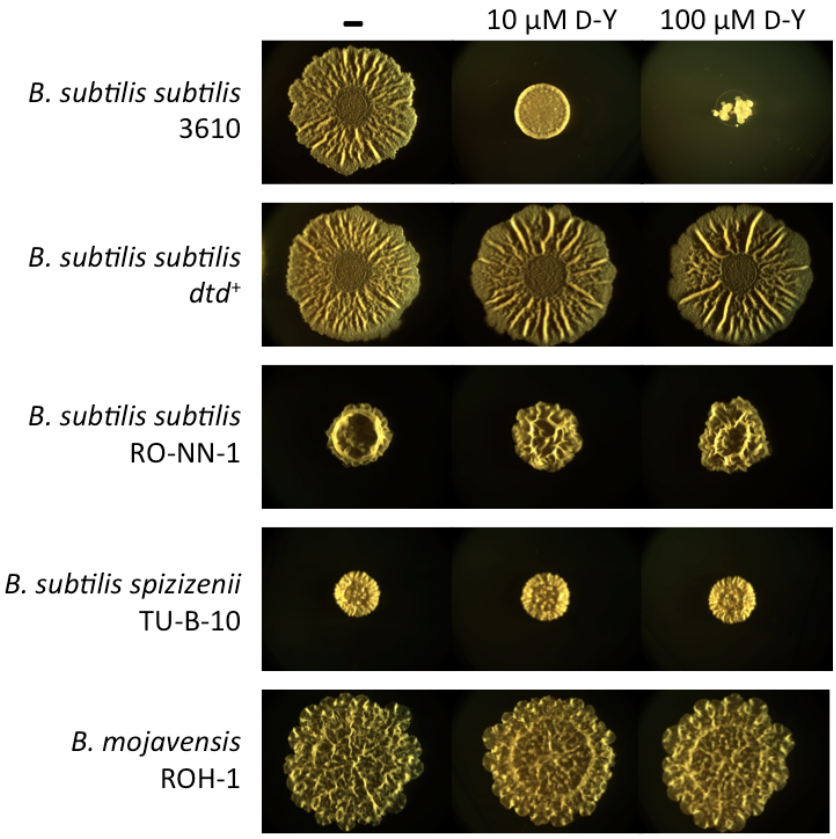

Figure 19. Relatives of *B. subtilis* that express *dtd* are insensitive to D-Tyr at high concentrations. *B. subtilis* 3610, the *dtd*$^+$ derivative of *B. subtilis* 3610 (SLH31), JRR4, JRR5, and JRR7 were spotted on solid MSgg containing no treatment or D-Tyr at either 10 µM or 100 µM. Plates were incubated at 30˚C and imaged after three days.

The conservation pattern of the D-aminoacyl tRNA deacylase encoded by *dtd* is informative; the presence or absence of *dtd* in a given organism's genome correlates closely with that organism's biosynthetic pathway for L-Tyr (Soutourina et al., 2000). Typically, L-Tyr is synthesized in one of two ways. Some microbes, including most cyanobacteria, convert the L-Tyr precursor prephenate into arogenate (pretyrosine) via aminotransferase activity. This is followed by the conversion of arogenate to L-Tyr by the L-stereospecific enzyme arogenate dehydrogenase. This pathway can only generate L-Tyr, and microbes that depend solely on this pathway tend not to express *dtd*[5]. Other microbes, including *B. subtilis* and *E. coli*, use prephenate dehydrogenase to convert prephenate to 4-hydroxyphenylpyruvate. When the final (aminotransferase) step of L-Tyr biosynthesis occurs, the amine group can be erroneously attached such that D-Tyr is formed instead of L-Tyr. Microbes reliant on this biosynthetic pathway do express *dtd*. One possible interpretation of this conservation pattern is that *B. subtilis* generates D-Tyr (as detected in Lam et al., 2009 and Kolodkin-Gal et al., 2010) not by one or more dedicated racemases[6], such as RacX and YlmE (Kolodkin-Gal et al., 2010), but by accident. In fact, not only is there no evidence that tyrosine is a substrate of RacX, a recent study showed that YlmE has no *in vitro* racemace activity at all (Ito et al., 2013).

D-amino acids do not inhibit biofilm except by way of growth inhibition

To summarize, the inhibition of biofilm formation by NCDAAs in *B. subtilis* is largely, and likely entirely, an indirect result of growth inhibition by D-Tyr, mediated by the mischarging of tRNAs. This conclusion rests on the following observations: (1) the biofilm-inhibitory effects

[5] Natural tyrosine auxotrophs also lack *dtd* (Soutourina et al., 2000).

[6] There is no evidence that any *B. subtilis* racemace produces D-Tyr, though I cannot eliminate that possibility. Some *B. subtilis* strains utilize D-Tyr for non-ribosomal peptide synthesis and it is unknown whether the amount of D-Tyr produced as a byproduct of L-Tyr biosynthesis is sufficient for this purpose.

of NCDAAs at concentrations previously reported and used here are not reversed by D-Ala but are reversed by their cognate L-amino acids; (2) concentrations of NCDAAs that inhibit biofilm formation also inhibit growth and the expression of the matrix operons *epsA* and *tapA*; (3) frameshift mutations in *tapA* are unrelated to biofilm inhibition by NCDAAs; and (4) cells corrected for the D-aminoacyl tRNA deacylase gene are resistant to the biofilm-inhibitory and growth-inhibitory effects of NCDAAs while retaining the ability to incorporate D-Trp into PG.

Notably, D-aminoacyl tRNA deacylase activity is not the only basis for resistance to NCDAAs. In the preceding chapter, I listed eight new potential D-LMWY-resistant mutations. Next, I discuss the nature of these mutations and the mechanisms by which they confer resistance to D-LMWY.

As a last point, I would like to draw attention to two elements currently missing from this investigation into NCDAAs, biofilm, and the findings reported in Kolodkin-Gal et al, 2010. First, is the issue of biofilm disassembly. Second, is the claim that NCDAAs also inhibit biofilm formation in *Staphylococcus aureus* and *Pseudomonas aeruginosa*. I address these topics in Appendix B and Appendix C, respectively.

Chapter 4

D-amino acid resistance mechanisms of *dtd*-null suppressors

In Chapter 3 I revealed that the standard *B. subtilis* laboratory strains 3610 and 168 are mutant for *dtd* and that this mutation renders them highly sensitive to D-Tyr. I also showed that strains repaired for *dtd* form pellicles in the presence of millimolar levels of NCDAAs, exhibiting an approximately 10,000-fold increase in resistance when compared to the parental strain 3610 (Leiman et al., 2013). Meanwhile, in Chapter 2 I briefly introduced seven mutants, with a total of eight mutations, which exhibit resistance to NCDAAs (Table 1 Reproduced). In this chapter, I confirm the mutations from the resistant strains, compare the growth and biofilm phenotypes of resistant mutants to the growth and biofilm phenotypes of the parental strain 3610, and investigate the mutations' mechanisms of action.

Table 1 Reproduced. Spontaneously arising mutations predicted to confer resistance to D-LMWY. Given positions are relative to the start of the open reading frame**.** n/a = not applicable.

Gene	Nucleotide Change	Amino Acid Change	Strain of Origin
tyrS	-38ΩC	n/a	SLH8
	-38C>T	n/a	SLH9
	605G>A	A202V	SLH16
trnD-Phe	35A>T	n/a	SLH13
hrcA	-8A>G	n/a	SLH15
ppaC	234A>T	E78D	SLH10
	434C>T	A145V	SLH7
	Δ496-498 (GCA)	ΔA166	SLH15

Identification of mutations conferring resistance to D-amino acids.

Having identified the mutation loci of putative D-LMWY-resistant strains, I constructed congenic derivatives of the parental strain 3610 that separately contain representative mutations. I constructed congenic mutants for *ppaC*^{A145V}, *tyrS*$^{-38C>T}$, *tyrS*^{A202V}, *trnD-Phe*$^{35A>T}$, and *hrcA*$^{-8A>G}$. Growth curves (Fig. 20) and biofilm assays (Fig. 21) revealed that the mutations in *ppaC*, *tyrS*, and *trnD-Phe* confer resistance to D-Tyr. Furthermore, these mutations conferred resistance as effectively against an equimolar mixture of D-LMWY as they did against D-Tyr (data not shown), consistent with my previous finding that D-Tyr is the only toxic component of this mixture at physiologically relevant concentrations (Leiman et al., 2013). In contrast, the mutation upstream of *hrcA* was ineffective against D-amino acid stress[1] (Fig. 20, 21). Given that the original source of this mutation (SLH15) harbored a second mutation in *ppaC* (*ppaC*$^{\Delta A166}$), and accounting for my finding that a separate mutation in *ppaC* (*ppaC*^{A145V}) protects *B. subtilis* from D-Tyr toxicity, I inferred that the active mutation of strain SLH15 is *ppaC*$^{\Delta A166}$.

[1] In retrospect, this is not surprising. The mutation interrupted the Shine Dalgarno sequence of *hrcA,* likely causing upregulation of the protein chaperones GroEL and DnaK. While increasing production of chaperones is in theory a reasonable solution to combat protein stress, the presence of one or more D-amino acids in a protein would likely prevent its proper folding regardless of the number of chaperones available.

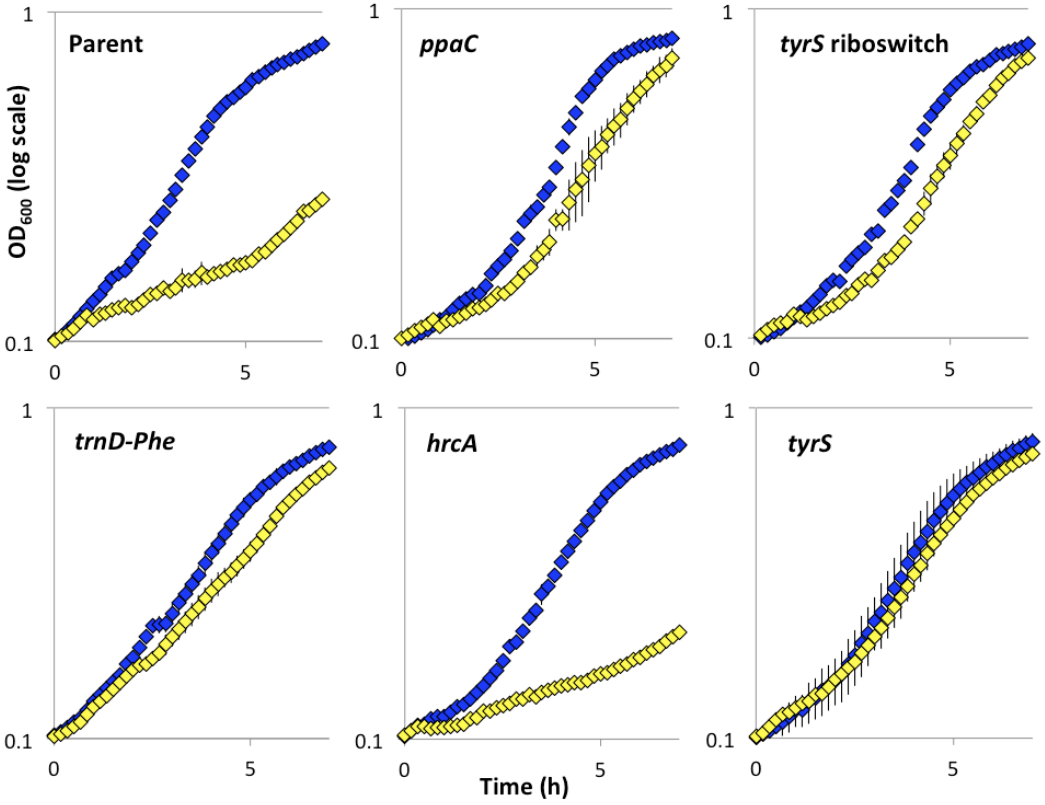

Figure 20. Mutations from spontaneously arising mutants confer resistance to growth inhibition by D-amino acids when moved to the parental strain. Optical density of cells grown in shaking MSgg was measured in the presence (yellow diamonds) or absence (blue diamonds) of 10 μM D-Tyr. Mutants were constructed by reconstituting select spontaneously arising mutations (Table 1) in the parent strain 3610. Results are shown as a semi-log plot and indicate the average of four replicates. Error bars show the standard deviation.

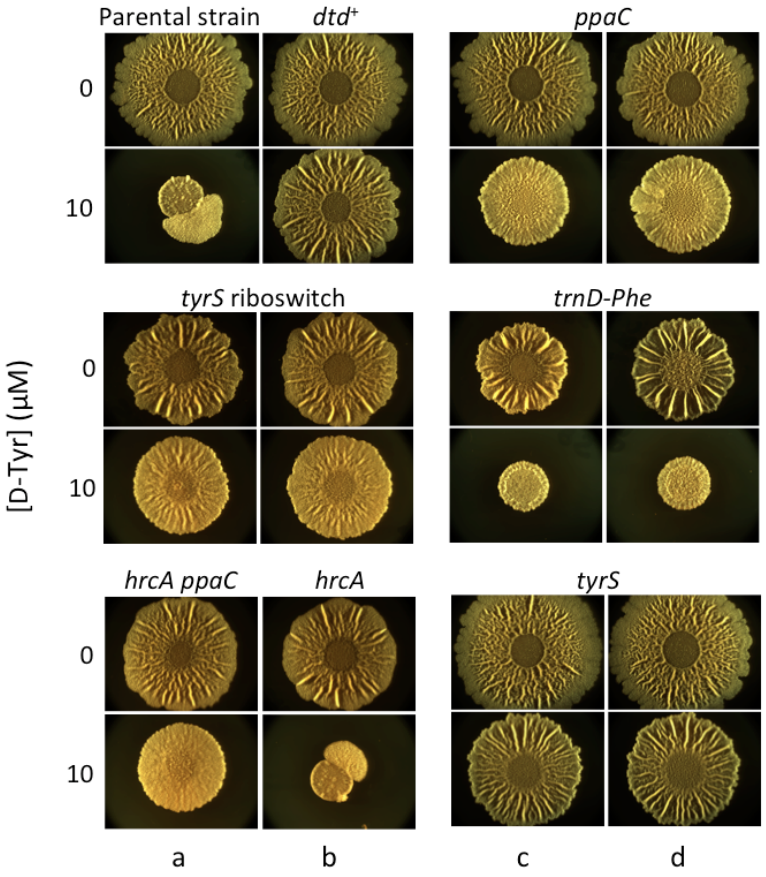

Figure 21. Congenic mutants exhibit resistance to biofilm inhibition by D-amino acids. Spontaneous mutants (Columns a, c) and their reconstituted counterparts (Columns b, d) were spotted on solid MSgg alone or solid MSgg containing 10 μM D-Tyr. The parental strain of the spontaneous mutants (3610, which is mutant for *dtd*) and a *dtd*$^+$ strain (SLH31) are included as a negative control and positive control, respectively. Images were taken after 72 h incubation at 30˚C.

TyrRS discriminates poorly between L-Tyr and D-Tyr

Tyrosyl $tRNA^{Tyr}$ synthetases are responsible for charging $tRNA^{Tyr}$ with L-Tyr. There are two classes of tyrosyl $tRNA^{Tyr}$ synthetase: TyrRS and TyrRZ, which have divergent protein sequences but highly similar structures (Tsunoda et al., 2007). Tyrosyl $tRNA^{Tyr}$ synthetase catalyzes the two steps of $tRNA^{Tyr}$ charging: L-Tyr activation, resulting in a TyrRS•L-Tyr-AMP intermediate, and aminoacylation, resulting in the transfer of L-Tyr to a $tRNA^{Tyr}$. The activation step, involving ATP hydrolysis, is rate limiting (Sheoran et al., 2008, Tsunoda et al., 2007).

As briefly mentioned in the introduction to my dissertation, all tyrosyl $tRNA^{Tyr}$ synthetases lack an editing site, instead relying on binding affinity for substrate selection (Nandi, 2012, Fersht et al., 1980). The flexibility inherent in a non-proofreading tRNA synthase has been used to great advantage by researchers in order to expand an organism's genetic code (Tsunoda et al., 2007). However, this characteristic also increases the likelihood that an organism will mischarge $tRNA^{Tyr}$, resulting in tRNA depletion and, in some cases, proteotoxicity.

Fortunately, substrate selection by binding affinity discriminates well between L-amino acids. For example, of the 19 other protein-building amino acids, L-Phe is closest in structure to L-Tyr, and the selectivity of TyrRS for L-Tyr over L-Phe is 10^4 (Fersht et al., 1980). However, this mechanism is far less effective at eliminating amino acids that are close in structure to L-Tyr but not canonically used in protein synthesis, such as 3-fluoro-L-Tyr, 3-hydroxy-L-Tyr, and D-Tyr (Calendar and Berg, 1966b).

In fact, the stereoselectivity of TyrRS is generally poor. In contrast to the 10,000-fold specificity of TyrRS for L-Tyr over L-Phe, the specificity of TyrRS for L-Tyr over D-Tyr has been reported as 24-fold in *G. stearothermophilus*, 23-fold in *E. coli*, and 3-fold in *B. subtilis*

(Calendar and Berg, 1966b, Sheoran et al., 2008). It has also been reported that while $tRNA^{Tyr}$ charging is notably slower for D-Tyr than it is for L-Tyr, L-Tyr-$tRNA^{Tyr}$ and D-Tyr-$tRNA^{Tyr}$ are equally stable once formed (Sheoran et al., 2008).

$TyrRS^{A202V}$ is more stereoselective than is wild-type TyrRS

Growth and biofilm assays (Fig. 20, 21) revealed that most effective D-LMWY-resistant mutation from my screen was *tyrS*^{A202V}, which caused an amino acid substitution proximal to the tyrosine-binding site of TyrRS (Brick et al., 1989). Because A202 is located in an alpha helix, it is reasonable to suppose that introducing the branched amino acid valine at this position alters the geometry of the tyrosine-binding site. This hypothesis is supported by the crystal structure of a divergent class of tyrosyl-$tRNA^{Tyr}$ synthetase known as TyrRZ. *B. subtilis* encodes TyrRZ in the cryptic gene *tyrZ*, and *B. subtilis* TyrRZ is structurally homologous to the synthetase expressed by *Thermus thermophilus*. In *B. subtilis* TyrRZ, the residue corresponding to *B. subtilis* TyrRS A202 is a methionine (hereafter M202). In the *T. thermophilus* enzyme it is a valine (hereafter V202). Although direct causation has not been established, the crystal structure of *T. thermophilus* TyrRZ reveals that the V202 helix more closely approaches the tyrosine-binding site than does the A202 helix. This is imperative because this helix (whether A202, V202, or M202) also contains a highly conserved glutamine (in *B. subtilis* TyrRS, this is Q195). In TyrRZ, this glutamine forms a hydrogen bond with L-Tyr; however, the TyrRS glutamine is not in the proper orientation to form this hydrogen bond (Tsunoda et al., 2007). According to preliminary work by the Henkin laboratory, *B. subtilis* TyrRZ is less efficient but more stereoselective than is *B. subtilis* TyrRS (T. Henkin and R. Williams-Wagner, personal communication). Perhaps the extended helix structure of TyrRZ – caused by a bulkier residue (valine or methionine versus alanine) – results in the formation of an L-stereospecific hydrogen

bond. If it is true that the Q195-L-Tyr hydrogen bond contributes to the enhanced specificity of TyrRZ, then it is possible that the A202V variant of *B. subtilis* TyrRS is also more specific for L-Tyr than for D-Tyr.

Of course, I also had to consider the possibility that the A202V substitution prevents TyrRS from functioning. Since *tyrS* is considered to be essential, the presence of a broken TyrRS could conceivably stimulate the expression of the cryptic, but more stereoselective TyrRZ. Thanks to helpful discussions with Becky Williams-Wagner in the Henkin laboratory, I was able to quickly eliminate this possibility. Expression of *tyrZ* requires compensatory mutations in the gene *ywaE* (T. Henkin and R. Williams-Wagner, personal communication), and I knew from whole genome sequencing that both the original resistance mutant harboring the *tyrS* mutation and the parental strain 3610 have wild-type *ywaE*.

A third and intermediate possibility was that the A202V substitution simply reduces the rate at which TyrRS charges $tRNA^{Tyr}$, thus reducing the accumulation of misacylated species. In other words, $TyrRS^{A202V}$ could be just *partially* broken[2]. To determine the mechanism by which $tyrS^{A202V}$ confers resistance to D-Tyr, I collaborated with Charles Richardson in the First laboratory at Louisiana State University Heath Sciences Center. I constructed C-terminally His_6-tagged $TyrRS^{WT}$ and $TyrRS^{A202V}$. Charles performed all of the kinetic analyses.

Charles Richardson performed steady-state kinetic analyses of *B. subtilis* $TyrRS^{WT}$ and $TyrRS^{A202V}$ (both of which were functional) in the presence of L-Tyr or D-Tyr. His findings support the hypothesis that the A202V substitution enhances enzyme stereoselectivity (Fig. 22, Table 2). Charles determined that $TyrRS^{WT}$ preferentially bound D-Tyr over L-Tyr, but that it still favored L-Tyr as a substrate; the catalytic efficiency (k_{cat}/K_M) of $TyrRS^{WT}$ was 0.173 for

[2] If true, $TyrRS^{A202V}$ would need to be efficient enough so as to maintain a near-wild-type growth rate (see Fig. 20).

L-Tyr and 0.057 for D-Tyr (Fig. 22, Table 2). While activation of L-Tyr (rather than D-Tyr) by $TyrRS^{WT}$ was three times as favorable, activation of L-Tyr by $TyrRS^{A202V}$ was 20 times as favorable. The second step of $tRNA^{Tyr}$ charging was not significantly changed by the A202V substitution (Fig. 22, Table 2). Since the L-Tyr binding site is distal to the $tRNA^{Tyr}$ binding site, I inferred that the A202V substitution does not induce widespread conformational changes in the protein structure (Brick et al., 1989). I concluded that *B. subtilis* $TyrRS^{WT}$ is a particularly poor discriminator with regard to L-Tyr and D-Tyr and that this is due to a higher binding affinity for D-Tyr (K_M = 4 μM) than for L-Tyr (K_M = 90 μM). D-Tyr can thus compete with L-Tyr in binding to TyrRS. In contrast to a classical competitive inhibitor, D-Tyr acts as a substrate of the enzyme, albeit with a sizable drop in catalytic efficiency. The introduction of a valine at position 202 alters the kinetics of the amino acid activation step, destabilizing the binding of D-Tyr relative to L-Tyr such that $TyrRS^{A202V}$ is nearly seven times as selective for L-Tyr over D-Tyr than is $TyrRS^{WT}$. Therefore, I concluded that $TyrRS^{A202V}$ is an improvement over $TyrRS^{WT}$ with regard to substrate specificity.

Table 2. Steady-state kinetics of wild-type and A202V variant TyrRS.

		K_M^{Tyr} (μM)	k_{cat} (s^{-1})	K_M^{tRNA} (μM)	k_{cat} (s^{-1})
$TyrRS^{WT}$	**L-Tyr**	90 ± 20	14 ± 3	0.27 ± 0.05	15 ± 5
	D-Tyr	4.0 ± 0.8	0.23 ± 0.04	2.2 ± 0.5	0.22 ± 0.01
$TyrRS^{A202V}$	**L-Tyr**	260 ± 20	14 ± 4	0.42 ± 0.08	11 ± 5
	D-Tyr	90 ± 20	0.27 ± 0.05	3.2 ± 0.8	0.23 ± 0.06

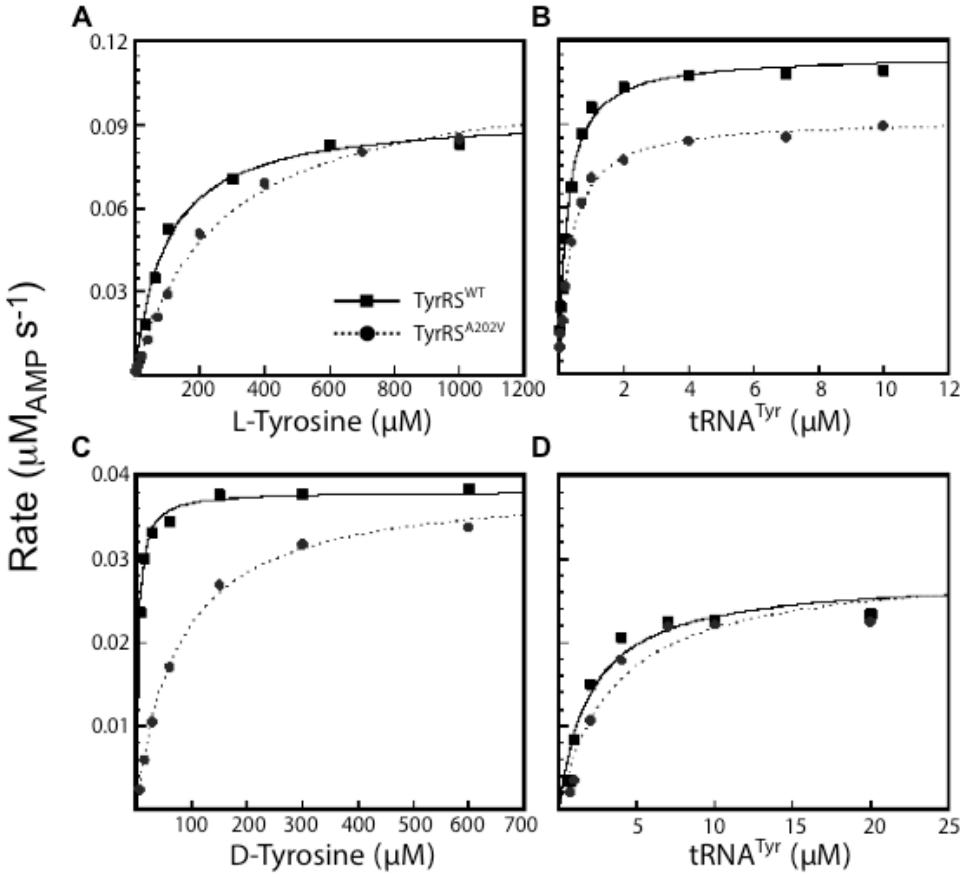

Figure 22. Representative steady-state kinetics of *B. subtilis* TyrRS. Representative data from eight independent trials are shown for the measurement of binding affinity (K_M) and turnover rate (k_{cat}) of wild type TyrRS (TyrRS^{WT}) and mutant TyrRS (TyrRS^{A202V}) for L-Tyr, D-Tyr, and tRNA^{Tyr}. The experimental conditions were as follows: A. 5 nM TyrRS and 2.5 μM tRNA^{Tyr}; B. 5 nM TyrRS and 1 mM L-Tyr; C. 125 nM TyrRS and 10 μM tRNA^{Tyr}; D. 125 nM TyrRS and 800 μM D-Tyr. All experiments included MgATP at 10 mM. .The results are summarized in Table 2.

Mutations in the *tyrS* riboswitch enhance *tyrS* expression.

Synthesis of TyrRS is controlled by a riboswitch upstream of the *tyrS* open reading frame (Grundy and Henkin, 1993, Wang and Nikonowicz, 2011). When L-Tyr is limiting, uncharged $tRNA^{Tyr}$ binds to the *tyrS* riboswitch at the Specifier Sequence (which contains the tyrosine codon UAC) as well as at the antiterminator region (Grundy et al., 1997) (Fig. 23). This stabilizes the antiterminator hairpin, thereby allowing transcriptional read-through from the riboswitch into *tyrS* and resulting in *tyrS* overexpression (Wang and Nikonowicz, 2011, Grundy and Henkin, 1993).

My selection for resistance mutations yielded two mutations in the terminator hairpin of the *tyrS* riboswitch. I hypothesized that these mutations destabilize the terminator hairpin, $tyrS^{-38C>T}$ by causing a base pair mismatch (from C-G to C-A), and $tyrS^{-38\Omega C}$ by introducing a bulge into the hairpin[3] (Fig. 23). I therefore expected that these *tyrS* riboswitch mutations would result in *tyrS* overexpression. Indeed, using a transcriptional fusion of the *tyrS* riboswitch to luciferase, I found that both mutations resulted in significantly higher luciferase activity than did the wild-type *tyrS* riboswitch (Fig. 24). These data suggest that $tyrS^{-38C>T}$ and $tyrS^{-38\Omega C}$ confer resistance to D-Tyr by increasing TyrRS levels in the cell.

[3] Both disruptions should also weaken base-stacking interactions. My hypothesis of decreased terminator hairpin stability is supported by calculations using the KineFold Web Server, estimating ΔG values of -19.6 kcal/mol (wild-type *tyrS*), -12.5 kcal/mol ($tyrS^{-38C>T}$), and -15.8 kcal/mol ($tyrS^{-38\Omega C}$).

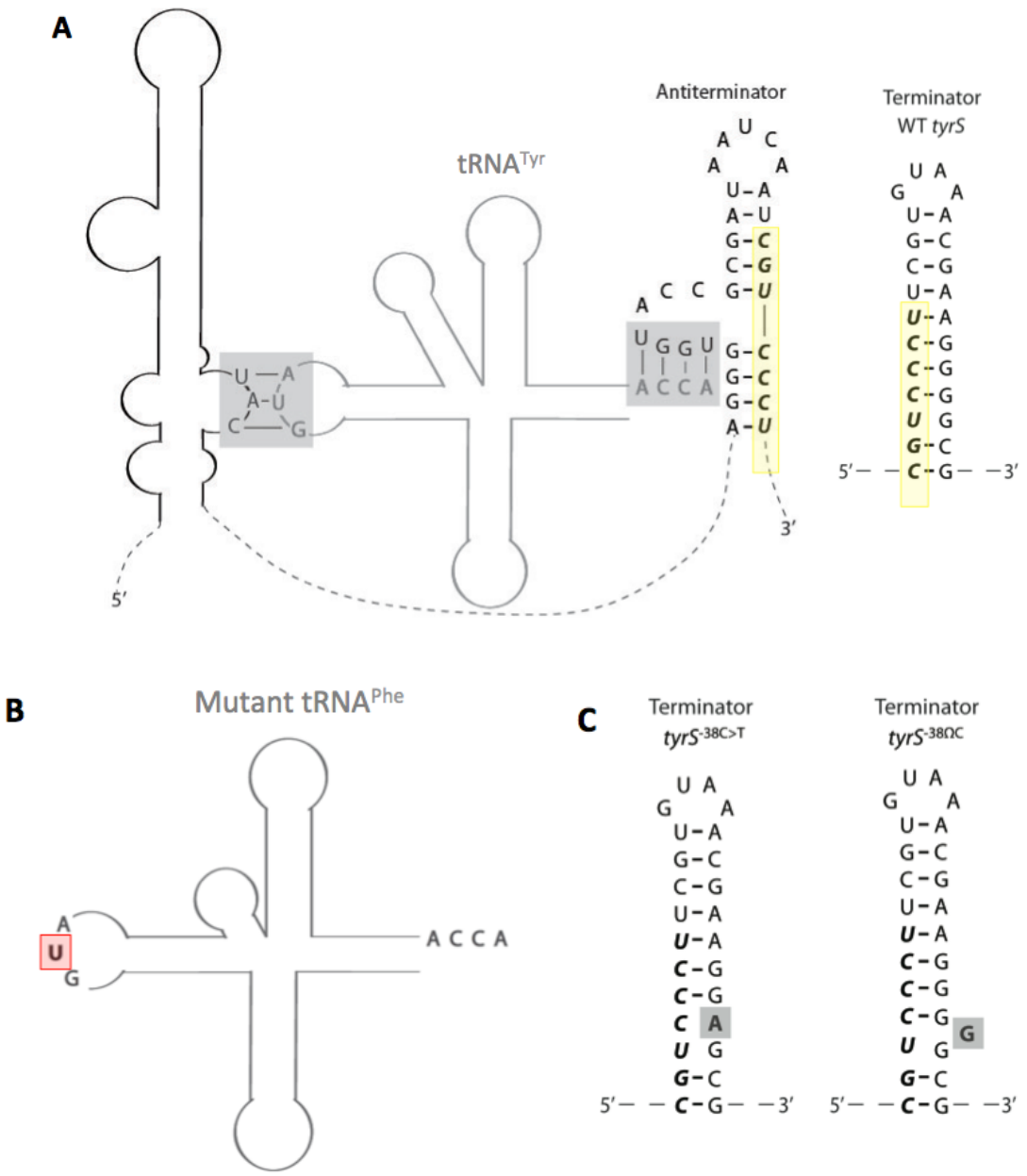

Figure 23. Schematic of the *B. subtilis tyrS* riboswitch. (A) The interaction sites of a tRNA^{Tyr} (grey) with the *tyrS* riboswitch (black) are highlighted with grey boxes. The grey box on the left shows binding between the tRNA^{Tyr} anticodon (AUG) and the riboswitch Specifier Sequence (UAC). The grey box on the right shows binding between the 3' end sequence of the tRNA^{Tyr} (ACCA) and the antiterminator. Dashed lines represent riboswitch sequence that is not significant for binding tRNA^{Tyr}. Bases shown in italics and highlighted in yellow are shared between the antiterminator and terminator hairpins. These secondary structures were originally depicted by Tina Henkin and others (Grundy et al., 1997, Gerdeman et al., 2002). (B) The mutant tRNA^{Phe} resulting from *trnD-Phe*$^{35A>T}$ harbors the AUG anticodon (A-to-U change highlighted in red) as well as the 3' ACCA sequence, and may therefore bind the *tyrS* riboswitch at the same locations as does tRNA^{Tyr}. (C) Proposed structures of mutant *tyrS* terminator hairpins. The relevant mutations are in bold and highlighted with grey boxes.

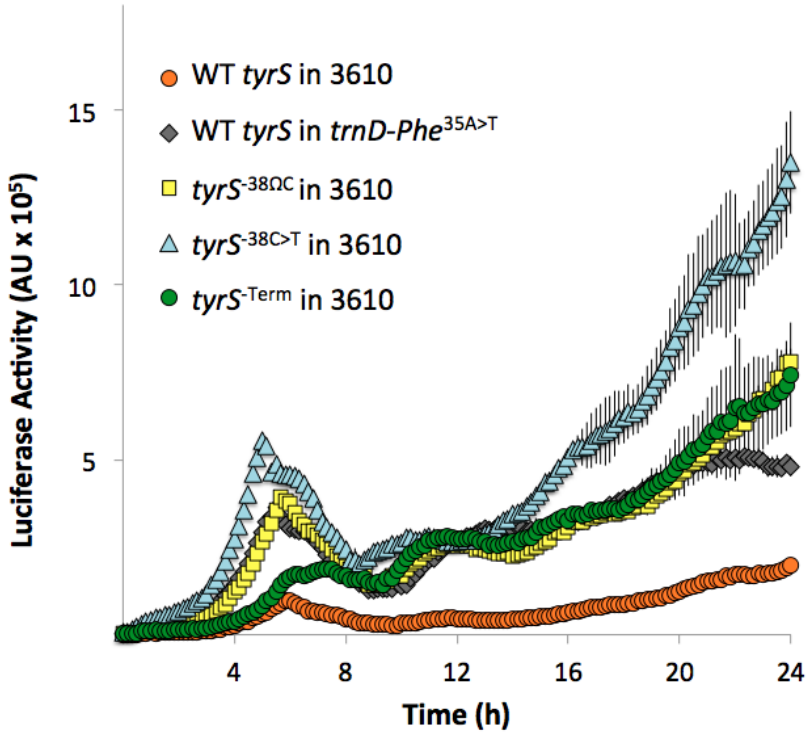

Figure 24. Mutations in the *tyrS* riboswitch and *trnD-Phe* cause read-through. Expression of a luciferase transcriptional fusion to the *tyrS* riboswitch was measured in shaking MSgg. Luciferase activity was determined by normalizing luminescence to optical density. Results shown are the average of three replicates and error bars indicate the standard deviation.

The *trnD-Phe*$^{35A>T}$ mutation converts the anticodon of tRNA^{Phe} from Phe to Tyr.

The recovery of a resistance mutation in *trnD-Phe* was surprising as *trnD-Phe* encodes a tRNA^{Phe}, and I did not use D-Phe in my screen for D-amino acid-resistant mutations. Interestingly, however, the 35A>T mutation in *trnD-Phe* changes the tRNA^{Phe} anticodon from AAG (for L-Phe) to AUG (for L-Tyr). I also noted that the sequence at the 3' end of tRNA^{Phe} is identical to the corresponding sequence of tRNA^{Tyr} that is known to base pair with the riboswitch antiterminator (Gerdeman et al., 2002). Thus, tRNA^{Phe} with the AAG to AUG anticodon switch contains both of the binding sites that dictate the tRNA^{Tyr}-*tyrS* riboswitch interaction (Gerdeman et al., 2002) (Fig. 23). I therefore postulated that the mutant tRNA^{Phe} binds the *tyrS* riboswitch and stimulates *tyrS* expression. Consistent with my hypothesis is a complementary observation,

made by Frank Grundy and Tina Henkin, that converting the *tyrS* riboswitch Specifier Sequence from UAC to UUC causes the riboswitch to become responsive to L-Phe limitation instead of L-Tyr limitation (Grundy and Henkin, 1993). As a test of my hypothesis, I measured *tyrS* expression using a transcriptional fusion of luciferase to the wild-type *tyrS* riboswitch. I found that luciferase activity in the *trnD-Phe* mutant was significantly higher than that of the parental strain and, in fact, was similar to that observed for the *tyrS* riboswitch mutants (Fig. 24). I also found that luciferase activity in the two *tyrS* riboswitch mutant strains and in the *trnD-Phe* mutant strain was comparable to or greater than that observed for a mutant lacking the *tyrS* riboswitch terminator hairpin (Fig. 24). Thus, $tyrS^{-38C>T}$, $tyrS^{-38\Omega C}$, and $trnD\text{-}Phe^{35A>T}$ result in constitutive or near-constitutive *tyrS* expression.

tyrS overexpression is sufficient to confer resistance to D-Tyr

To confirm the causal relationship between *tyrS* overexpression and resistance to D-Tyr, I constructed derivatives of *B. subtilis* 3610 that harbor isopropyl β-D-1-thiogalactopyranoside (IPTG)-inducible *tyrS* at the *amyE* locus. Overexpression of the *tyrS* open reading frame yielded robust D-Tyr resistance (Fig. 25). Overexpression of the *tyrS* riboswitch and open reading frame together also yielded D-Tyr resistance, albeit to a lesser degree (Fig. 25). This finding is consistent with evidence that the *tyrS* riboswitch normally occupies a terminator hairpin conformation, which would attenuate *tyrS* overexpression even in the presence of IPTG (Grundy and Henkin, 1993).

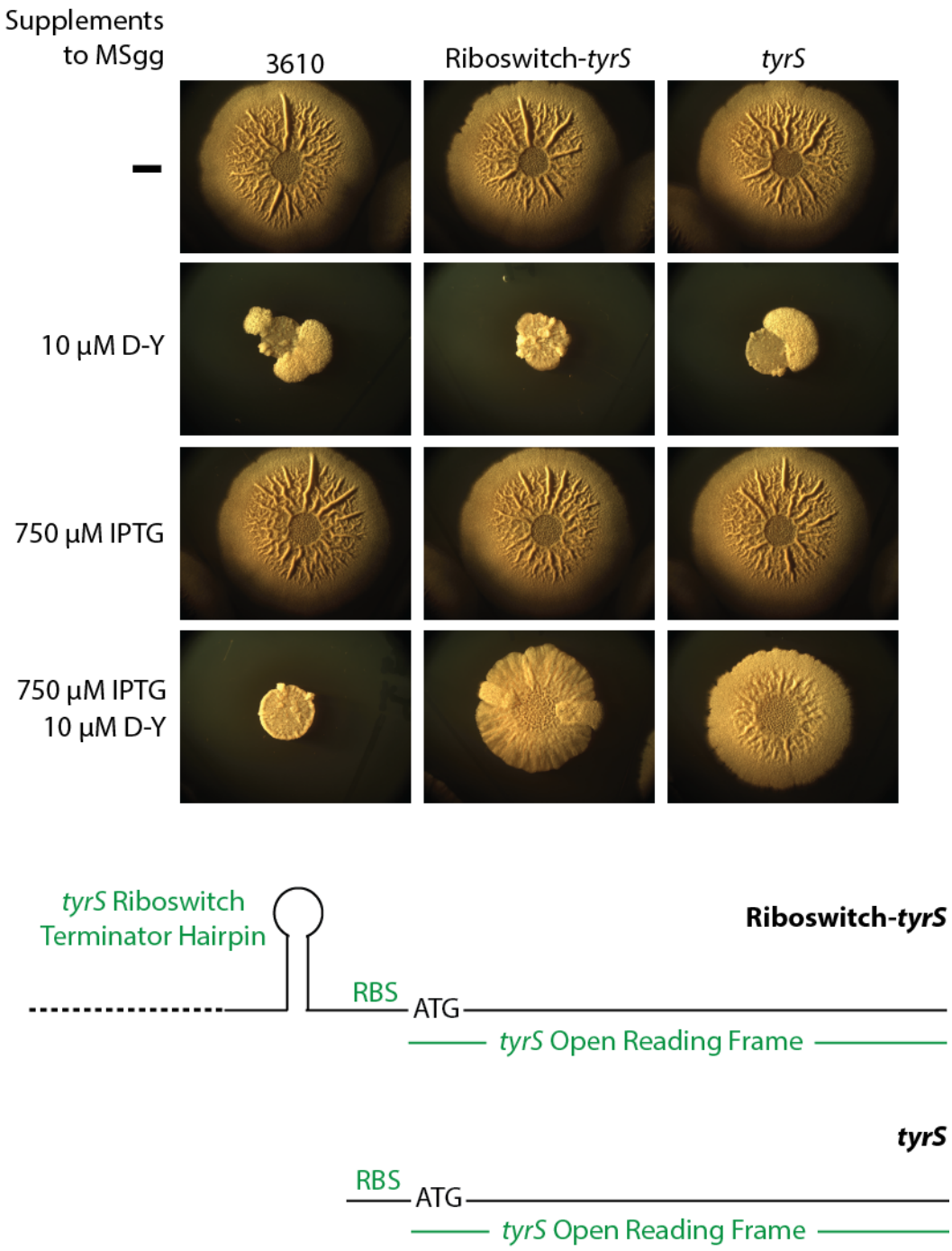

Figure 25. Overexpression of *tyrS* is sufficient to induce D-Tyr resistance. *B. subtilis* 3610, SLH69, and SLH70 were spotted on solid MSgg containing supplements as indicated. Plates were incubated at 30˚C and imaged after three days. Schematics illustrate the constructs used to overexpress the *tyrS* riboswitch, RBS, and open reading frame (in SLH69) or to overexpress the *tyrS* RBS and open reading frame (in SLH70).

Mutations in *ppaC* may disadvantage mischarging of $tRNA^{Tyr}$ with D-Tyr

It is interesting that mutations in the inorganic pyrophosphatase gene *ppaC* impart resistance to NCDAAs (Fig. 20 and 21; Table 1). I speculate that these mutations do so by slowing the rate of NTP-driven reactions, including the charging (or mischarging) of tRNAs (Halonen et al., 2005). By fortunate coincidence, Halonen et al. previously constructed a *B. subtilis* $ppaC^{E78D}$ mutant, which I independently recovered in my selection for NCDAA resistance. The authors found that the E78D substitution enhanced the affinity of inorganic pyrophosphatase for its metal ion cofactor, Mn^{2+}, but simultaneously changed the metal ion specificity of the enzyme from Mn^{2+} to Mg^{2+} (Halonen et al., 2005). I posit that these changes hamper the enzyme's efficiency, and suggest that $ppaC^{A145V}$ and $ppaC^{\Delta A166}$ also confer resistance to NCDAAs by impairing NTP-driven reactions.

PpaC is essential to drive biological reactions to completion in *B. subtilis*, implying that any reduction in enzyme efficiency caused by $ppaC^{E78D}$, $ppaC^{A145V}$, and $ppaC^{\Delta A166}$ must be minor enough to sustain continued cell growth and proliferation. How could a small global impairment in inorganic pyrophosphatase activity lead to protection from D-Tyr toxicity? Kinetic analyses of a *B. subtilis* TyrRS homolog may provide an answer. Using *G. stearothermophilus* TyrRS, the First laboratory showed that pyrophosphate (PP_i) binds to the TyrRS•D-Tyr-AMP complex with 14-fold higher affinity than it binds to the TyrRS•L-Tyr-AMP complex (Sheoran et al., 2008). This difference contributes to the lower relative turnover rate for TyrRS bound to D-Tyr. The *B. subtilis* TyrRS, which is 69% identical (and 89% similar) in protein sequence to *G. stearothermophilus* TyrRS, also exhibits a lower turnover rate for D-Tyr than for L-Tyr (Fig. 22, Table 2). Likely, the PP_i binding affinities of the *B. subtilis* TyrRS and the *G. stearothermophilus* TyrRS are similar. This is crucial, because by accounting for the higher

binding affinity of the TyrRS•D-Tyr-AMP complex to PP_i, it becomes plausible that mildly reduced pyrophosphatase activity could preferentially disadvantage activation of D-Tyr by TyrRS.

Mechanisms to avoid $tRNA^{Tyr}$ mischarging: A review

D-Tyr-$tRNA^{Tyr}$ misacylation may be avoided in several ways. One way is to bias reactions in favor of proper $tRNA^{Tyr}$ charging events. This bias could be introduced by, for example, altering the TyrRS binding site to disfavor D-Tyr binding (e.g., $TyrRS^{A202V}$), expressing the alternative, more stereoselective tyrosyl-$tRNA^{Tyr}$ synthetase TyrRZ, or disfavoring ATP hydrolysis when D-Tyr is bound to TyrRS. I propose that this last mechanism is, at least in part, how mutations in *ppaC* confer resistance to D-Tyr in *B. subtilis*.

Possibly another way to bias proper $tRNA^{Tyr}$ charging events is to overproduce TyrRS. While an excess of TyrRS would not change the ratio of proper charging-to-mischarging events, excess TyrRS would increase the absolute number of properly charged species. As such, excess TyrRS could help compensate for TyrRS sequestration by D-Tyr and thus increase the protein translation rate of D-Tyr-treated cells. A related hypothesis, based on our kinetic analyses of *B. subtilis* $TyrRS^{WT}$ and $TyrRS^{A202V}$, is that excess TyrRS confers resistance to D-Tyr by acting as a D-Tyr sink. In other words, a subset of the excess TyrRS would bind D-Tyr with high affinity but then proceed to activate and transfer D-Tyr with low catalytic efficiency. Meanwhile, the remaining TyrRS would bind L-Tyr and (with greater efficiency) transfer this substrate to $tRNA^{Tyr}$. According to our calculations, the *B. subtilis* 3610 TyrRS produces about 60 molecules of L-Tyr-$tRNA^{Tyr}$ for every one D-Tyr-$tRNA^{Tyr}$ (Table 2). Therefore, when combined with downstream selection – for instance, properly charged tRNAs interact more favorably with EF-

Tu (Yamane et al., 1981) – excess TyrRS could facilitate the exclusion of D-Tyr from nascent proteins[4]. One lingering question, however, is why excess TyrRS may be beneficial for *B. subtilis* when it is highly toxic for other organisms. For example, in *E. coli,* excess TyrRS results in the erroneous charging of non-tyrosyl tRNAs with tyrosine (Bedouelle et al., 1990).

Another possible mechanism to avoid D-Tyr-tRNA^{Tyr} misacylation would be to maintain high levels of L-Tyr in order to augment the probability that TyrRS encounters L-Tyr before encountering D-Tyr. Having a large pool of free L-Tyr in the cytoplasm seems particularly beneficial for *B. subtilis*, given the favorable binding affinity of its wild-type TyrRS for D-Tyr versus L-Tyr. Additionally, the *tyrS* riboswitch acts as a sensor of low intracellular L-Tyr concentrations, meaning that *B. subtilis* already has a system in place that could signal for an increase in the production or import of L-Tyr (Grundy and Henkin, 1994)[5]. In other words, rather than excess TyrRS conferring D-Tyr resistance directly, either *tyrS* overexpression or the signals for *tyrS* overexpression (low L-Tyr, or an accumulation of uncharged tRNA^{Tyr}) might result in the biosynthesis or import of L-Tyr. While such a feedback system exists for other amino acids, including L-Leu and L-Trp[6] (Grundy and Henkin, 1994, Shimotsu and Henner, 1984), it has not been established whether L-Tyr levels can be similarly regulated. That said, changes in amino acid import and production have been previously associated with D-Tyr resistance in *B. subtilis*. In one instance, a mutation that prevented noncompetitive inhibition of prephenate dehydrogenase by D-Tyr resulted in L-Tyr overproduction and resistance to D-Tyr

[4] That said, I would be surprised for TyrRS to so heavily bias proper charging/protein incorporation events as to elicit the strong D-Tyr resistance we observed experimentally.

[5] Arguably it is more beneficial to the cell to increase L-Tyr uptake rather than increase L-Tyr biosynthesis, as some L-Tyr biosynthetic enzymes (e.g., prephenate dehydrogenase) are product-inhibited.

[6] Most of the L-Trp and L-Tyr biosynthetic genes are clustered in an operon. A riboswitch preceding the gene *trpE* is responsive to limiting L-Trp and is thought to control the expression of both L-Trp and L-Tyr biosynthesis genes.

toxicity (Champney and Jenson, 1969). In another case, D-Tyr resistance was linked to a defect in D-Tyr uptake (Jenson et al., 1972)[7]. For my part, I attempted to measure intracellular L-Tyr levels in various *B. subtilis* strains by an established LC-MS protocol but was unable to obtain reproducible or conclusive results. My data on the transcription levels of two L-Tyr biosynthesis genes (*tyrA*, which encodes prephenate dehydrogenase, and *aroH,* which encodes chorismate mutase) were also inconclusive. I am currently trying to address whether *tyrS* overexpression influences L-Tyr uptake. These studies involve taking a candidate gene approach, as amino acid transporters – particularly aromatic amino acid transporters – are poorly characterized for Gram-positive organisms.

In summary, I have found that *B. subtilis* acquires resistance to D-Tyr through single mutations that influence the fidelity of translation. I found that *tyrS* overexpression can be driven by destabilizing mutations in the *tyrS* riboswitch terminator hairpin or by a mutant $tRNA^{Phe}$, and that *tyrS* overexpression leads to D-Tyr resistance. My collaboration with Charles Richardson at LSUHSC revealed that *B. subtilis* TyrRS does not strongly select against D-Tyr and that a mutation of A202 to a valine enhances the enzyme's stereoselectivity. Together, these results offer new insights into how *B. subtilis* strains lacking D-aminoacyl tRNA deacylase activity can overcome exposure to D-amino acids and prevent proteotoxicity.

[7] The decrease in uptake was shown experimentally; however, the mutation(s) responsible were not identified.

Chapter 5

Biofilm formation and cyclic di-GMP in *Pseudomonas aeruginosa*

Pseudomonas aeruginosa infections are the leading cause of mortality for cystic fibrosis patients (Kirov et al., 2007). Work over the past ten years has demonstrated that the danger of *P. aeruginosa* infections rests not only in the bacteria's genetic resistance to many antibiotics, but also in their propensity to live in a biofilm (Foweraker, 2009). *P. aeruginosa* biofilms comprise a mixture of metabolically active and dormant cells encased by a self-produced exopolymer matrix (Kirov et al., 2007). The biofilm matrix has a drastic therapeutic consequence, magnifying the minimum inhibitory concentrations of antibiotics as much as 1000-fold when compared to planktonic *P. aeruginosa* (Hill et al., 2005). Improved strategies to treat and clear chronic *P. aeruginosa* infections must overcome the biofilm matrix, and it is therefore imperative to learn how *P. aeruginosa* builds, maintains, and breaks down its biofilms.

Decades of research into *P. aeruginosa* biofilms have revealed many of the key biofilm genes and matrix components. Much of the work in this field is performed using the lab strains PAO1 or PA14. While many factors are conserved between lab strains and clinical isolates, including quorum sensing molecules, the secondary messenger cyclic di-GMP, and a subset of genes responsible for making matrix, some aspects of biofilm regulation are strain-specific. For the most part, this introduction will focus on PA14, the strain in which I have conducted my experiments.

Pel is the main component of the PA14 biofilm matrix

The *P. aeruginosa* biofilm matrix has many constituents and varies between strain types. Generally, the *P. aeruginosa* biofilm matrix comprises some combination of exopolysaccharide, protein, and extracellular DNA (eDNA). Of the biofilm matrix components, the exopolysaccharides alginate, Psl, and Pel are particularly well studied. Though not significant for biofilm matrix in the lab strains PA14 or PAO1, alginate is the major biofilm exopolysaccharide for clinical *P. aeruginosa* isolates, and acts as a source of structural stability, protection, and nutrient retention (Wei and Ma, 2013, Wozniak et al., 2003). Psl, which is not produced by PA14, is the primary matrix exopolysaccharide for PAO1. Psl builds and maintains the PAO1 biofilm structure by facilitating cell-cell and cell-surface interactions (Ma et al., 2006, Ma et al., 2009). In contrast, PA14 biofilm matrices are constructed primarily from Pel, which is required for both pellicles and surface-attached biofilms (Friedman and Kolter, 2004). Pel is also associated with resistance to aminoglycoside antibiotics (Colvin et al., 2011).

While proteins (particularly attachment factors such as fimbriae, type IV pili, and flagella) and eDNA are also established *P. aeruginosa* biofilm matrix components, their importance to biofilm structure is highly strain-specific. For example, while DNaseI treatment of PAO1 is sufficient to inhibit biofilm formation (Whitchurch et al., 2002), the same treatment has no affect on the development of PA14 biofilms (Fig. 26). Similarly, I found that PA14 produces robust biofilms in the presence of Proteinase K at 500 μg/ml, suggesting that the protein components of the PA14 biofilm matrix are not necessary (Fig. 26). This result is not entirely surprising, as others have demonstrated that Pel can compensate for the loss of protein attachment factors (Vasseur et al., 2005).

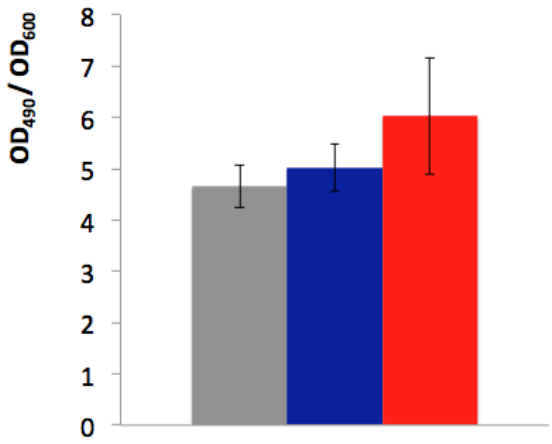

Figure 26. PA14 biofilms are neither eDNA- nor protein-dependent. PA14 day cultures were diluted 1:1000 in M6301R and treated with a water control (grey), 90 U/mL DNaseI (blue), or 500 µg/mL Proteinase K (red). The cultures were incubated at 25˚C for 24 hours, after which time the culture density was measured at 600 nm and a crystal violet assay was performed. Crystal violet absorbance, indicative of biofilm biomass, was measured at 490 nm and was normalized to culture density. The results shown represent the average of five technical replicates and error bars represent the standard deviation. Results are representative of duplicate experiments.

The role and regulation of cyclic di-GMP in *P. aeruginosa* biofilm formation

Bis-(3'-5')-cyclic dimeric guanosine monophosphate (cyclic di-GMP) is a common bacterial secondary messenger often associated with enhanced biosynthesis of adhesins and exopolyssaccharide, as well as with inhibition of motility (Ha et al., 2014, Hengge, 2009, Wei and Ma, 2013). In many organisms, including *P. aeruginosa*, high cyclic di-GMP levels facilitate a shift from a motile, planktonic state to a sessile, biofilm state. Cyclic di-GMP is produced from two molecules of GTP by diguanylate cyclases (DGCs), which canonically have a GG(D/E)EF motif. Cyclic di-GMP is then degraded to 5'-phosphoguanylyl-(3'-5')-guanosine (pGpG) by phosphodiesterases (PDEs), which typically have an E(A/E/V)L motif[1] (Hengge, 2009). *P. aeruginosa* is known to encode 17 DGCs, 5 PDEs, and 16 proteins with both DGC and PDE functional domains, adding complexity to the regulation of intracellular cyclic di-GMP levels (Ha et al., 2014, Merritt et al., 2010). In addition, the importance of each of these proteins for biofilm formation can vary between the strains PAO1 and PA14, likely indicating that certain DGCs or PDEs are dedicated to strain-specific aspects of biofilm formation, such as the biosynthesis of biofilm matrix components (Ha et al., 2014).

[1] In rare cases, cyclic di-GMP PDEs have an HD-GYP motif.

Cyclic di-GMP signaling in *P. aeruginosa* is mediated by binding to cyclic di-GMP receptors (known as effectors)[2]. Generally, cyclic di-GMP effectors have a degenerate GG(D/E)EF or E(A/E/V)L domain and/or RxxD motifs (Romling et al., 2013). There are four established cyclic di-GMP effectors involved in *P. aeruginosa* biofilm formation: PilZ, a type IV fimbrial biogenesis protein involved in twitching motility; Alg44, a protein involved in the biosynthesis of alginate; PelD, a product of the *pel* operon necessary for Pel biosynthesis; and the transcription factor FleQ (Romling et al., 2013). FleQ is an interesting case because when cyclic di-GMP is not bound to FleQ, this protein acts as a positive regulator of flagella biosynthesis and a negative regulator of the *pel* operon; however, upon binding cyclic di-GMP, FleQ activates transcription of *pel*, thus contributing to exopolysaccharide biosynthesis and biofilm formation.

An ongoing question in the *P. aeruginosa* biofilm field is whether the dozens of cyclic di-GMP regulators (DGCs, PDEs, and DGC/PDEs) simply contribute to the cell's net intracellular cyclic di-GMP concentration, or whether these proteins have more nuanced roles. On one hand, some mutational analyses demonstrate a clear correlation between biofilm wrinkling (indicative of Pel production in PA14) and cyclic di-GMP levels. For example, the DGC AdcA is repressed by the biofilm state regulator AmrZ, and a Δ*amrZ* strain has both a robustly rugose biofilm colony morphology and elevated cyclic di-GMP levels (Jones et al., 2014). Similarly, deleting the gene that encodes the DGC RoeA results in lower global cyclic-di-GMP levels as well as a flat colony morphology comparable to that of a mutant unable to synthesize Pel (Δ*pelA*) (Merritt et al., 2010). On the other hand, while deleting the DGC gene *sadC* yields similarly low global cyclic di-GMP levels when compared with a *roeA* deletion mutant, SadC has minimal effect on Pel biosynthesis (Merritt et al., 2010). Hence, it is possible to uncouple the global cyclic di-GMP concentration from biofilm matrix production. Furthermore, the O'Toole laboratory

[2] Cyclic di-GMP-binding riboswitches have also been found, but so far none have been identified in *P. aeruginosa.*

reported that RoeA and SadC are differentially localized in the cell, adding credence to the hypothesis that local pools of cyclic di-GMP – regulated by specific DGCs or PDEs – might be responsible for biofilm regulation (Merritt et al., 2010).

Identification of Novel Biofilm Genes

Genes relevant for biofilm formation, maintenance, and/or disassembly have traditionally been identified through transposon mutagenesis followed by measurement of biofilm biomass by crystal violet staining (O'Toole, 2011). While this method has proven effective, many gaps in the genetic pathways governing biofilm remain. This may be, in part, because crystal violet assays are not reliable for detecting subtle changes in biofilm formation. Moreover, these assays are destructive, creating the risk that a mutant's measured biofilm integrity reflects artifacts of the assay's staining or washing steps. In the next chapter, I describe a non-destructive, high-throughput, and successful transposon mutagenesis screen that takes advantage of the distinctive biofilm colony morphologies of wild-type and mutant *P. aeruginosa* strains. All of the work described in the next chapter was done in collaboration with Matt Cabeen, a postdoctoral fellow in the Losick laboratory.

Chapter 6

Identification and preliminary characterization of *P. aeruginosa* biofilm genes

To achieve a more thorough understanding of *P. aeruginosa* biofilms, Matt Cabeen and I performed a genetic screen in which wrinkled colony morphology was used as an indicator of Pel production and thus biofilm formation. Our selection approach, developed by Matt, entailed mutagenizing *P. aeruginosa* using a *Mariner*-based transposon (Kulasekara et al., 2005), arraying mutants on the biofilm-promoting medium M6301, and picking those mutants that exhibited non-parental colony morphology. Here, we selected the mutant PA14 Δ*amrZ* as our parental strain. An *amrZ*-null background provided three advantages. First, the transcriptional regulator AmrZ controls the switch between the mucoid state (via alginate production) and the wrinkled biofilm state (via Pel and/or Psl production)[1]. The PA14 Δ*amrZ* strain overproduces Pel and leads to hyper-wrinkled biofilms (Jones et al., 2014). By using an *amrZ*-null strain to lock *P. aeruginosa* in the wrinkled, non-mucoid biofilm state, we became better positioned to probe the regulation of *P. aeruginosa* biofilm formation. The second advantage of the Δ*amrZ* background is that the Δ*amrZ* biofilm colony morphology is reproducible and robust, allowing us to easily and confidently identify enhanced or diminished biofilm production by eye. Third, the PA14 Δ*amrZ* mutant has approximately two-fold greater intracellular cyclic di-GMP when compared to wild-type PA14 (Jones et al., 2014). Mutagenesis of the Δ*amrZ* strain background may therefore help tackle the question of how and under what conditions cyclic di-GMP levels correlate with biofilm formation.

[1] This switch is physiologically relevant and occurs in the lungs of cystic fibrosis patients (Romling et al., 2013).

A colony morphology-based screen yields both established and novel biofilm genes

We were pleased to learn that our screen yielded mutations in genes with known effects on biofilm. For example, we were able to identify genes involved in cyclic di-GMP degradation (*bifA*) (Kuchma et al., 2007); surface attachment (*pilR*, *cupA5*) (Kulasekara et al., 2005, Klausen et al., 2003, Hobbs et al., 1993); quorum sensing and virulence (*hpd*, *phzA*, *pqsL*) (Legendre et al., 2012, Mavrodi et al., 2001, Sall et al., 2014); arginine metabolism (*argG*) (Bernier et al., 2011); and exopolysaccharide production (*pelA*, *lemA*) (Wei and Ma, 2013), though notably these pathways are interconnected (Wei and Ma, 2013, Bernier et al., 2011, Ueda and Wood, 2009) (Fig. 27). Our ability to identify genes spanning many different biofilm-related pathways indicates that our non-destructive, colony morphology-based screen reveals biofilm genes in an accurate, efficient, and unbiased manner.

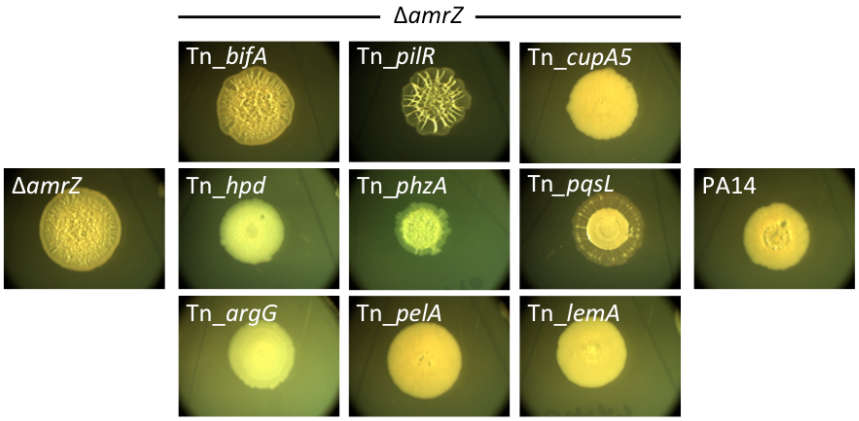

Figure 27. Screening by colony morphology yields expected mutations. Mutagenesis of a biofilm-forming mutant of PA14 (Δ*amrZ*) using a *Mariner*-based transposon yielded both diminished and enhanced wrinkled colony morphology, indicative of hypo- or hyper-biofilm formation, respectively. The mutant genes shown here all have known roles in biofilm formation. For comparison, the biofilm phenotype of PA14 is shown on the right.

In addition to genes with previously established roles in *P. aeruginosa* biofilm formation, our screen also revealed numerous new avenues for exploration. We decided to focus on three genes of unknown or unclear relevance to *P. aeruginosa* biofilm: two uncharacterized genes, *PA14_16550* and *PA14_69700* (hereafter *16550* and *69700*, respectively), and the phosphoenolpyruvate-protein phosphotransferase gene *ptsP*.

What is known about these genes? Based on structural homology, the protein product of *16550* belongs to the class of TetR-family transcriptional repressors. Very little knowledge exists on the 16550 regulon, and while excess 16550 has been shown to reduce the expression of the quorum sensing gene *lasR*, the opposite was not found to be true for a *16550* deletion (Longo et al., 2013). The protein product of *ptsP* is also thought to negatively regulate quorum sensing (Xu et al., 2005). Quorum sensing is required for *P. aeruginosa* biofilm formation, and so it is curious that a deletion of *ptsP*, which leads to an increase in the expression of quorum sensing genes, would manifest as biofilm deficiency. Intriguingly, both 69700 and PtsP have a GAF domain and multiple RxxD motifs, the latter of which are commonly found in proteins that bind cyclic di-GMP. Furthermore, the crystal structure of 69700 (PDB ID: 3E98) is similar to that of *Acinetobacter* PtsP (PDB ID: 3C16) (Bernstein et al., 1977) and shows homology to the known cyclic di-GMP effector PelD (Whitney et al., 2012). No studies to date have implicated 69700 or PtsP as cyclic di-GMP effectors, DGCs, or PDEs.

Evaluation of putative PA14 biofilm genes

We confirmed the biofilm phenotypes of the *ptsP*, *16550*, and *69700* transposon mutants using clean gene deletions and complementations (Fig. 28). Using the clean deletion mutants, we quantified biofilm formation with a standard Congo Red binding assay, wherein the amount of bound Congo Red is proportional to Pel production in PA14 and its derivatives (Ueda and Wood, 2009). We determined that Congo Red binding agreed with the degree of wrinkling observed by eye using colony morphology assays, further verifying the applicability of our screen (Fig. 29A). Intracellular cyclic di-GMP levels also tracked fairly well with colony morphology (Fig. 29B).

We did, however, note subtle but interesting discrepancies between Congo Red binding and cyclic di-GMP concentration. Although the Δ*69700* and Δ*amrZ* Δ*69700* strains exhibited a significant rise in biofilm wrinkling and Congo Red binding, they did not exhibit a significant increase in cyclic di-GMP ($p > 0.5$ and $p > 0.2$, respectively). Compared to PA14, Δ*16550* demonstrated comparable (if not slightly flatter) colony morphology, and this was reflected by the Congo Red assay results; however, Δ*16550* exhibited slightly *elevated* cyclic di-GMP levels when compared to PA14. While Congo Red binding and cyclic di-GMP levels were well correlated for Δ*ptsP* in an *amrZ*-null background (both decreased when compared to Δ*amrZ*), this was not the case for Δ*ptsP* in an $amrZ^+$ background (only cyclic di-GMP concentration decreased when compared to PA14).

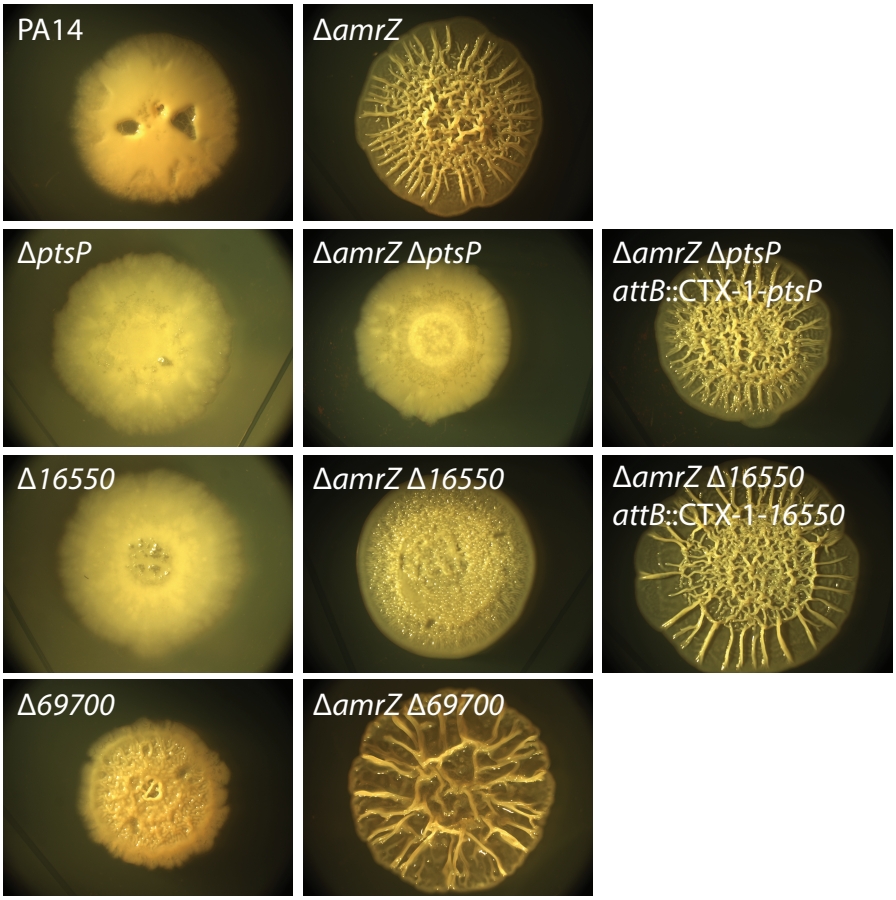

Figure 28. Screening by colony morphology yields mutations at loci with unknown roles in biofilm formation. Transposon mutagenesis of a biofilm-forming mutant of PA14 (Δ*amrZ*) yielded both under-producers and over-producers of biofilm matrix. The mutant genes featured here (*ptsP*, *16550*, and *69700*) do not have known roles in biofilm formation. Clean deletions and complementations of these genes confirm their respective biofilm phenotypes. The leftmost column shows the colony morphologies of clean gene deletions in a wild-type PA14 background. The center column shows the colony morphologies of clean gene deletions in a PA14 Δ*amrZ* background. The rightmost column shows the colony morphologies of double mutants in which the gene of interest is complemented at an ectopic locus to restore the Δ*amrZ* biofilm phenotype. The complementation strain for *69700* has not yet been made successfully.

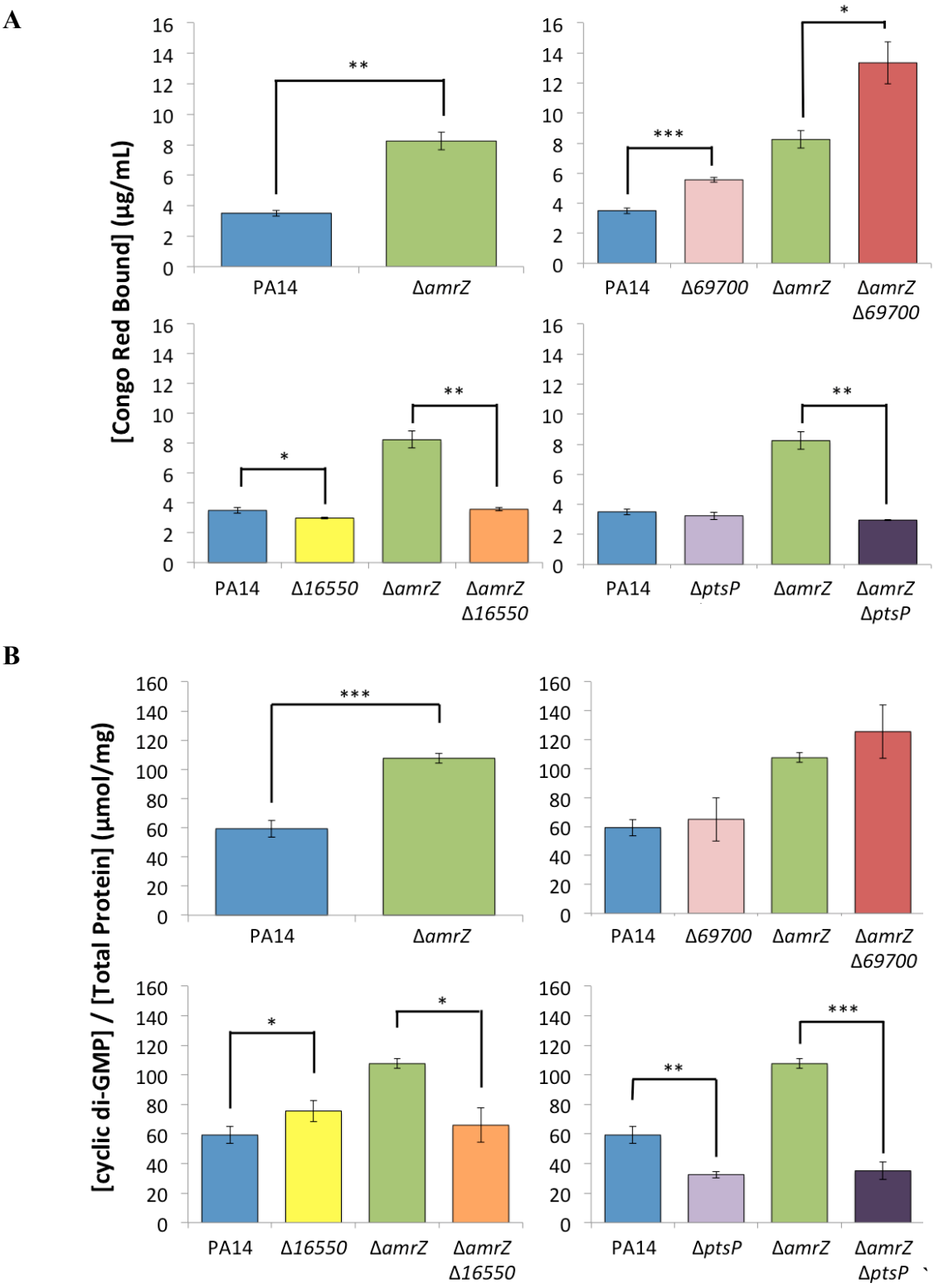

Figure 29. Quantification of rugosity and intracellular cyclic di-GMP concentration of *P. aeruginosa* biofilm mutants. Results represent the average of triplicate experiments using six-day-old (A) or four-day-old (B) biofilms. Error bars show the standard deviation, and statistical significance was determined by an unpaired T-test (* $p < 0.05$; ** $p < 0.01$; *** $p < 0.001$).

Interpretations and implications of mutant cyclic di-GMP levels

We believe that the cyclic di-GMP concentrations of the single and double mutants may provide clues as to how *ptsP*, *16550*, and *69700* contribute to the regulation of *P. aeruginosa* biofilm. In the case of *ptsP*, we observed low cyclic di-GMP levels independent of *amrZ*, and these levels were always below those of wild-type PA14. Such data suggest that *ptsP* operates upstream of cyclic di-GMP production, or that its protein product interacts with DGCs and/or PDEs. In contrast, *69700* does not appear to influence cyclic di-GMP levels significantly. Thus the protein 69700 may act downstream of cyclic di-GMP regulation, possibly as a stimulator of Pel production. We determined that the cyclic di-GMP levels of Δ*16550* and Δ*amrZ* Δ*16550* are comparable and slightly higher than those of wild-type PA14. Deleting *16550* had a minimal effect on cyclic di-GMP in the wild-type background but led to a 1.6-fold drop in cyclic di-GMP in the absence of *amrZ*. It is possible that the protein 16550 interacts with or regulates the transcription of a DGC or PDE under the control of AmrZ, such as the DGC AdcA, which is responsible for the hyper-wrinkled phenotype of an *amrZ*-null mutant (Jones et al., 2014).

ptsP* and *69700*, but not *16550*, regulate the expression of *adcA

To test whether 16550 regulates expression of the gene encoding AdcA, we constructed a transcriptional fusion of the *adcA* promoter to luciferase. By comparing the luciferase activities of the Δ*amrZ* and Δ*amrZ* Δ*16550* strains, we determined that 16550 does not affect *adcA* transcription (Fig. 30). Surprisingly, we instead found striking increases in luciferase activity in the Δ*amrZ* Δ*ptsP* and Δ*amrZ* Δ*69700* mutants (Fig. 30). Further study is required to explain the effects of PtsP and 69700 on AdcA production and to reconcile the increase in *adcA* expression with decreased (for Δ*ptsP*) or unchanged (for Δ*69700*) intracellular cyclic di-GMP concentration.

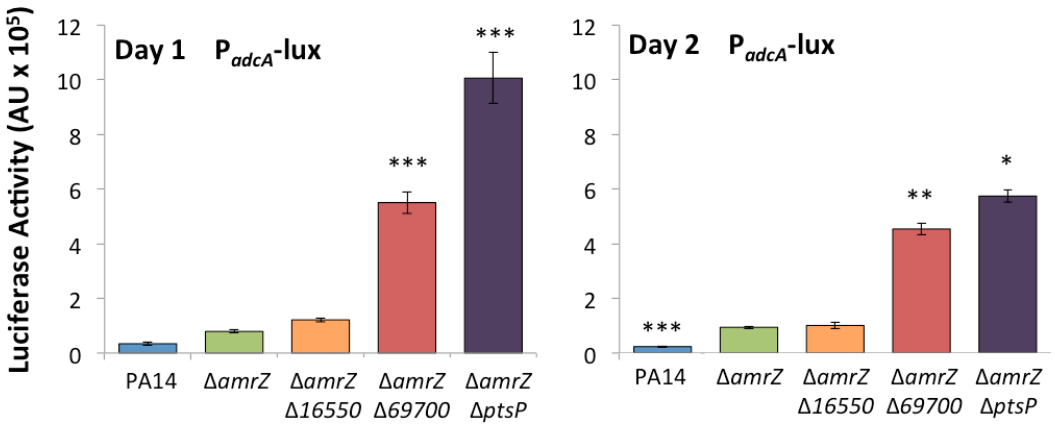

Figure 30. Expression of *adcA* is regulated by *amrZ*, *69700*, and *ptsP*. Luciferase activity was calculated by normalizing luminescence to culture optical density. Results represent the average of three biological replicates (each having four technical replicates) using cultures grown on M6301 agar for 24 or 48 hours. Error bars show the standard deviation. Statistical significance was determined by an unpaired T-test (* $p < 0.05$; ** $p < 0.005$; *** $p < 0.0005$) by comparing all strains to Δ*amrZ*. Luciferase activity was also assessed at days 3 and 4, and was comparable to the results shown for day 2.

While research into the roles that *ptsP*, *16550*, and *69700* play in *P. aeruginosa* biofilm formation is ongoing, we can draw conclusions about the colony morphology-based screen used to identify these genes. Overall, we found that the colony morphology-based screen had the same functionality as traditional (i.e., crystal violet-based) screens; both types of screens may be implemented in a high-throughput manner, both accurately identify biofilm mutants, and both are unbiased. However, screening by colony morphology also offers an improvement over crystal violet assays, because this new approach does not require destructive processing steps.

It is also worth noting that the colony morphology-based screen is simple to implement and modify, and is therefore applicable for various laboratory or clinical strains, genetic mutants, mixtures of strains, or treatment conditions, and may be performed iteratively.

Moving forward, we have several avenues of investigation to pursue. Pull-downs of 69700 or PtsP may be useful to reveal their respective interaction partners. As 16550 is a putative TetR-family transcriptional repression, we may take an RNA-seq approach to uncover

its regulon. We can test for epistasis by comparing the biofilm phenotypes and cyclic di-GMP levels in strains harboring additional mutations, particularly deletions of known or predicted DGCs or PDEs. For example, we are currently testing the effects of combining a deletion of the PDE gene *bifA* with Δ*16550*, Δ*69700*, or Δ*ptsP*. A Δ*bifA* background has high levels of intracellular cyclic di-GMP independent of AmrZ, and thus will help reveal whether our gene candidates have a general effect on cyclic di-GMP concentration or if they act in more specific signaling cascades. Finally, *ptsP*, *16550*, and *69700* are only three of many genes that we identified in our screen with no ascribed function in biofilm regulation. Therefore, we may also learn more about *P. aeruginosa* biofilm formation by analyzing other candidate biofilm genes either individually or in combination with the mutations discussed here.

Conclusions

Applications of biofilm research extend from industry (e.g., eliminating biofouling), to agriculture (e.g., promoting plant growth), to medicine (e.g., treating chronic infection), and rely on an understanding of the genetic underpinnings and environmental cues that control biofilms in nature. My research has been motivated by the possibility that small molecule natural products trigger biofilm disassembly (Chapters 1-4, Appendices A-C) as well as by the opportunity to identify novel biofilm genes in a pathogenic microbe (Chapters 5-6).

My thesis work began under the assumption that cell wall incorporation of non-canonical D-amino acids (NCDAAs) regulates biofilm formation in *Bacillus subtilis* (Kolodkin-Gal et al., 2010). I collaborated with Janine May and Matt Lebar in the Kahne laboratory to analyze the role of penicillin binding protein 1 (PBP1) in *B. subtilis* NCDAA incorporation. We determined that PBP1 incorporates NCDAAs *in vitro* (Lebar et al., 2014) but is not required for NCDAA incorporation *in vivo.* While I noted that biofilm-producing strains of *B. subtilis* (e.g., the wild strain 3610) are more dependent on PBP1 for cell growth than are biofilm-attenuated strains (e.g., the domesticated strain 168), I did not find evidence that PBP1 directly influences biofilm formation or disassembly.

Much of my thesis work was driven by discrepancies between Kolodkin-Gal et al., 2010 and my own research on NCDAAs and biofilm formation. I summarize a few key points here, though a more comprehensive comparison of my results and those reported by Kolodkin-Gal et al. appears in Table 3. Briefly, Kolodkin-Gal et al. showed that four NCDAAs, D-LMWY, work synergistically to inhibit biofilm formation and disassemble established biofilms. The authors attributed this behavior to the incorporation of NCDAAs into peptidoglycan and the subsequent

release of cell wall-anchored biofilm matrix proteins. In contrast, my research demonstrates that D-LMWY does not inhibit biofilm formation directly or specifically, nor does it trigger biofilm disassembly at all. Instead, D-LMWY inhibits growth. I found D-Tyr to be the most potent growth inhibitor of the D-LMWY mixture due to the inherent inaccuracies of the tyrosyl-$tRNA^{Tyr}$ synthetase TyrRS and the absence of D-aminoacyl tRNA deacylase (encoded by *dtd*). I also found that repairing the *dtd* gene in *B. subtilis* confers resistance to NCDAA-induced toxicity. As for incorporation of NCDAAs into peptidoglycan, I confirmed that this occurs but determined it to have no bearing on biofilm formation or stability (Leiman et al., 2013). Overall, I believe that my thorough analysis of *B. subtilis* biofilms (Chapter 3, Appendices A and B) and my brief studies on *Staphylococcus aureus* and *Pseudomonas aeruginosa* biofilms (Appendix C), present a strong case against the paradigm set by Kolodkin-Gal et al. in their 2010 *Science* publication and offer a convincing explanation (the absence of D-aminoacyl tRNA deacylase) for the perceived biofilm-inhibitory activities of NCDAAs against *B. subtilis*.

Table 3. A comparison and summary of findings about D-amino acids and biofilm.

Previously Thought	Conclusions From My Thesis Work	Notes or Unresolved Points
Secretion of D-LMWY into the biofilm supernatant coincides with *B. subtilis* pellicle disassembly.	*B. subtilis* pellicles do not disassemble as depicted previously.	Supernatant levels of D-LMWY were not assessed. In my experience, the amino acid quantification method is subject to variability.
Biofilms are inhibited by 8.5 mM D-L, 2 mM D-M, 5 mM D-W, and 3 µM D-Y. Cultures do not recover pellicle formation after treatment (Cells treated with 3 µM D-Y are inhibited for biofilm formation days later).	Biofilm is not produced in the presence of 8.5 mM D-L or 5 mM D-W; however, lower concentrations of D-L or D-W merely delay biofilm formation for one day. Cells also recover from 3 µM D-Y within one day.	I was unable to find conditions in which 2 mM D-M inhibits biofilm formation.
Biofilm-inhibitory concentrations of D-LMWY, together or individually, do not inhibit growth.	All biofilm-inhibitory concentrations of D-LMWY, together or individually, delay or inhibit growth. This inhibition is largely, if not entirely, eliminated in a *dtd*$^+$ strain.	The growth defect caused by D-L is delayed, likely due to a high abundance of L-L in exponentially-growing cells (Hsiao et al., 2010).
Biofilm-inhibitory concentrations of D-LMWY, together or individually, do not change transcription levels of *epsA-O* or *tapA-sipW-tasA.*	Biofilm-inhibitory concentrations of D-LMWY, together or individually, significantly reduce transcription of *epsA-O* and *tapA-sipW-tasA.*	
D-LMWY act synergistically to inhibit or disassemble biofilms.	The potency of the D-LMWY mixture may be attributed to D-Y alone.	At non-physiologic concentrations, other NCDAAs also inhibit growth.
Deleting *racX* and *ylmE* delays biofilm disassembly and prevents accumulation of D-Y.	D-Y is a known byproduct of L-Y biosynthesis, and ought to accumulate regardless of racemace activity. Pellicle disassembly, *per se*, does not occur, and therefore cannot be delayed.	YlmE is not a racemace (Ito et al., 2013). There is no evidence that RacX produces D-Tyr.
Excess D-A rescues biofilm formation in NCDAA-treated cells.	Excess D-A does not rescue biofilm formation, except when it improves growth.	D-W is not removed from PG in the presence of excess D-A, invalidating the old model.
NCDAA incorporation into PG is associated with biofilm inhibition or disassembly.	D-W incorporation into PG is inconsequential to biofilm formation or stability.	
Frameshift mutations in TapA overcome biofilm inhibition by one or more NCDAAs. These mutations prevent release of TapA and TasA.	The C-terminus of TapA is dispensable. Mutations in this region do not influence biofilm formation in the presence or absence of NCDAAs.	I did not study the localization of TapA and TasA in the presence of NCDAAs. That said, transcriptional reporter assays suggest the proteins are not efficiently produced due to growth inhibition.
D-Y or D-LMWY can disassemble *B. subtilis* pellicles.	Neither D-Y nor D-LMWY can disassemble *B. subtilis* pellicles.	
NCDAAs inhibit biofilms in other species, specifically *P. aeruginosa* and *S. aureus*.	NCDAAs do not inhibit biofilm in *P. aeruginosa* or *S. aureus.*	NCDAAs are similarly ineffective against other organisms that produce a D-aminoacyl tRNA deacylase.

Having reaffirmed that NCDAAs, particularly D-Tyr, inhibit cell growth (Champney and Jensen, 1969, Champney and Jensen, 1970, Grula, 1960, Jensen et al., 1972, Soutourina et al., 2000, Soutourina et al., 2004), I sought to advance the current understanding of D-Tyr-induced stress. I identified and analyzed mutations in or upstream of *tyrS*, *trnD-Phe*, and *ppaC* that overcome D-Tyr toxicity. In doing so, I uncovered mechanisms that reduce the incidence of D-Tyr-tRNA^{Tyr} misacylation events in the absence of D-aminoacyl tRNA deacylase. I found that mutations that destabilize the *tyrS* riboswitch terminator hairpin lead to *tyrS* overexpression, and verified a causal relationship between *tyrS* overexpression and resistance to D-Tyr. I determined that mutating the tRNA^{Phe} anticodon to AUG transforms tRNA^{Phe} into a *tyrS* riboswitch ligand, again resulting in *tyrS* overexpression and D-Tyr resistance. My collaboration with Charles Richardson in the First laboratory revealed that an A202V variant of *B. subtilis* TyrRS improves the enzyme's stereoselectivity. Finally, I presented an argument for how a less efficient inorganic pyrophosphatase (PpaC) could preferentially disadvantage the formation of D-Tyr-tRNA^{Tyr}.

There are, of course, remaining questions about these D-Tyr resistance mechanisms. We do not yet know why *tyrS* overexpression confers such strong resistance to D-Tyr. It would be interesting to learn whether *tyrS* overexpression signals for, or is perhaps concurrent with, the increased production or import of L-Tyr. The identification of the A202V variant of *B. subtilis* TyrRS also raises new opportunities for exploration. Obtaining a crystal structure of TyrRS^{A202V} would help settle the mechanism by which this mutant discriminates against D-Tyr, and may serve as a useful comparison to TyrRZ structures. The TyrRS^{A202V} structure could also provide insight into new ways to strengthen or, in contrast, broaden the substrate specificity of aminoacyl-tRNA synthetases.

In addition to my work on NCDAAs and bacterial biofilms, I embarked on a new project with a postdoctoral fellow in the Losick laboratory, Matt Cabeen, to probe for unidentified *P. aeruginosa* biofilm genes. Our research, though preliminary, demonstrates that a colony morphology-based transposon mutagenesis screen successfully uncovers genes involved in *P. aeruginosa* biofilm formation. The screen, using a hyper-wrinkled mutant (PA14 Δ*amrZ*) as the parental strain, yielded not only a diverse array of known biofilm genes, but also yielded new biofilm gene candidates. Through analyses of intracellular cyclic di-GMP concentrations and gene expression, we have begun to unravel how three candidate genes (*ptsP*, *PA14_16550*, and *PA14_69700*) contribute to biofilm formation in *P. aeruginosa*.

In conclusion, the experiments and analyses that I have described here offer new insights into how *B. subtilis* maintains protein quality control and advances our knowledge about bacterial biofilms. My work on NCDAAs and biofilms clears up several misconceptions about the manner in which NCDAAs interact with *B. subtilis*, and likely extends to interactions between NCDAAs and other species as well. In continuation of my NCDAA research, I demonstrated how an organism with no D-Tyr proofreading capabilities adapts to limit the formation of D-Tyr-tRNA^{Tyr} and D-Tyr-containing proteins. Finally, I showed the effectiveness of a simple, non-destructive biofilm-screening tool and presented preliminary steps in the characterization of three putative *P. aeruginosa* biofilm genes.

Materials and Methods

Strains and growth conditions

Bacillus subtilis NCIB3610, 168, or PY79; *Escherichia coli* Turbo (New England Biolabs, USA), DH5α, or SM10; *Staphylococcus aureus* HG003 or SC01; and *Pseudomonas aeruginosa* PA14 were grown in Luria-Bertani (LB) broth (10 g/L tryptone, 5 g/L yeast extract, 5 g/L NaCl) or on LB agar plates containing 1.5% Bacto agar at 37˚C. When appropriate, 1 μg/mL erythromycin and 25 μg/mL lincomycin, 5 μg/mL chloramphenicol, 100 μg/mL spectinomycin, 100 μg/mL ampicillin, 10 μg/mL kanamycin, 25 μg/mL irgasan and 75 μg/mL tetracycline, 25 μg/mL irgasan and 75 μg/mL gentamicin, 25 μg/mL tetracycline, or 20 μg/mL gentamicin was added to liquid or solid medium. Strains used in this work are listed in Table 4.

D-amino acid-resistant mutant isolation and identification

Spontaneous mutants resistant to D-amino acids were isolated by growing *B. subtilis* 3610 on solid LB supplemented with D-leucine, D-methionine, D-tryptophan, and D-tyrosine (D-LMWY), each at 500 μM. The frequency at which mutations conferring resistance arose was calculated by plating dilutions on solid LB alone or supplemented with 500 μM D-LMWY. Genomic DNA libraries for whole genome sequencing were prepared using the NEBNext kit according to the manufacturer's instructions. Individual barcodes for multiplexed sequencing were supplied by Illumina.

Strain construction

All strains were constructed using standard molecular biology techniques (Harwood and Cutting, 1990, Gibson et al., 2009). All primers and plasmids used in this study are listed in Table 4.

Marked *ponA* knockouts were built using long flanking homology (Harwood and Cutting, 1990) and primers JMM1-4. The resulting construct, a deletion of bases 343-1745 of *ponA*, was transformed into *B. subtilis* PY79 or 168 as described (Harwood and Cutting, 1990), generating SLH1 and SLH2, respectively. This mutation deleted both PBP1 catalytic sites as well as the sites of the putative D-amino acid-resistant *ponA* mutations. The *ponA* deletion was transferred by phage transduction into 3610, DS2569, and AM373 (Kearns et al., 2005) to generate SLH3, SLH4, and SLH5, respectively. Transformants and transductants were selected on LB agar plus kanamycin and were confirmed by amplifying the 4.5kb region surround *ponA* with primers JMM5 and JMM6 and sequencing the product using primers JMM7-12.

The markerless repair of *dtd* in *B. subtilis* was accomplished using the pMiniMAD protocol as described by Patrick and Kearns (Patrick and Kearns, 2008) and using primers 51-54 in Table 4. Successful double-crossover events leading to the *dtd*$^+$ strain were confirmed by re-streaking individual clones on 1% agar plates containing LB, LB plus erythromycin and lincomycin, or LB plus 400 μM D-LMWY. Isolates which grew on LB and on LB plus D-LMWY, but not on LB plus erythromycin and lincomycin, were submitted for sequencing using primers 7 and 8.

Luciferase reporters for *epsA* and *tapA* operon expression were constructed as described (Leiman et al., 2014) and transferred by phage transduction into *dtd*$^+$ cells (Kearns et al., 2005).

Mutations in *trnD-Phe*, *hrcA*, *tyrS*, and *ppaC* were markerlessly reconstructed in *B. subtilis* 3610 using the pMiniMAD protocol as described (Patrick and Kearns, 2008) and primers 39-42 and 45-50. Successful double-crossover events were indicated by the absence of growth in the presence of erythromycin and lincomycin. Mutations were subsequently verified using primers 45, 46, 49, 50, and 57-60.

Luciferase reporters for readthrough of the *tyrS* riboswitch were constructed as follows. pAH328 (Chen et al., 2012) was digested with EcoRI and BamHI and a fragment of approximately 6 kb, containing the optimized, promoterless *luxABCDE* operon, was isolated by gel extraction. The *amyE* integrating vector pDG1662 (Guerout-Fleury et al., 1996) was digested with EcoRI and BamHI and a fragment of approximately 7 kb was isolated by gel extraction. The fragments were ligated and transformed into *E. coli* DH5α, generating pLF007, and the construct was confirmed by restriction digestion using HindIII and PstI. The promoter region of *tyrS* (Henkin et al., 1992) was amplified from *B. subtilis* 3610, SLH8, and SLH9 using primers 70 and 71, or from 3610 using primers 70 and 72, and combined by isothermal assembly (Gibson et al., 2009) with pLF007 linearized with NotI and EcoRI to yield pSL001, pSL002, pSL003, and, pSL008, respectively. The plasmids were maintained in *E. coli* Turbo in the presence of ampicillin, the promoter region sequences were verified with primers LF002F and LF002R, and the plasmids were transformed into *B. subtilis* 168. The constructs were moved by phage transduction into 3610 or SLH36 to yield SLH57-59, SLH61, and SLH75. Movement of the plasmids into *B. subtilis* was confirmed by growth on LB agar containing chloramphenicol and proper insertion at *amyE* was verified by the strains' inability to metabolize starch.

To construct the wild-type *tapA* complementation strain, primers AE1 and AE2 were used to amplify a fragment containing the *tapA* operon, including 200 bp upstream of the operon

representing the promoter, from *B. subtilis* 3610 chromosomal DNA. To generate the mutated *tapA* variants we created two fragments of the *tapA* operon overlapping at the desired mutation site, including the promoter, using primers AE1-AE6. The corresponding fragments were then joined in an isothermal assembly reaction (Gibson et al., 2009) with pDG364 (Harwood and Cutting, 1990) linearized with BamHI and EcoRI to produce pAE164 (wild-type *tapA*), pAE165 ($tapA^{558\Delta}$), or pAE166 ($tapA^{724\Omega G}$). The plasmids were maintained in *E. coli* DH5α using selection with ampicillin. After verifying the *tapA* sequences with primers 55 and 56, the plasmids were transformed directly into SLH63, a derivative of *B. subtilis* 3610 lacking the *tapA* operon at the native locus. SLH63 was generated by phage transduction (Kearns et al., 2005) of *tapA-sipW-tasA*::*spec* from strain RL4602. Movement of the plasmids into *B. subtilis* was confirmed by growth on LB agar containing chloramphenicol and proper insertion at *amyE* was verified by the strains' inability to metabolize starch.

The *tyrS* overexpression strains were constructed as follows. Primers 76 and 77 were used to amplify the fragment containing the *tyrS* riboswitch, ribosome binding site (RBS), and open reading frame (ORF) from *B. subtilis* 3610 chromosomal DNA. Primers 76 and 86 were used to amplify the fragment containing the *tyrS* RBS and ORF from *B. subtilis* 3610 chromosomal DNA. The resulting fragments were then joined in an isothermal assembly reaction (Gibson et al., 2009) with pDR111 (Ben-Yehuda et al., 2003) linearized with HindIII and SphI to produce pSL004 (*tyrS* riboswitch, RBS, and ORF) or pSL005 (*tyrS* RBS and ORF). The plasmids were maintained in *E. coli* Turbo using selection with ampicillin. After verifying the plasmid inserts with primers pDR111F and pDR111R, the plasmids were transformed directly into *B. subtilis* 3610 to generate strains SLH69 and SLH70. Movement of the plasmids

into *B. subtilis* was confirmed by growth on LB agar containing spectinomycin and proper insertion at *amyE* was verified by the strains' inability to metabolize starch.

Deletions, complementations, and luciferase reporters in *P. aeruginosa* PA14 were constructed as described (Cabeen, 2014) using primers MTCP259-62, MTCP573-6, MTCP593-600, MTCP607-10, and MTCP641-2 (Table 4).

Pellicle assays

B. subtilis cultures were grown to early stationary phase and then diluted 1:1000 into MSgg (Branda et al., 2001) or modified MSgg, as indicated. Amino acids were stored as stock solutions of 40 mM or 60 mM in deionized water (dH_2O), except for D-Tyr and L-Tyr, which were stored as 10 mM stock solutions in 25 mM HCl. Treatments were diluted from stock solutions to achieve the indicated final concentrations, and volumes were normalized using dH_2O. All experiments were conducted in BD Falcon 24-well plates with low evaporation lids (BD Biosciences, USA) in a final volume of 2 mL. Plates were incubated at 30˚C or 25˚C as indicated and photographs were taken every 24 hours.

Solid medium biofilm assays

B. subtilis colony biofilms were grown by spotting 2 μL of early stationary phase cultures on unmodified solid MSgg (Branda et al., 2006) or solid MSgg without L-FTW, as indicated in the text. D-Tyr was stored as a 10 mM stock solution in 25 mM HCl and diluted to achieve the indicated final concentrations. Plates were incubated at 30˚C and photographs were taken after 72 hours.

P. aeruginosa biofilm studies were conducted using liquid or solid (1% agar) M6301 or M6301R medium. The recipe for M6301 medium is 100 μM KH_2PO_4, 15.14 mM $(NH_4)_2SO_4$, and 0.36 μM $FeSO_4 \cdot H_2O$ (Cabeen, 2014) along with 0.5% glycerol, 1 mM $MgSO_4$, and 0.2% casamino acids (BD Bacto, USA). M6301R, which favors more robust wrinkled colony morphology in the lab strain PA14, was made by supplementing M6301 with 5 mM L-arginine.

Plates containing 40 mL of M6301 and 1% agar were poured fresh for each experiment and laid to dry in a single layer for 6-7 hours. *P. aeruginosa* day cultures in 3 mL LB were back-diluted to an OD_{600} of 1.0 and 2 μL of the diluted cultures were spotted on the M6301 agar plates. The plates were incubated at 25˚C and photographed after four, five, or six days, as indicated. Colonies were harvested from the agar surface and resuspended in 1 mL sterile 1x phosphate-buffered saline (PBS, 20 mM potassium phosphate, 150 mM NaCl). 100 μL were removed from the resuspension to measure the optical density at 600 nm using a Genesys 20 spectrophotometer (Thermo Scientific, USA). The remaining volume was pelleted at 13000 rpm for 3 minutes at room temperature and the supernatant was discarded. Pellets were resuspended in 40 μg/mL Congo Red and incubated, shaking, for at least 90 minutes. The samples were again pelleted at 13000 rpm for 3 minutes at room temperature, and the optical density of the supernatants was measured at 490 nm. A standard curve was constructed by measuring the optical density at 490 nm of Congo Red at 40, 20, 10, 5, 2, 1, and 0.5 μg/mL. 1x PBS was used as a blank and as a diluent for the standard curve.

For *P. aeruginosa* biofilm assays conducting using a 96-well-plate format, stationary phase day cultures (grown in LB) were diluted 1:100 in M6301 or M6301R with or without treatment (e.g., D-amino acids, DNaseI, or Proteinase K) as indicated in the text. Treated cultures were immediately plated in transparent Costar 96-well plates with lids (Fisher Scientific,

USA) and incubated at 25˚C for 24 hours. The optical density in each well was measured using a BioTek Synergy 2 luminometer (BioTek, USA) at 600 nm. The wells were then washed three times with dH_2O and stained with 0.1% crystal violet. After a 20-minute incubation at room temperature, the crystal violet was removed and the wells were again washed three times with dH_2O. After air-drying the plates overnight, the crystal violet was solubilized using 95% ethanol and the optical density at 600 nm was measured as described above. Biofilm biomass was calculated for each sample as the ratio of crystal violet staining to culture density.

S. aureus SC01 or HG003 were grown as day cultures in 3 mL LB at 37˚C. Stationary-phase cultures were diluted 1:100 in tryptic soy broth (TSB; EMD Millipore, USA) + 0.5% glucose and D-amino acid treatments as indicated in the text. All experiments were carried out in transparent Costar 96-well plates with lids (Fisher Scientific, USA) in a total volume of 200 µL/well. Biofilm biomass was determined after 24 hours (25˚C) by resuspending submerged biofilms (following three thorough washes with 1x PBS) in PBS and measuring the optical density at 600 nm.

Growth measurements

Unless otherwise indicated, growth curves done manually were performed as follows. Cells were grown to mid-exponential phase and diluted to a final OD_{600} of ~0.015 into MSgg medium to which amino acid or the equivalent volume of dH_2O was added to a final volume of 20 mL. Cells were grown in shaking culture at 200 rpm at 37˚C, and OD_{600} was measured every hour for seven hours.

In Chapter 3, automated growth curves were performed as follows. Cells grown to mid-exponential phase were diluted 1:1000 into MSgg plus amino acids or the equivalent volume of

dH_2O, and 250 µL aliquots were transferred to a Costar polystyrene 96-well plate with low evaporation lid (Fisher Scientific, USA). OD_{600} was measured every 10 minutes for 24 hours in a BioTek Synergy 2 luminometer (BioTek, USA) with continuous slow shaking at 30˚C.

In Chapter 4, automated growth curves were performed as follows. Cells were grown to mid-exponential phase in MSgg, diluted to an OD_{600} of 0.03 in fresh MSgg, and treated with 10 µM D-Tyr or an equivalent volume of dH_2O. Aliquots of 250 µL were transferred to a Costar polystyrene 96-well plate with low evaporation lid (Fisher Scientific, USA). OD_{600} was measured every 10 minutes for 7 hours in a BioTek Synergy 2 luminometer (BioTek, USA) with continuous medium shaking at 37˚C.

Kinetic luciferase assay

Cultures of *B. subtilis* cells were grown in LB to mid-exponential phase and diluted 1:1000 in fresh MSgg with the indicated amino acid treatment or an equivalent volume of dH_2O. Dilutions were plated in triplicate (250 µl each) in a 96-well polystyrene Costar plate (white with a clear bottom; Fisher Scientific, USA). Luciferase activity was measured on a BioTek Synergy 2 luminometer (BioTek, USA) with continuous slow shaking at 30°C. Luciferase luminescence was measured at a sensitivity setting of 200, and culture optical density was measured at 600 nm every 10 minutes for 24 hours. Final luciferase activity values were calculated by normalizing luciferase luminescence to culture density.

Cultures of *P. aeruginosa* cells were grown in LB to stationary phase and diluted to an OD_{600} of 1.0 in fresh LB. 2 µL of the resulting cultures were spotted on solid M6301 and plates were incubated at 25˚C for 24, 72, or 120 hours. At the indicated time points, colonies were harvested in 1 mL sterile 1x PBS, homogenized for 20 seconds, and plated in quadruplet (200 µL

each) in a 96-well polystyrene Costar plate (white with a clear bottom; Fisher Scientific, USA). Luciferase activity and optical density was measured on a BioTek Synergy 2 luminometer (BioTek, USA). Luciferase luminescence was measured at a sensitivity setting of 200, and culture optical density was measured at 600 nm. In cases in which the culture optical density exceeded the dynamic range of the luminometer, the analysis was repeated with two- or four-fold culture dilutions. Final luciferase activity values were calculated by normalizing luciferase luminescence to culture density.

tyrS overexpression assay

B. subtilis strains 3610, SLH69, and SLH70 were grown to early stationary phase in 3 mL LB, shaking at 37˚C, and 2 μL of each culture were spotted on MSgg agar, MSgg agar with 750 μM isopropyl β-D-1-thiogalactopyranoside (IPTG), MSgg agar with 10 μM D-Tyr, or MSgg agar with both 750 μM IPTG and 10 μM D-Tyr. The plates were incubated at 30˚C and photographed at 72 hours.

Evaluation of D-amino acid incorporation into peptidoglycan

Three mL LB was inoculated with a single colony of *dtd*$^{+}$ *B. subtilis* and incubated in a roller drum at 37˚C. After three hours, these cultures were diluted 1:1000 into MSgg and 48.5 mL of culture were transferred into a glass dish containing a total of 1.5 mL treatment (D-tryptophan) or water (untreated). These biofilm cultures were incubated statically at 25˚C for 48 hours, at which time cells were harvested by centrifugation at 4000 rpm for 25 minutes.

Pelleted cells were resuspended in 2 mL cold distilled H_2O, added drop-wise to boiling 50 mL solutions of 5% SDS, and boiled for 15 minutes. After cooling to room temperature, the

samples were pelleted at 4000 rpm for 25 minutes at room temperature. SDS was removed from the pellets by several rounds of washing in warm distilled H_2O and re-pelleting. Pellets were resuspended in a solution of 100 mM Tris-HCl, 20 mM $MgSO_4$, pH 7.5. 20 µg/mL DNase I, 40 µg/mL RNAse, and 80 µg/mL α-amylase (final concentrations from 10 mg/ml stocks in 50% glycerol) were added and samples were incubated shaking at 37˚C for 2 hours. 80 µg/mL trypsin (10 mg/ml stock) was added as well as $CaCl_2$ to a final concentration of 10 mM, and the samples were incubated shaking at 37˚C overnight. The following day, SDS was added to achieve a final SDS concentration of 1%, and samples were boiled for 2 hours. After washing out the SDS with warm water as described above, the sample was pelleted and resuspended in 0.02% NaN_3.

To digest the cell wall for LC-MS analysis, 50 µL of the cell wall sample was moved to a fresh Eppendorf™ tube, mixed with 10 µL 500 mM sodium phosphate buffer (pH 6.0), 2.5 µL 4000 U/mL mutanolysin, and 37.5 µL dH_2O, and incubated shaking overnight at 37˚C. Another aliquot of mutanolysin was added the next morning, and the samples were incubated shaking at 37˚C for at least three hours. The samples were centrifuged at 16000 rpm for 10 min at 4˚C, and the supernatant was transferred to fresh 1.5 mL Eppendorf™ tubes. One volume of freshly dissolved 10 mg/mL $NaBH_4$ (in dH_2O) was added for every two volumes of supernatant. The solution was mixed gently every 10 minutes for 30 minutes, and the reaction was quenched with 20% H_3PO_4 (1.2 µL of acid was added for every 10 µL of base). After centrifuging until all bubbles disappeared, the samples were frozen in liquid nitrogen, lyophilized, and resuspended in 25 µL dH_2O.

LC-MS chromatograms were obtained on an Agilent Technologies 1100 series LC-MSD instrument using electrospray ionization (ESI) in positive mode and a Waters Symmetry Shield RP18 column (5 µm, 3.9X150 mm) with matching column guard. The fragments were separated

by water for 5 minutes followed by a gradient of 0% acetonitrile in water to 20% acetonitrile in water for 40 minutes, always at a constant flow rate of 0.5 mL/min. Both the water and acetonitrile contained 0.1% formic acid to aid in ionization. (M+2H)/2 ions were extracted from the chromatograms for selected disaccharide fragments.

To confirm the structure of the D-Trp incorporation peaks, high-resolution LC-MS/MS was performed on the peptidoglycan isolated from *dtd*$^{+}$ cells treated with 1 mM D-Trp. Chromatograms were obtained in positive mode (ES) on a Bruker maXis impact Q-Tof with Agilent 1290 HPLC using the same column and method as the nominal mass LC-MS above. Differences in retention times between the nominal and high-resolution chromatograms can be attributed to dead volume differences between instruments.

TyrRS protein purification and kinetic analyses

Materials were obtained from the following sources: Arctic Express (De3) *E. coli* cells (Agilent), Rosetta 2 (De3) and BL21 (De3) *E. coli* cells (EMD Biosciences), HisPur NiNTA resin (Promega), Biosafe II scintillation cocktail (Research Products International Corporation), and [^{14}C]L-Tyr (Moravek). All other reagents were obtained from VWR International or Fisher Scientific. Curve fitting and graphing was performed using GraFit (Erithacus Software, LTD, Horley, Surrey, UK) and Kaleidograph (Synergy Software, Reading, PA).

Plasmids for the expression of C-terminally His_6-tagged TyrRS (wild-type and A202V variant) were constructed as follows. pET-28a (Novagen) was linearized with NcoI and XhoI such that the C-terminal His_6 tag was preserved but the N-terminal His_6 tag was removed. Primers 73 and 74 were used to amplify the fragment containing *tyrS* from *B. subtilis* 3610 chromosomal DNA. The resulting fragments were then joined in an isothermal assembly

reaction (Gibson et al., 2009) with linearized and gel-purified pET-28a to produce pSL006 (for the production of $TyrRS^{WT}$-His_6) or pSL007 (for the production of $TyrRS^{A202V}$-His_6). The plasmids were maintained in Arctic Express (De3), Rosetta 2 (De3), or BL21 (De3) *E. coli* cells using selection with kanamycin at 25 μg/mL. Plasmid inserts were verified by sequencing using primers 73 and 74.

To verify expression, BL21 (De3) cells harboring pSL006 or pSL007 were grown overnight at 37˚C in 5 mL LB with kanamycin at 30 μg/mL. Overnight cultures were diluted 1:100 into fresh 25 mL LB with kanamycin at 50 μg/mL and grown at 37˚C. When the cultures reached an optical density (600 nm) of 0.3-0.35, the cultures were either left untreated or treated with 500 μM or 1 mM IPTG. After growth for four hours at 30˚C, aliquots were collected, pelleted, boiled, and run on an SDS-PAGE gel. Expression was confirmed by western blot as described (Foulston et al., 2014) except the primary antibody was rabbit anti-His_6 (ab9108, Abcam) used at a dilution of 1:5000.

The AMP deaminase and IMP dehydrogenase were expressed in *E. coli* Rosetta 2 (De3) and the inorganic pyrophosphatase, cyclodityrosine synthase, and D-tyrosyl-$tRNA^{Tyr}$ deacylase, were expressed in *E. coli* BL21 (De3) cells, as described in First 2014 and First and Richardson 2014 (manuscripts submitted). T7 RNA polymerase was isolated using standard procedures. The pET28-based *B. subtilis* tyrosyl-$tRNA^{Tyr}$ synthetase wild-type and A202V variant encoding plasmids (pSL006 and pSL007) were transformed into Arctic Express (De3) cells. Single colonies were grown in 5 mL 2xYT (16 g/L tryptone, 10 g/L yeast extract, and 5 g/L NaCl) with 50 μg/mL kanamycin overnight at 37˚C. Four 500 mL Delong flasks containing 2xYT with kanamycin were inoculated with 1 mL of overnight culture. Flasks were incubated at 37˚C at 250 rpm in a platform shaker until the optical density at 600 nm was 0.4-0.6. Flasks were chilled for

about 30 minutes before protein expression was induced with IPTG at a final concentration of 0.5 mM. Flasks were incubated at 13˚C for at least 24 hours prior to protein purification.

Recombinant enzymes were isolated using NiNTA affinity chromatography, as previously described (Kleeman et al., 1997). Both *B. subtilis* tyrosyl-tRNA^{Tyr} synthetase wild-type and A202V variant were initially dialyzed against buffer containing 0.1 mM inorganic pyrophosphate, followed by three more rounds of dialysis to remove pyrophosphate and released substrate. Proteins were isolated to >95% homogeneity based on SDS-PAGE. Extinction coefficients and molecular weights were calculated using the ExPASy ProtParam tool. Purified proteins were stored in the buffers described in First and Richardson, 2014 (manuscript submitted). Both *B. subtilis* tyrosyl-tRNA^{Tyr} synthetase wild-type and A202V variant were stored in 20 mM Tris, pH 7.8, 1 mM EDTA, 10 mM β-mercaptoethanol, and 50% v/v glycerol.

Geobacillus stearothermophilus tRNA^{Tyr} was synthesized by runoff transcription using T7 RNA polymerase using pGFX-WT, as previously described (Kleeman et al., 1997).

The concentration of tyrosyl-tRNA synthetase was determined using a filter-based active site titration assay that monitors the formation of the enzyme-bound tyrosyl-adenylate intermediate complex in the absence of tRNA. Reactions contained 10 mM [^{14}C]L-Tyr, 10 mM MgATP, 2 U/mL inorganic pyrophosphatase, and 1-5 mM enzyme being tested, based on A_{280} measurements, in 100 mM Tris pH 7.8 and 10 mM $MgCl_2$. Reactions were incubated at 25˚C, and samples were filtered over Protran BA-85 nitrocellulose discs presoaked with 100 mM Tris pH 7.8 and 10 mM $MgCl_2$. Filters were washed three times with cold buffer, dried, and counted in 5.5 mL Biosafe II scintillation cocktail by a Beckman LS-6500 scintillation counter.

Real time, continuous AMP detection assays was performed as elaborated in First 2014 and First and Richardson 2014 (manuscripts submitted). Reactions contained 50 mM Tris pH

7.78, 10 mM KCl, 0.1 mM dithiothreitol, 10 mM $MgCl_2$, 10 mM MgATP, 5 mM NAD^+, 160 nM AMP deaminase, 640 nM IMP dehydrogenase, 2 U/mL inorganic pyrophosphatase, 5 nM to 0.5 mM TyrRS, and variable [$tRNA^{Tyr}$] and [Tyr]. NAD^+ and ATP solutions were adjusted to pH 7.0 prior to use. Assays were performed in a 96-well plate (100 or 200 µL per well) at 25˚C by monitoring the change in absorbance at 340 nm (A_{340}) that occurs with the conversion of NAD^+ to NADH. This reaction provides a readout for the consumption of ATP to form AMP, which is converted to IMP and XMP by AMP deaminase and IMP dehydrogenase, respectively. Under these conditions, the formation of tyrosyl-$tRNA^{Tyr}$ is the rate-limiting step and substrate is non-limiting due to the addition of recycling enzymes: 8 µM cyclodityrosine synthase or 50 µM D-tyrosyl-$tRNA^{Tyr}$ deacylase for L- and D-Tyr, respectively. The values for K_M^{tRNA} and k_{cat} were obtained by varying the tRNA concentration under conditions where the L- or D-Tyr concentration is saturating (1 mM). The values for $K_M^{L\text{-}Tyr}$, $K_M^{D\text{-}Tyr}$, and k_{cat} were obtained by varying the L- or D-Tyr concentration under conditions where the tRNA concentration is saturating (i.e., 5 µM).

Initial rates were determined for each substrate concentration by a linear fit of a plot of A_{340} against time. K_M and V_{max} values were determined by subtracting the no substrate rate and plotting the initial rate against substrate concentration and fitting the curve to the Henri-Michaelis-Menten equation: $v_o = V_{max}[S]/(K_M+[S])$, where K_M is the affinity for the substrate and v_o is the initial rate. The k_{cat} values were calculated by the equation: $V_{max} = k_{cat}[E]$, where [E] is the molar concentration of the enzyme in the assay.

Intracellular L-Tyr quantification

B. subtilis 3610, SLH31, SLH34, SLH35, SLH36, and SLH38 were grown, shaking at 220 rpm, in 25 mL modified Belitzky Medium (15 mM $(NH_4)_2SO_4$, 8 mM $MgSO_4$, 27 mM KCl, 7 mM $Na_3C_6H_5O_7 \bullet 2H_2O$, 50 mM Tris HCl (pH 7.5), 1 mM KH_2PO_4, 2 mM $CaCl_2 \bullet 2H_2O$, 1 μM $FeSO_4 \bullet 7H_2O$, 10 μM $MnSO_4 \bullet 1H_2O$, 2% glucose) (Stulke et al., 1993) at 37˚C and harvested at an OD_{600} of 0.2. The cells were pelleted at 4˚C at 3000 rpm for 10 minutes and, after removing the supernatant, the cells were immediately snap frozen in liquid nitrogen. Resuspension, metabolite extraction, Marfey derivatization, desalting, and LC-MS of the snap frozen samples were performed essentially as described (Jamindar and Gutheil, 2010).

Transposon mutagenesis and biofilm colony morphology screen

P. aeruginosa PA14 Δ*amrZ* (MTC590) and *E. coli* SM10 pBT24 (MTC33) were grown as separate day cultures in 3 mL LB. 50 μL of MTC33 was spot-dried on LB agar plates, and 100 μL of MTC590 was spot-dried on top of the dried MTC33. The plates were incubated overnight at 37˚C. The following day, the cells were harvested in 500 μL sterile 1x PBS and plated for single colonies on LB agar containing irgasan and gentamicin. Individual single colonies were picked and used to inoculate LB (150 μL/ well) in twenty 96-well plates (Costar, Fisher Scientific, USA). The 96-well plates were incubated overnight at 37˚C. Each plate contained a culture of PA14 and a culture of MTC590 for reference.

Cells from the 96-well plate cultures were deposited by pin array onto M6301 agar plates and grown at 25˚C. At day four, colonies exhibiting a biofilm morphology that differed from that of MTC590 were imaged and streaked out for single colonies on LB agar with gentamicin. These colonies were then grown in 3 mL LB culture with gentamicin and aliquots were saved as

glycerol (25% final concentration) frozen stocks. Two µL of each culture were spotted on M6301 agar to verify the initially observed colony morphologies. Colonies that exhibited reproducible colony morphologies were submitted for sequencing with primer BT20TnMSeq following two rounds of amplification. Primers Rnd1-ARB1, Rnd1-ARB2, Rnd1-ARB3, and Rnd1-TnM20 were used for the first round of amplification. Primers Rnd2-ARB and Rnd2-TnM20 (Kulasekara et al., 2005) were used for the second round of amplification.

Quantification of intracellular cyclic di-GMP

P. aeruginosa PA14 and mutants thereof were grown in 3 mL LB day cultures and spotted (2 µL each) at an OD_{600} of 1.0 on 40 mL M6301 agar as described above. Using a sterile spatula, the colonies were deposited into 5 mL Eppendorf™ tubes (Fisher Scientific, USA) containing 1 mL sterile 1x PBS and homogenized for 20 seconds with an Argos pestle (Cole Parmer, USA). Cyclic di-GMP concentrations were measured in triplicate as described (Roy et al., 2013).

Table 4. Strains, plasmids, and primers used in this study.

Strain	Genotype or description	Source
NCIB3610	Parental strain (wild-strain) *B. subtilis*	Laboratory stock
168	Lab strain of *B. subtilis, trpC2*	Laboratory stock
PY79	Prototrophic derivative of 168	Laboratory stock
DS2569	NCIB3610 cured of plasmid	McLoon et al., 2011
AM373	168 *sfp*$^{+}$ *epsC*$^{+}$ *swrA*$^{+}$ *degQ*$^{+}$ *amyE*::P$_{rapP}$-*rapP phrP*, Cm^{R}	McLoon et al., 2011
SLH1	Δ*ponA*::kan in PY79	This study
SLH2	Δ*ponA*::kan in 168	This study
SLH3	Δ*ponA*::kan in NCIB3610	This study
SLH4	Δ*ponA*::kan in DS2569	This study
SLH5	Δ*ponA* in ALM373	This study
SLH7	Spontaneous D-LMWY resistance mutant, *ppaC*$^{434C>T}$	This study
SLH8	Spontaneous D-LMWY resistance mutant, *tyrS*$^{-38\Omega C}$	This study
SLH9	Spontaneous D-LMWY resistance mutant, *tyrS*$^{-38C>T}$	This study
SLH10	Spontaneous D-LMWY resistance mutant, *ppaC*$^{234A>T}$	This study
SLH13	Spontaneous D-LMWY resistance mutant, *trnD-Phe*$^{35A>T}$	This study
SLH15	Spontaneous D-LMWY resistance mutant, *hrcA*$^{-8A>G}$ *ppaC*$^{\Delta 496-498}$	This study
SLH16	Spontaneous D-LMWY resistance mutant, *tyrS*$^{605G>A}$	This study
SLH31	*dtd*$^{2T>A}$ in NCIB3610	This study
ALM89	*sacA::P$_{epsA}$-lux* in NCIB3610, Cm^{R}	Leiman et al., 2014
SLH32	*sacA::P$_{epsA}$-lux* in SLH31, Cm^{R}	This study
ALM91	*sacA::P$_{tapA}$-lux* in NCIB3610, Cm^{R}	Leiman et al., 2014
SLH33	*sacA::P$_{tapA}$-lux* in SLH31, Cm^{R}	This study
SLH34	*ppaC*$^{434C>T}$ in NCIB3610	This study
SLH35	*tyrS*$^{-38C>T}$ in NCIB3610	This study
SLH36	*trnD-Phe*$^{35A>T}$ in NCIB3610	This study
SLH37	*hrcA*$^{-8A>G}$ in NCIB3610	This study
SLH38	*tyrS*$^{605G>A}$ in NCIB3610	This study
SLH49	*amyE*::P$_{aroH}$-lux in NCIB3610, Cm^{R}	This study
SLH50	*amyE*::P$_{aroH}$-lux in SLH31, Cm^{R}	This study
SLH51	*amyE*::P$_{aroH}$-lux in SLH35, Cm^{R}	This study
SLH52	*amyE*::P$_{aroH}$-lux in SLH36, Cm^{R}	This study
SLH53	*amyE*::P$_{tyrA}$-lux in NCIB3610, Cm^{R}	This study
SLH54	*amyE*::P$_{tyrA}$-lux in SLH31, Cm^{R}	This study

Table 4 (Continued). Strains, plasmids, and primers used in this study.

Strain	Genotype or description	Source
SLH55	*amyE*::P_{tyrA}-lux in SLH35, Cm^R	This study
SLH56	*amyE*::P_{tyrA}-lux in SLH36, Cm^R	This study
SLH57	*amyE*::P_{tyrS}-*lux* (from NCIB3610) in NCIB3610, Cm^R	This study
SLH58	*amyE*::P_{tyrS}-*lux* (from NCIB3610) in SLH36, Cm^R	This study
SLH59	*amyE*::P_{tyrS}-*lux* (from SLH8) in NCIB3610, Cm^R	This study
SLH61	*amyE*::P_{tyrS}-*lux* (from SLH9) in NCIB3610, Cm^R	This study
SLH63	*tapA-sipW-tasA*::*spec*	This study
SLH64	*tapA-sipW-tasA*::*spec*, *amyE*::*tapA-sipW-tasA*, Cm^R	This study
SLH65	*tapA-sipW-tasA*::*spec*, *amyE*::*tapA2-sipW-tasA*, Cm^R	This study
SLH66	*tapA-sipW-tasA*::*spec*, *amyE*::*tapA6-sipW-tasA*, Cm^R	This study
SLH69	*amyE*::$P_{hyspank}$-*tyrS*$^{-366\text{-}1269}$, $Spec^R$	This study
SLH70	*amyE*::$P_{hyspank}$-*tyrS*$^{-16\text{-}1269}$, $Spec^R$	This study
SLH75	*amyE*::P_{tyrS}-*lux* (no terminator) in NCIB3610, Cm^R	This study
RL4602	*tapA-sipW-tasA::spec, amyE::*Δ*tapA(13-234)-sipW-tasA,* Cm^R	Laboratory stock
JRR4	*B. subtilis subtilis* RO-NN-1	Laboratory stock
JRR5	*B. subtilis spizizenii* TU-B-10	Laboratory stock
JRR7	*B. mojavensis* ROH-1	Laboratory stock
Turbo *E. coli*	*recA*$^+$ *endA1* Δ*(hsdS-mcrB)5*	NEB
DH5α	*recA1 endA1 hsdR17* (r_K^-, m_K^+) *relA1*	Invitrogen
BL21 (De3)	F^- *ompT hsdS*B (r_B^- m_B^-) *gal dcm* (DE3)	EMD Biosciences
Arctic Express (De3)	BL21 derivative for improved protein folding and solubility	Agilent
AE-pET28-BsubTyrRS-WT	Arctic Express cells harboring pSL006	This study
AE-pET28-BsubTyrRS-AV	Arctic Express cells harboring pSL007	This study
Rosetta (De3)	F^- *ompT hsdS*$_B$(r_B^- m_B^-) *gal dcm* (DE3) pRARE2 (Cam^R)	EMD Biosciences
SM10	*E. coli* strain for mating with *P. aeruginosa*	Laboratory stock
HG003	Lab strain of *S. aureus*	Laboratory stock
SC01	Lab strain of *S. aureus*	Laboratory stock
PA14	Lab strain of *P. aeruginosa*	Laboratory stock
MTC33	SM10 pBT24 (mating strain for Tn mutagenesis), $Gent^R$	Kulasekara et al., 2005
MTC590	PA14 Δ*amrZ*	This study
MTC1231	PA14 Δ*amrZ* Tn*bifA*, $Gent^R$	This study
MTC1234	PA14 Δ*amrZ* Tn*cupA5* isolate 1, $Gent^R$	This study
MTC1238	PA14 Δ*amrZ* Tn*phzA,* $Gent^R$	This study
MTC1240	PA14 Δ*amrZ* Tn*69700* isolate 1, $Gent^R$	This study

Table 4 (Continued). Strains, plasmids, and primers used in this study.

Strain	Genotype or description	Source
MTC1241	PA14 Δ*amrZ* Tn*16550*, $Gent^R$	This study
MTC1247	PA14 Δ*amrZ* Tn*cupA5* isolate 2, $Gent^R$	This study
MTC1249	PA14 Δ*amrZ* Tn*argG*, $Gent^R$	This study
MTC1271	PA14 Δ*amrZ* Tn*lemA* isolate 1, $Gent^R$	This study
MTC1279	PA14 Δ*amrZ* Tn*lemA* isolate 2, $Gent^R$	This study
MTC1281	PA14 Δ*amrZ* Tn*ptsP*, $Gent^R$	This study
MTC1284	PA14 Δ*amrZ* Tn*69700* isolate 2, $Gent^R$	This study
MTC1290	PA14 Δ*amrZ* Tn*pelA*, $Gent^R$	This study
MTC1294	PA14 Δ*amrZ* Tn*hpd* isolate 1, $Gent^R$	This study
MTC1295	PA14 Δ*amrZ* Tn*pilR*, $Gent^R$	This study
MTC1305	PA14 Δ*amrZ* Tn*hpd* isolate 2, $Gent^R$	This study
MTC1308	PA14 Δ*amrZ* Tn*pqsL*, $Gent^R$	This study
MTC1336	SM10 pEXG2-Δ*16550*, $Gent^R$	This study
MTC1346	SM10 pEXG2-Δ*69700*, $Gent^R$	This study
MTC1348	SM10 pEXG2-Δ*ptsP*, $Gent^R$	This study
MTC1381	PA14 Δ*amrZ* Δ*16550*	This study
MTC1387	PA14 Δ*amrZ* Δ*ptsP*	This study
MTC1398	PA14 Δ*amrZ* Δ*69700*	This study
MTC1408	SM10 CTX-1-*16550*, Tet^R	This study
MTC1448	PA14 Δ*16550*	This study
MTC1450	PA14 Δ*ptsP*	This study
MTC1512	PA14 Δ*69700*	This study
MTC1533	PA14 *attB*::CTX-1-P_{adcA}-lux, Tet^R	This study
MTC1535	PA14 Δ*amrZ attB*::CTX-1-P_{adcA}-lux	This study
MTC1537	PA14 Δ*amrZ* Δ*16550 attB*::CTX-1-P_{adcA}-lux, Tet^R	This study
MTC1539	PA14 Δ*amrZ* Δ*69700 attB*::CTX-1-P_{adcA}-lux, Tet^R	This study
MTC1541	PA14 Δ*amrZ* Δ*ptsP attB*::CTX-1-P_{adcA}-lux, Tet^R	This study
MTC1543	PA14 Δ*amrZ* Δ*ptsP* CTX-1-*ptsP*, Tet^R	This study
MTC1549	PA14 Δ*amrZ* Δ*16550* CTX-1-*16550*, Tet^R	This study
MTC1551	SM10 CTX-1-*ptsP*, Tet^R	This study

Table 4 (Continued). Strains, plasmids, and primers used in this study.

Plasmid	Genotype or description	Source
pDG364	*amyE*-integration vector, Amp^R, Cm^R	Harwood and Cutting, 1990
pDG1662	*amyE*-integration vector, Amp^R, Cm^R	Guerout-Fleury et al., 1996
pAH328	*sacA*-integration vector with *luxABCDE*, Amp^R, Cm^R	Chen et al., 2012
pAE164	*amyE*-integration vector with *tapA-sipW-tasA*, Amp^R, Cm^R	This study
pAE165	*amyE*-integration vector with $tapA^{558\Delta}$-*sipW-tasA*, Amp^R, Cm^R	This study
pAE166	*amyE*-integration vector with $tapA^{724\Omega G}$-*sipW-tasA*, Amp^R, Cm^R	This study
pLF007	*amyE*-integration vector with *luxABCDE*, Amp^R, Cm^R	This study
pSL001	*amyE*-integration vector with P_{tyrS} from NCIB3610 fused to *luxABCDE*, Amp^R, Cm^R	This study
pSL002	*amyE*-integration vector with P_{tyrS} from SLH8 fused to *luxABCDE*, Amp^R, Cm^R	This study
pSL003	*amyE*-integration vector with P_{tyrS} from SLH9 fused to *luxABCDE*, Amp^R, Cm^R	This study
pDR111	*amyE* integration vector with $P_{hyspank}$, $Spec^R$	Ben-Yehuda et al., 2003
pSL004	Derived from pDR111, $P_{hyspank}$-$tyrS^{-366-1269}$, $Spec^R$	This study
pSL005	Derived from pDR111, $P_{hyspank}$-$tyrS^{-16-1269}$, $Spec^R$	This study
pET-28a	T7 promoter, *lac* operator, His_6 tag (N or C)	Novagen
pSL006	Derived from pET-28a to express IPTG-inducible TyrRS-His_6 (*tyrS* from NCIB3610)	This study
pSL007	Derived from pET-28a to express IPTG-inducible TyrRS-His_6 (*tyrS* from SLH38)	This study
pSL008	*amyE*-integration vector with P_{tyrS} lacking the terminator hairpin sequence fused to *luxABCDE*, Amp^R, Cm^R	This study

Table 4 (Continued). Strains, plasmids, and primers used in this study.

Primer	Sequence	Primary Use
JMM1	ACGGCAGAAAATCAATTCGAAAAGATGAGTTGG	delete *ponA*
JMM2	CAATTCGCCCTATAGTGAGTCGTTGTCGCGATAAAGGCTTCTTTTACAACATCG	delete *ponA*
JMM3	CCAGCTTTTGTTCCCTTTAGTGAGTGAAGTCAAAAGGTACAATATCGCTAGCGGT	delete *ponA*
JMM4	TTAATTTGTTTTTTCAATGGATGATGAGTTTGTTTGTGTTTTATTA	delete *ponA*
JMM5	AAACCAGTCACTTAAATAAAAAGGAATCGTGTC	sequence *ponA*
JMM6	AGTGTTGGCTTCCTATGAGCAATACT	sequence *ponA*
JMM7	AGAAGCTTTCTGATGGCCTGTTGTT	sequence *ponA*
JMM8	GATTTCTCTTGGATACGCACCCAGAAT	sequence *ponA*
JMM9	GCACGAGCTCATGTCAGATCAATTTAACAGCCGTGAAG	sequence *ponA*
JMM10	TTAAGCAAATTGACTGTCGAACAGGCT	sequence *ponA*
JMM11	AGCATTCCAGGCAGTCGGTAAAGATA	sequence *ponA*
JMM12	GAGTATTTGTTAAAGGCACAGCTCCTT	sequence *ponA*
7	CCAGCTTTTGTTCCCTTTAGTGAGGATCGAAAGCGGATTAGAGAAATAC	sequence *yrvI* (*dtd*)
8	AATGAAGAGGATATGTACGCGGC	sequence *yrvI* (*dtd*)
39	CGTTGTAAAACGACGGCCAGTGAATTCGTAGCTATGTGCGGACGGGA	amplify *trnD-Phe*
40	AACAGCTATGACCATGATTACGCCAAGCTTCATGGATCTCATAAAGTGTCAACGTATTTC	amplify *trnD-Phe*
41	CGTTGTAAAACGACGGCCAGTGAATTCGCTTTTGACAAGTCCGAAGTC	amplify *hrcA*
42	AACAGCTATGACCATGATTACGCCAAGCTTCTGATGGATATGATCAACCGCG	amplify *hrcA*
45	CGTTGTAAAACGACGGCCAGTGAATTCGCTTGGGAGATGTTGATGGC	amplify *tyrS* riboswitch
46	AACAGCTATGACCATGATTACGCCAAGCTTCGGAAGTCATCAGATGGGGAC	amplify *tyrS* riboswitch
47	CGTTGTAAAACGACGGCCAGTGAATTCCCGTCTTACAACCTTTCTGAACTGTT	amplify *ppaC*
48	AACAGCTATGACCATGATTACGCCAAGCTTCGATGAGGGGGCTGAAGATGAA	amplify *ppaC*
49	CGTTGTAAAACGACGGCCAGTGAATTCGTACTTTCACTCGTCTTCCTGAGCG	amplify *tyrS*
50	AACAGCTATGACCATGATTACGCCAAGCTTCCAGAAGCGGAAAGATCATGAGGC	amplify *tyrS*
51	CGTTGTAAAACGACGGCCAGTGAATTCGTCTGGAAACGGCTCTCTAAACAA	amplify *yrvI* (*dtd*)
52	GAAATGAGATTAGTTGTTCAGCGAG	amplify *yrvI* (*dtd*)
53	CTAATCTCATTTCTAACCCCTTTAGTTC	amplify *yrvI* (*dtd*)
54	AACAGCTATGACCATGATTACGCCAAGCTTTCTGTTCCGATTGACTTTTCTTACCG	amplify *yrvI* (*dtd*)
55	GTATACCCAAACACTGCCGGCTCTC	sequence *tapA*
56	GAGCAATACTGAGCAAGACTTTGTA	sequence *tapA*
57	CCCAAGCGTGTTAAAAGACC	sequence *hrcA*
58	GCAGCAAGACGTGTTAAACT	sequence *ppaC*
59	CATCTTCAATGTCCACTGTGT	sequence *ppaC*

Table 4 (Continued). Strains, plasmids, and primers used in this study.

Primer	Sequence	Primary Use
60	GCTCTCCGCCACTGATACTTATAC	sequence *trnD-Phe*
66	CTATTGCCGATGATAAGCTGTCAAACATGAGAATTCGTTTGATTGGAAATTCATTGCTC	construct P_{tyrA}-lux strains
67	GAGAGTCCTCCTGTCGACCTTACTAGTTATGCGGCCGCATGACGGTCCAGACAGATGT	construct P_{tyrA}-lux strains
68	CTATTGCCGATGATAAGCTGTCAAACATGAGAATTCCTCCGGCTGTTAAATATCTCAT	construct P_{aroH}-lux strains
69	GAGAGTCCTCCTGTCGACCTTACTAGTTATGCGGCCGCGCGTTTATCAGGAGCGGTCT	construct P_{aroH}-lux strains
70	CTATTGCCGATGATAAGCTGTCAAACATGAGAATTCAGATCTGTCAACAATGGAGGAT	construct pSL001, pSL002, pSL003
71	GAGAGTCCTCCTGTCGACCTTACTAGTTATGCGGCCGCTCTAGAAATCTGGACAGCTGG	construct pSL001, pSL002, pSL003
72	GAGAGTCCTCCTGTCGACCTTACTAGTTATGCGGCCGCGGTACCACCCTACTAATAAGAG	construct pSL008
73	TTGTTTAACTTTAAGAAGGAGATATACCATGACTAACTTACTTGAAGACTTA	construct pSL006, pSL007
74	GGATCTCAGTGGTGGTGGTGGTGCTCGAGTTTATACGTCACAAGGAAGT	construct pSL006, pSL007
76	TGATGACCTCGTTTCCACCGAATTAGCTTGCATGC TTATTTATACGTCACAAGGAAGT	construct pSL004, pSL005
77	TGTGTAATTGTGAGCGGATAACAATTAAGCTTAGATCTGTCAACAATGGAGGAT	construct pSL004
86	TGTGTAATTGTGAGCGGATAACAATTAAGCTTAAAGGAGCTTTATCTTATGACTAACTTAC	construct pSL005
pDR111F	TGTGTAATTGTGAGCGGATAACAATTAAGCTT	sequence pSL004, SL005
pDR111R	TGATGACCTCGTTTCCACCGAATTAGCTTGCATGC	sequence pSL004, SL005
LF002F	TGAGCGTAGCGAAAAATCCT	sequence *amyE*
LF002R	TGAGAAAATTGGGGAGGTTG	sequence *amyE*
AE1	GGTAGCGACCGGCGCTCAGGATCCGATCATCATGCTGTCACCCTTTCTTTG	construct pAE164, pAE165, pAE166
AE2	GCCGATGATAAGCTGTCAAACATGAGAATTCTTAATTTTTATCCTCGCTATGCGCTTTT	construct pAE164, pAE165, pAE166
AE3	GAGGCTTGCAAATGCGATGAAAAAC	construct pAE165
AE4	GTTTTTCATCGCATTTGCAAGCCTC	construct pAE165
AE5	GAAGGAAAGCGGGGGAAGAGGATG	construct pAE166
AE6	CATCCTCTTCCCCCGCTTTCCTTC	construct pAE166
Rnd1-ARB1	GGCCACGCGTCGACTAGTACNNNNNNNNNNAGAG	amplify Tn insertion site
Rnd1-ARB2	GGCCACGCGTCGACTAGTACNNNNNNNNNNACGCC	amplify Tn insertion site
Rnd1-ARB3	GGCCACGCGTCGACTAGTACNNNNNNNNNNGATAT	amplify Tn insertion site
Rnd1-TnM20	TATAATGTGTGGAATTGTGAGCGG	amplify Tn insertion site
Rnd2-ARB	GGCCACGCGTCGACTAGTAC	amplify Tn insertion site

Table 4 (Continued). Strains, plasmids, and primers used in this study.

Primer	Sequence	Primary Use
Rnd2-TnM20	ACAGGAAACAGGACTCTAGAGG	amplify Tn insertion site
BT20TnMSeq	CACCCAGCTTTCTTGTACAC	sequence Tn insertion site
MTCP259	GGGCTTCGGCGGTGCCGAGGAAGCGTTCATTG	delete *amrZ*
MTCP260	TGCGCACCCGTGGAAATTAATTAAGGTACCGAATTCCGCTGAGGCGGTTGACCAG	delete *amrZ*
MTCP261	CCTCGGCACCGCCGAAGCCCACGCGTAG	delete *amrZ*
MTCP262	TTATACGAGCCGGAAGCATAAATGTAAAGCAAGCTTGGCATCCGTGGCTCAGCG	delete *amrZ*
MTCP573	GACGCTCAGGGGTGTTTCCTCCGCTCGC	delete *16550*
MTCP574	TGCGCACCCGTGGAAATTAATTAAGGTACCGAATTCCTGGAGCAGCCGCACTTC	delete *16550*
MTCP575	AGGAAACACC CCTGAGCGTCAACCCCG	delete *16550*
MTCP576	TTATACGAGCCGGAAGCATAAATGTAAAGCAAGCTTGGCCTCGACGAACACGTC	delete *16550*
MTCP593	CGAGGAGAAGAAGCGTCTCGGTTCTCGCG	delete *69700*
MTCP594	TGCGCACCCGTGGAAATTAATTAAGGTACCGAATTCCTTCGTTCAGGACAAGCGCC	delete *69700*
MTCP595	CGAGACGCTT CTTCTCCTCGCCGCTGC	delete *69700*
MTCP596	TTATACGAGCCGGAAGCATAAATGTAAAGCAAGCTTCTTGTTGCCCTTGCCGCG	delete *69700*
MTCP597	CCGGGTTGATGCTCGGGGCCTTGTCTCC	delete *ptsP*
MTCP598	TGCGCACCCGTGGAAATTAATTAAGGTACCGAATTCTTGCCGGCCCTGTATCCTC	delete *ptsP*
MTCP599	GGCCCCGAGCATCAACCCGGCGGCTACC	delete *ptsP*
MTCP600	TTATACGAGCCGGAAGCATAAATGTAAAGCAAGCTTGCGCTGCTGCAACTCCAG	delete *ptsP*
MTCP607	TCTAGAACTAGTGGATCCCCCGGGCTGCAGGAATTCCGCCGCAACAGTCCATGG	complement *16550*
MTCP608	CCCCCTCGAGGTCGACGGTATCGATAAGCTTCGGGGTTGACGCTCAGG	complement *16550*
MTCP609	ATGTCCCAGCGGAGACAAGGCCCCGAGC	complement *ptsP*
MTCP610	CCCCCTCGAGGTCGACGGTATCGATAAGCTTAAGCGCCGCACGACGAAG	complement *ptsP*
MTCP641	GACGGTATCGATAAGCTTGATATCGAATTCCTGGGCGTCCTGCTGCAC	construct P_{adcA}-lux strains
MTCP642	TTTACCGGCAGATTTCTAAAGAAGAATTGGGGATCCGACGCGCTTCTTTCGTGGTC	construct P_{adcA}-lux strains

References

Amory, A., Kunst, F., Aubert, E., Klier, A. & Rapoport, G. 1987. Characterization of the *sacQ* genes from *Bacillus licheniformis* and *Bacillus subtilis*. *J Bacteriol,* 169**,** 324-33.

Barnett, T. A., Valenzuela, D., Riner, S. & Hageman, J. H. 1983. Production by *Bacillis subtilis* of brown sporulation-associated pigments. *Can J Microbiol,* 29**,** 96-101.

Barnhart, M. M. & Chapman, M. R. 2006. Curli biogenesis and function. *Annu Rev Microbiol,* 60**,** 131-47.

Bedouelle, H., Guez, V., Vidal-Cros, A. & Hermann, M. 1990. Overproduction of tyrosyl-tRNA synthetase is toxic to *Escherichia coli*: a genetic analysis. *J Bacteriol,* 172**,** 3940-5.

Ben-Yehuda, S., Rudner, D. Z. & Losick, R. 2003. RacA, a bacterial protein that anchors chromosomes to the cell poles. *Science,* 299**,** 532-6.

Bernier, S. P., Ha, D. G., Khan, W., Merritt, J. H. & O'Toole, G. A. 2011. Modulation of *Pseudomonas aeruginosa* surface-associated group behaviors by individual amino acids through c-di-GMP signaling. *Res Microbiol,* 162**,** 680-8.

Bernstein, F. C., Koetzle, T. F., Williams, G. J., Meyer, E. F., JR., Brice, M. D., Rodgers, J. R., Kennard, O., Shimanouchi, T. & Tasumi, M. 1977. The Protein Data Bank: a computer-based archival file for macromolecular structures. *J Mol Biol,* 112**,** 535-42.

Branda, S. S., Chu, F., Kearns, D. B., Losick, R. & Kolter, R. 2006. A major protein component of the *Bacillus subtilis* biofilm matrix. *Mol Microbiol,* 59**,** 1229-38.

Branda, S. S., Gonzalez-Pastor, J. E., Ben-Yehuda, S., Losick, R. & Kolter, R. 2001. Fruiting body formation by *Bacillus subtilis*. *Proc Natl Acad Sci U S A,* 98**,** 11621-6.

Brick, P., Bhat, T. N. & Blow, D. M. 1989. Structure of tyrosyl-tRNA synthetase refined at 2.3 Å resolution. Interaction of the enzyme with the tyrosyl adenylate intermediate. *J Mol Biol,* 208**,** 83-98.

Cabeen, M. T. 2014. Stationary phase-specific virulence factor overproduction by a *lasR* mutant of *Pseudomonas aeruginosa*. *PLoS One,* 9**,** e88743.

Calendar, R. & Berg, P. 1966a. Purification and physical characterization of tyrosyl ribonucleic acid synthetases from *Escherichia coli* and *Bacillus subtilis*. *Biochemistry,* 5**,** 1681-90.

Calendar, R. & Berg, P. 1966b. The catalytic properties of tyrosyl ribonucleic acid synthetases from *Escherichia coli* and *Bacillus subtilis*. *Biochemistry,* 5**,** 1690-5.

Calendar, R. & Berg, P. 1967. D-Tyrosyl RNA: formation, hydrolysis and utilization for protein synthesis. *J Mol Biol,* 26**,** 39-54.

Cava, F., De Pedro, M. A., Lam, H., Davis, B. M. & Waldor, M. K. 2011. Distinct pathways for modification of the bacterial cell wall by non-canonical D-amino acids. *EMBO J,* 30**,** 3442-53.

Champney, W. S. & Jensen, R. A. 1969. D-Tyrosine as a metabolic inhibitor of *Bacillus subtilis.* *J Bacteriol,* 98**,** 205-14.

Champney, W. S. & Jensen, R. A. 1970. Molecular events in the growth inhibition of *Bacillus subtilis* by D-tyrosine. *J Bacteriol,* 104**,** 107-16.

Chen, Y., Cao, S., Chai, Y., Clardy, J., Kolter, R., Guo, J. H. & Losick, R. 2012. A *Bacillus subtilis* sensor kinase involved in triggering biofilm formation on the roots of tomato plants. *Mol Microbiol,* 85**,** 418-30.

Colvin, K. M., Gordon, V. D., Murakami, K., Borlee, B. R., Wozniak, D. J., Wong, G. C. & Parsek, M. R. 2011. The Pel polysaccharide can serve a structural and protective role in the biofilm matrix of *Pseudomonas aeruginosa*. *PLoS Pathog,* 7**,** e1001264.

Cramton, S. E., Gerke, C., Schnell, N. F., Nichols, W. W. & Gotz, F. 1999. The intercellular adhesion (*ica*) locus is present in *Staphylococcus aureus* and is required for biofilm formation. *Infect Immun,* 67**,** 5427-5433.

Epstein, A. K., Pokroy, B., Seminara, A. & Aizenberg, J. 2011. Bacterial biofilm shows persistent resistance to liquid wetting and gas penetration. *Proc Natl Acad Sci U S A,* 108**,** 995-1000.

Fersht, A. R., Shindler, J. S. & Tsui, W. C. 1980. Probing the limits of protein-amino acid side chain recognition with the aminoacyl-tRNA synthetases. Discrimination against phenylalanine by tyrosyl-tRNA synthetases. *Biochemistry,* 19**,** 5520-4.

Fitzpatrick, F., Humphreys, H. & O'Gara, J. P. 2005. Evidence for *icaADBC*-independent biofilm development mechanism in methicillin-resistant *Staphylococcus aureus* clinical isolates. *J Clin Microbiol,* 43**,** 1973-1976.

Foulston, L., Elsholz, A. K., DeFrancesco, A. S. & Losick, R. 2014. The extracellular matrix of *Staphylococcus aureu*s biofilms comprises cytoplasmic proteins that associate with the cell surface in response to decreasing pH. *MBio,* 5**,** e01667-14.

Foweraker, J. 2009. Recent advances in the microbiology of respiratory tract infection in cystic fibrosis. *Br Med Bull,* 89**,** 93-110.

Friedman, L. & Kolter, R. 2004. Two genetic loci produce distinct carbohydrate-rich structural components of the *Pseudomonas aeruginosa* biofilm matrix. *J Bacteriol,* 186**,** 4457-65.

Gerdeman, M. S., Henkin, T. M. & Hines, J. V. 2002. In vitro structure-function studies of the *Bacillus subtilis tyrS* mRNA antiterminator: evidence for factor-independent tRNA acceptor stem binding specificity. *Nucleic Acids Res,* 30**,** 1065-72.

Gibson, D. G., Young, L., Chuang, R. Y., Venter, J. C., Hutchison, C. A., 3rd & Smith, H. O. 2009. Enzymatic assembly of DNA molecules up to several hundred kilobases. *Nat Methods,* 6**,** 343-5.

Grula, E. A. 1960. Cell division in a species of *Erwinia*. I. Inhibition of division by D-amino acids. *J Bacteriol,* 80**,** 375-85.

Grundy, F. J. & Henkin, T. M. 1993. tRNA as a positive regulator of transcription antitermination in *B. subtilis*. *Cell,* 74**,** 475-82.

Grundy, F. J. & Henkin, T. M. 1994. Conservation of a transcription antitermination mechanism in aminoacyl-tRNA synthetase and amino acid biosynthesis genes in gram-positive bacteria. *J Mol Biol,* 235**,** 798-804.

Grundy, F. J., Hodil, S. E., Rollins, S. M. & Henkin, T. M. 1997. Specificity of tRNA-mRNA interactions in *Bacillus subtilis tyrS* antitermination. *J Bacteriol,* 179**,** 2587-94.

Guerout-Fleury, A. M., Frandsen, N. & Stragier, P. 1996. Plasmids for ectopic integration in *Bacillus subtilis*. *Gene,* 180**,** 57-61.

Ha, D. G., Richman, M. E. & O'Toole, G. A. 2014. Deletion mutant library for investigation of functional outputs of cyclic diguanylate metabolism in *Pseudomonas aeruginosa* PA14. *Appl Environ Microbiol,* 80**,** 3384-93.

Halonen, P., Tammenkoski, M., Niiranen, L., Huopalahti, S., Parfenyev, A. N., Goldman, A., Baykov, A. & Lahti, R. 2005. Effects of active site mutations on the metal binding

affinity, catalytic competence, and stability of the family II pyrophosphatase from *Bacillus subtilis*. *Biochemistry,* 44**,** 4004-10.

Harwood, C. R. & Cutting, S. M. 1990. *Molecular biological methods for Bacillus,* Chichester ; New York, Wiley.

Hengge, R. 2009. Principles of c-di-GMP signalling in bacteria. *Nat Rev Microbiol,* 7**,** 263-73.

Henkin, T. M., Glass, B. L. & Grundy, F. J. 1992. Analysis of the *Bacillus subtilis tyrS* gene: conservation of a regulatory sequence in multiple tRNA synthetase genes. *J Bacteriol,* 174**,** 1299-306.

Hill, D., Rose B., Pajkos, A., Robinson, M., Bye, P., Bell, S., Elkins, M., Thompson, B., Macleod, C., Aaron, S. D. & Harbour, C. 2005. Antibiotic susceptabilities of *Pseudomonas aeruginosa* isolates derived from patients with cystic fibrosis under aerobic, anaerobic, and biofilm conditions. *J Clin Microbiol,* 43**,** 5085-90.

Hobbs, M., Collie, E. S., Free, P. D., Livingston, S. P. & Mattick, J. S. 1993. PilS and PilR, a two-component transcriptional regulatory system controlling expression of type 4 fimbriae in *Pseudomonas aeruginosa. Mol Microbiol,* 7**,** 669-82.

Hobley, L., Ostrowski, A., Rao, F. V., Bromley, K. M., Porter, M., Prescott, A. R., MacPhee, C. E., Van Aalten, D. M. & Stanley-Wall, N. R. 2013. BslA is a self-assembling bacterial hydrophobin that coats the *Bacillus subtilis* biofilm. *Proc Natl Acad Sci U S A,* 110**,** 13600-5.

Hochbaum, A. I., Kolodkin-Gal, I., Foulston, L., Kolter, R., Aizenberg, J. & Losick, R. 2011. Inhibitory effects of D-amino acids on *Staphylococcus aureus* biofilm development. *J Bacteriol,* 193**,** 5616-22.

Homuth, G., Mogk, A. & Schumann, W. 1999. Post-transcriptional regulation of the *Bacillus subtilis dnaK* operon. *Mol Microbiol,* 32**,** 1183-97.

Hsaio, T. L., Revelles, O., Chen, L., Sauer, U. & Vitkup, D. 2010. Automatic policing of biochemical annotations using genomic correlations. *Nat Chem Biol,* 6**,** 34-40.

Ito, T., Iimori, J., Takayama S., Moriyama, A., Yamauchi, A., Hemmi, H. & Yoshimura, T. 2013. Conserved pyridoxal protein that regulates Ile and Val metabolism. *J Bacteriol,* 195**,** 5439-49.

Jamindar, D. & Gutheil, W. G. 2010. A liquid chromatography-tandem mass spectrometry assay for Marfey's derivatives of L-Ala, D-Ala, and D-Ala-D-Ala: application to the *in vivo* confirmation of alanine racemase as the target of cycloserine in *Escherichia coli. Anal Biochem,* 396**,** 1-7.

Jensen, R. A., Stenmark, S. L. & Champney, W. S. 1972. Molecular basis for the differential anti-metabolite action of D-tyrosine in strains 23 and 168 of *Bacillus subtilis*. *Arch Mikrobiol,* 87**,** 173-80.

Jones, C. J., Newsom, D., Kelly, B., Irie, Y., Jennings, L. K., Xu, B., Limoli, D. H., Harrison, J. J., Parsek, M. R., White, P. & Wozniak, D. J. 2014. ChIP-Seq and RNA-Seq reveal an AmrZ-mediated mechanism for cyclic di-GMP synthesis and biofilm development by *Pseudomonas aeruginosa*. *PLoS Pathog,* 10**,** e1003984.

Kearns, D. B., Chu, F., Branda, S. S., Kolter, R. & Losick, R. 2005. A master regulator for biofilm formation by *Bacillus subtilis. Mol Microbiol,* 55**,** 739-49.

Kirov, S. M., Webb, J. S., O'May C, Y., Reid, D. W., Woo, J. K., Rice S. A. & Kjelleberg, S. 2007. Biofilm differentiation and dispersal in mucoid *Pseudomonas aeruginosa* isolates from patients with cystic fibrosis. *Microbiology,* 153**,** 3264-74.

Klausen, M., Heydorn, A., Ragas, P., Lambertsen, L., Aaes-Jorgensen, A., Molin, S. & Tolker-Nielsen, T. 2003. Biofilm formation by *Pseudomonas aeruginosa* wild type, flagella and type IV pili mutants. *Mol Microbiol,* 48**,** 1511-24.

Kleeman, T. A., Wei, D., Simpson, K. L. & First, E. A. 1997. Human tyrosyl-tRNA synthetase shares amino acid sequence homology with a putative cytokine. *J Biol Chem,* 272**,** 14420-5.

Kobayashi, K. & Iwano, M. 2012. BslA(YuaB) forms a hydrophobic layer on the surface of *Bacillus subtilis* biofilms. *Mol Microbiol,* 85**,** 51-66.

Kolodkin-Gal, I., Romero, D., Cao, S., Clardy, J., Kolter, R. & Losick, R. 2010. D-amino acids trigger biofilm disassembly. *Science,* 328**,** 627-9.

Kuchma, S. L., Brothers, K. M., Merritt, J. H., Liberati N. T., Ausubel, F. M. & O'Toole, G. A. 2007. BifA, a cyclic-Di-GMP phosphodiesterase, inversely regulates biofilm formation and swarming motility by *Pseudomonas aeruginosa* PA14. *J Bacteriol,* 189**,** 8165-78.

Kulasekara, H. D., Ventre, I., Kulasekara, B. R., Lazdunski, A., Filloux, A. & Lory, S. 2005. A novel two-component system controls the expression of *Pseudomonas aeruginosa* fimbrial cup genes. *Mol Microbiol,* 55**,** 368-80.

Lam, H., Oh, D. C., Cava, F., Takacs, C. N., Clardy, J., De Pedro, M. A. & Waldor, M. K. 2009. D-amino acids govern stationary phase cell wall remodeling in bacteria. *Science,* 325**,** 1552-5.

Lebar, M. D., May, J. M., Meeske, A. J., Leiman, S. A., Lupoli, T. J., Tsukamoto, H., Losick, R., Rudner, D. Z., Walker, S. & Kahne, D. 2014. Reconstitution of peptidoglycan cross-linking leads to improved fluorescent probes of cell wall synthesis. *J Am Chem Soc,* 136**,** 10874-7.

Leiman, S. A., Arboleda, L. C., Spina, J. S. & McLoon, A. L. 2014. SinR is a mutational target for fine-tuning biofilm formation in laboratory-evolved strains of Bacillus subtilis. *BMC Microbiol,* 14**,** 301.

Leiman, S. A., May, J. M., Lebar, M. D., Kahne, D., Kolter, R. & Losick, R. 2013. D-Amino acids indirectly inhibit biofilm formation in *Bacillus subtilis* by interfering with protein synthesis. *J Bacteriol,* 195**,** 5391-5.

Longo, F., Rampioni, G., Bondi, R., Imperi, F., Fimia, G. M., Visca, P., Zennaro, E. & Leoni, L. 2013. A new transcriptional repressor of the *Pseudomonas aeruginosa* quorum sensing receptor gene *lasR*. *PLoS One,* 8**,** e69554.

Lupoli, T. J., Lebar, M. D., Markovski, M., Bernhardt, T., Kahne, D. & Walker, S. 2014. Lipoprotein activators stimulate *Escherichia coli* penicillin-binding proteins by different mechanisms. *J Am Chem Soc,* 136**,** 52-5.

Lupoli, T. J., Tsukamoto, H., Doud, E. H., Wang, T. S., Walker, S. & Kahne, D. 2011. Transpeptidase-mediated incorporation of D-amino acids into bacterial peptidoglycan. *J Am Chem Soc,* 133**,** 10748-51.

Ma, L., Conover, M., Lu, H., Parsek, M. R., Bayles, K. & Wozniak, D. J. 2009. Assembly and development of the *Pseudomonas aeruginosa* biofilm matrix. *PLoS Pathog,* 5**,** e1000354.

Ma, L., Jackson K. D., Landry, R. M., Parsek, M. R. & Wozniak, D. J. 2006. Analysis of *Pseudomonas aeruginosa* conditional *psl* variants reveals roles for the *psl* polysaccharide in adhesion and maintaining biofilm structure postattachment. *J Bacteriol,* 188**,** 8213-21.

Mavrodi, D. V., Bonsall, R. F., Delaney, S. M., Soule, M. J., Phillips, G. & Thomashow, L. S. 2001. Functional analysis of genes for biosynthesis of pyocyanin and phenazine-1-carboxamide from *Pseudomonas aeruginosa* PAO1. *J Bacteriol,* 183**,** 6454-65.

McLoon, A. L., Guttenplan, S. B., Kearns, D. B., Kolter, R. & Losick, R. 2011. Tracing the domestication of a biofilm-forming bacterium. *J Bacteriol,* 193**,** 2027-34.

Merritt, J. H., Ha, D. G., Cowles, K. N., Lu, W., Morales, D. K., Rabinowitz, J., Gitai, Z. & O'Toole, G. A. 2010. Specific control of *Pseudomonas aeruginosa* surface-associated behaviors by two c-di-GMP diguanylate cyclases. *MBio,* 1.

Nandi, N. 2012. Chirality in Biological Nanospaces: Reactions in Active Sites. *Chirality in Biological Nanospaces: Reactions in Active Sites***,** 1-183.

Ongena, M. & Jacques, P. 2008. *Bacillus* lipopeptides: versatile weapons for plant disease biocontrol. *Trends Microbiol,* 16**,** 115-25.

O'Toole, G. A. 2011. Microtiter dish biofilm formation assay. *J Vis Exp*.

Patrick, J. E. & Kearns, D. B. 2008. MinJ (YvjD) is a topological determinant of cell division in *Bacillus subtilis*. *Mol Microbiol,* 70**,** 1166-79.

Perego, M., Glaser, P., Minutello, A., Strauch, M. A., Leopold, K. & Fischer, W. 1995. Incorporation of D-alanine into lipoteichoic acid and wall teichoic acid in *Bacillus subtilis*. Identification of genes and regulation. *J Biol Chem,* 270**,** 15598-606.

Romero, D., Aguilar, C., Losick, R. & Kolter, R. 2010. Amyloid fibers provide structural integrity to *Bacillus subtilis* biofilms. *Proc Natl Acad Sci U S A,* 107**,** 2230-4.

Romero, D., Vlamakis, H., Losick, R. & Kolter, R. 2011. An accessory protein required for anchoring and assembly of amyloid fibres in *B. subtilis* biofilms. *Mol Microbiol,* 80**,** 1155-68.

Romero, D., Vlamakis, H., Losick, R. & Kolter, R. 2014. Functional analysis of the accessory protein TapA in *Bacillus subtilis* amyloid fiber assembly. *J Bacteriol,* 196**,** 1505-13.

Romling, U., Galperin, M. Y. & Gomelsky, M. 2013. Cyclic di-GMP: the first 25 years of a universal bacterial second messenger. *Microbiol Mol Biol Rev,* 77**,** 1-52.

Roy, A., Petrova, O. & Sauer, K. 2013. Extraction and quantification of cyclic di-GMP from *Pseudomonas aeruginosa*. *Bio-protocol,* 3**,** e828.

Sall, K. M., Casabona, M. G., Bordi, C., Huber, P., De Bentzmann, S., Attree, I. & Elsen, S. 2014. A *gacS* deletion in *Pseudomonas aeruginosa* cystic fibrosis isolate CHA shapes its virulence. *PLoS One,* 9**,** e95936.

Sheoran, A., Sharma, G. & First, E. A. 2008. Activation of D-tyrosine by *Bacillus stearothermophilus* tyrosyl-tRNA synthetase: 1. Pre-steady-state kinetic analysis reveals the mechanistic basis for the recognition of D-tyrosine. *J Biol Chem,* 283**,** 12960-70.

Shimotsu, H. & Henner, D. J. 1984. Characterization of the *Bacillus subtilis* tryptophan promoter region. *Proc Natl Acad Sci U S A,* 81**,** 6315-9.

Soutourina, J., Blanquet, S. & Plateau, P. 2000. D-tyrosyl-tRNA^{Tyr} metabolism in *Saccharomyces cerevisiae*. *J Biol Chem,* 275**,** 11626-30.

Soutourina, O., Soutourina, J., Blanquet, S. & Plateau, P. 2004. Formation of D-tyrosyl-tRNA^{Tyr} accounts for the toxicity of D-tyrosine toward *Escherichia coli*. *J Biol Chem,* 279**,** 42560-5.

Stulke, J., Hanschke, R. & Hecker, M. 1993. Temporal activation of beta-glucanase synthesis in B*acillus subtilis* is mediated by the GTP pool. *J Gen Microbiol,* 139**,** 2041-5.

Tsunoda, M., Kusakabe, Y., Tanaka, N., Ohno, S., Nakamura, M., Senda, T., Moriguchi, T., Asai, N., Sekine, M., Yokogawa, T., Nishikawa, K. & Nakamura, K. T. 2007. Structural basis for recognition of cognate tRNA by tyrosyl-tRNA synthetase from three kingdoms. *Nucleic Acids Res,* 35**,** 4289-300.

Ueda, A. & Wood, T. K. 2009. Connecting quorum sensing, c-di-GMP, Pel polysaccharide, and biofilm formation in *Pseudomonas aeruginosa* through tyrosine phosphatase TpbA (PA3885). *PLoS Pathog,* 5**,** e1000483.

Van Heijenoort, J. 2007. Lipid intermediates in the biosynthesis of bacterial peptidoglycan. *Microbiol Mol Biol Rev,* 71**,** 620-35.

Vannieuwenhze, M. S., Mauldin, S. C., Zia-Ebrahimi, M., Aikins, J. A. & Blaszczak, L. C. 2001. The total synthesis of Lipid I. *J Am Chem Soc,* 123**,** 6983-8.

Vasseur, P., Vallet-Gely, I., Soscia, C., Genin, S. & Filloux, A. 2005. The *pel* genes of the *Pseudomonas aeruginosa* PAK strain are involved at early and late stages of biofilm formation. *Microbiology,* 151**,** 985-97.

Vlamakis, H., Chai, Y., Beuaregard, P., Losick, R. & Kolter, R. 2013. Sticking together: building a biofilm the *Bacillus subtilis* way. *Nat Rev Microbiol,* 11**,** 157-68.

Vollmer, W., Blanot, D. & De Pedro, M. A. 2008. Peptidoglycan structure and architecture. *FEMS Microbiol Rev,* 32**,** 149-67.

Wang, J. & Nikonowicz, E. P. 2011. Solution structure of the K-turn and Specifier Loop domains from the *Bacillus subtilis tyrS* T-box leader RNA. *J Mol Biol,* 408**,** 99-117.

Wei, Q. & Ma, L. Z. 2013. Biofilm matrix and its regulation in *Pseudomonas aeruginosa*. *Int J Mol Sci,* 14**,** 20983-1005.

Whitchurch, C. B., Tolker-Nielsen, T., Ragas, P. C. & Mattick, J. S. 2002. Extracellular DNA required for bacterial biofilm formation. *Science,* 295**,** 1487.

Whitney, J. C., Colvin, K. M., Marmont, L. S., Robinson, H., Parsek, M. R. & Howell, P. L. 2012. Structure of the cytoplasmic region of PelD, a degenerate diguanylate cyclase

receptor that regulates exopolysaccharide production in *Pseudomonas aeruginosa*. *J Biol Chem,* 287**,** 23582-93.

Wozniak, D. J., Wyckoff, T. J., Starkey, M., Keyser, R., Azadi, P., O'Toole, G. A. & Parsek, M. R. 2003. Alginate is not a significant component of the extracellular polysaccharide matrix of PA14 and PAO1 *Pseudomonas aeruginosa* biofilms. *Proc Natl Acad Sci U S A,* 100**,** 7907-12.

Xu, H., Lin, W., Xia, H., Xu, S., Li, Y., Yao, H., Bai, F., Zhang, X., Bai, Y., Saris, P. & Qiao, M. 2005. Influence of *ptsP* gene on pyocyanin production in *Pseudomonas aeruginosa*. *FEMS Microbiol Lett,* 253**,** 103-9.

Yamane, T., Miller, D. L. & Hopfield, J. J. 1981. Discrimination between D- and L-tyrosyl transfer ribonucleic acids in peptide chain elongation. *Biochemistry,* 20**,** 7059-64.

Yang, H., Zheng, G., Peng, X., Qiang, B. & Yuan, J. 2003. D-Amino acids and D-Tyr-tRNA^{Tyr} deacylase: stereospecificity of the translation machine revisited. *FEBS Lett,* 552**,** 95-8.

Zafra, O., Lamprecht-Grandio, M., De Figueras, C. G. & Gonzalez-Pastor, J. E. 2012. Extracellular DNA release by undomesticated *Bacillus subtilis* is regulated by early competence. *PLoS One,* 7**,** e48716.

Appendix A

A Rebuttal of Uncoupling Biofilm Inhibition from Growth Inhibition

The assertion that pellicle inhibition and growth inhibition may be uncoupled, albeit under very particular growth conditions (Leiman et al., 2013), ignores crucial caveats. Pellicle assays are inherently condition-dependent[1]. The degree of pellicle wrinkling changes with the humidity inside the incubator, culture volume, and sample position in a pellicle assay plate. This last factor can be particularly misleading. As such, claims about subtle pellicle phenotypes must be reproducible when samples are moved from one location in a multi-well plate to another (e.g., from an edge well to a center well). The uncoupling phenomenon that the Kolter laboratory reported was poorly reproducible, both in the hands of Kolter group members and my own. Furthermore, in the instances in which I observed pellicle rescue by excess D-Ala, I also observed comparable or stronger pellicle rescue by excess L-Ala[2] (Fig. A1). Notably, these experiments were performed in a nutrient-poor medium, where possibly alanine racemace converts excess D-Ala to L-Ala to maintain a chemical equilibrium. Alternatively, D-Ala aminotransferase could convert excess D-Ala to pyruvate, thus providing an important nutrient precursor. Growth curves

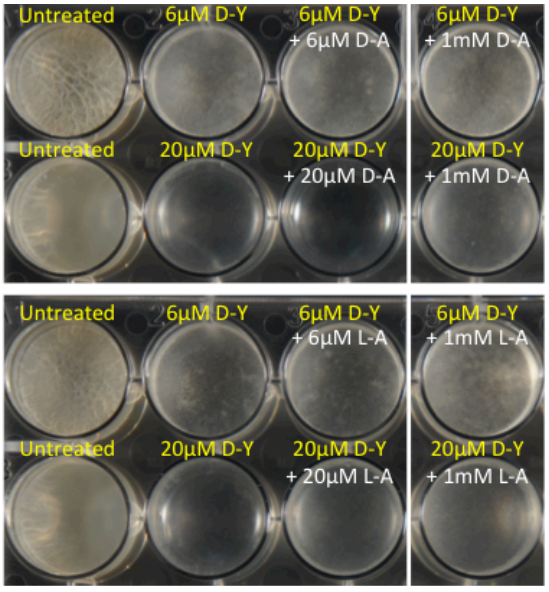

Figure A1. L-Ala rescues pellicle formation as well as or better than D-Ala. *B. subtilis* 3610 was grown in MSgg with the indicated treatments, incubated at 30˚C, and photographed at 72 hours.

[1] For this reason, most of the biofilm assays after the publication of Leiman et al., 2013 were performed on agar.

[2] To my knowledge, the Kolter laboratory did not perform this control.

support the hypothesis that, in a low-nutrient environment, excess D-Ala contributes to the growth of NCDAA-treated *B. subtilis* (Fig. A2).

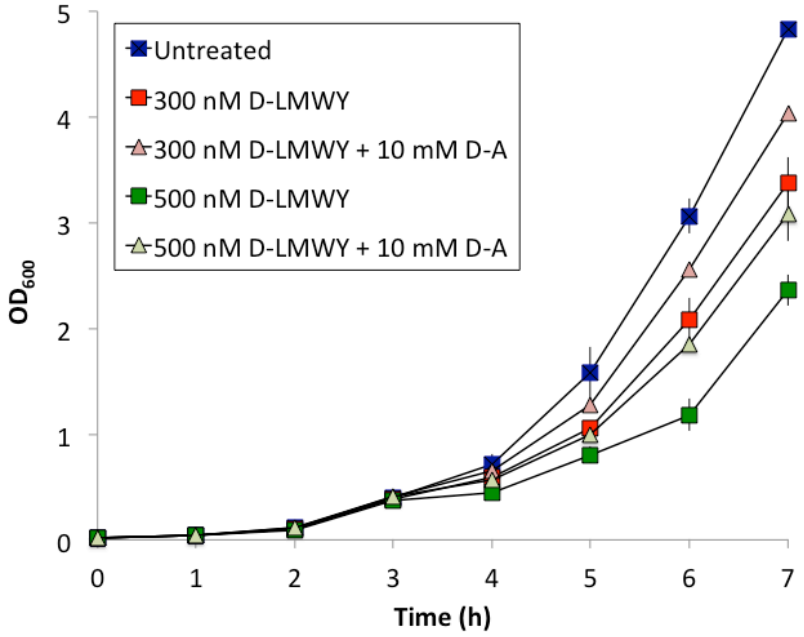

Figure A2. Excess D-Ala can contribute to growth rate. *B. subtilis* 3610 was grown in shaking MSgg lacking L-FTW and containing the indicated treatments. Optical density was measured every hour for seven hours. Results shown indicated the average of duplicate trials and error bars represent the standard deviation.

An alternative explanation is that excess D-Ala rescues pellicle formation in conditions that lead to too much muropeptide NCDAA incorporation, which would disturb the cell wall structure, limit osmotic protection to the cell, and inhibit cell division (Grula, 1960). This scenario is attractive, as it presents a middle ground between my argument that NCDAAs inhibit biofilm as a side effect of inhibiting growth, and the argument – put forth by Kolodkin-Gal et al. and reiterated by the Kolter laboratory – that NCDAAs act through their incorporation into PG. Unfortunately, the evidence does not support this theory. As shown in Chapter 3 (Fig. 13), excess D-Ala does not replace NCDAAs at the fifth position of the PG muropeptide.

As to the claim that D-Leu inhibits biofilm but not growth at 700 µM, I believe this result stems from limitations in the detection of a growth defect, rather than a true uncoupling of biofilm inhibition from growth inhibition. This assertion is based on two pieces of evidence. As shown in Figure A3, I am able to detect a minimal growth defect using D-Leu at 500 µM. More importantly, sub-lethal concentrations of D-Leu delay, but do not abolish, pellicle formation (Fig. A4). Clearly, growth inhibition by D-Leu requires higher doses and more time than does growth inhibition by D-Tyr. This is due, at least in part, to the ability of leucyl-tRNA^{Leu} synthetase to eliminate D-amino acids such as D-Leu (Nandi, 2011), and to the fact that L-Leu is one of the most abundantly produced amino acids by exponential-phase *B. subtilis* (Hsiao et al., 2010).

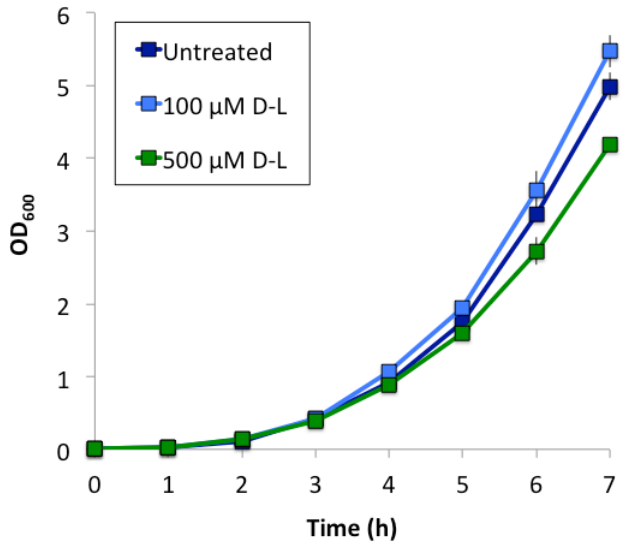

Figure A3. D-Leu at 500 µM causes a subtle growth defect. *B. subtilis* 3610 was grown in shaking MSgg at 37˚C and treated as indicated. Results represent the average of duplicate experiments and error bars show the standard devation.

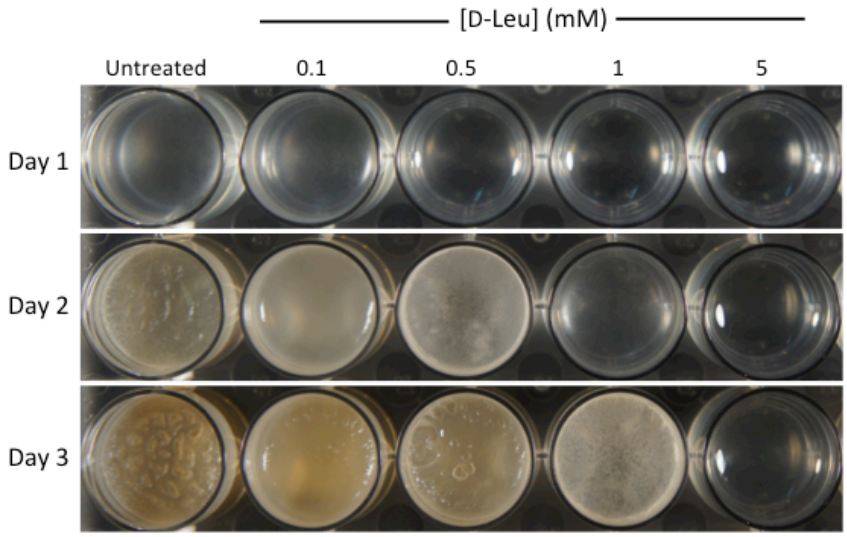

Figure A4. *B. subtilis* treated with D-Leu recovers pellicle formation. *B. subtilis* 3610 was grown in MSgg at 30˚C and imaged at 24, 48, and 72 hours post-treatment.

Appendix B

D-amino acids do not trigger biofilm disassembly

Before addressing the claim that NCDAAs cause biofilm disassembly, I would like to address the claim that *B. subtilis* pellicles naturally disassemble after six to eight days (Kolodkin-Gal et al., 2010). I, as well as other members of the Losick laboratory who routinely perform pellicle assays, do not see natural disassembly of *B. subtilis* pellicles at these time points (Fig. B1) or even weeks later. It is fair to say, though, that the structural integrity of the biofilm – as indicated by the robustness of pellicle wrinkles – may change or weaken as time progresses. It is also possible, even likely, that disassembly occurs in nature; *B. subtilis* biofilms in the soil or on plant roots may very well have a particular life span. Unlike in nature, however, *B. subtilis* living in plastic wells with limiting nutrients cannot travel to and occupy a new, habitable niche. It is my opinion, based on the brown coloration of mature pellicles and their underlying medium, the lack of visible pellicle breakdown over time, and the lack of turbidity in the medium underneath mature pellicles, that aging *B. subtilis* pellicles are increasingly populated by spores but do not truly disassemble (Barnett et al., 1983, Kolodkin-Gal et al., 2010).

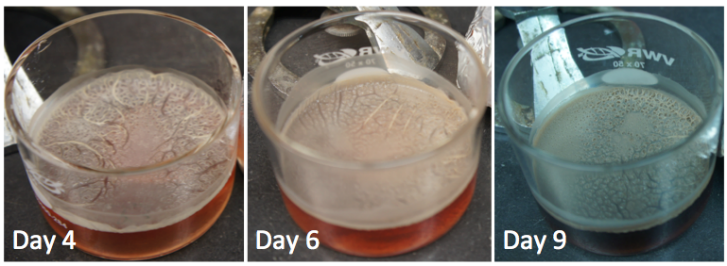

Figure B1. Representative *B. subtilis* pellicles. Nine dishes of 50 mL MSgg were inoculated with a 1:1000 dilution of *B. subtilis* 3610 and incubated at 30˚C. Because these pellicles were harvested for subsequent experiments, these pictures do not represent a time-course of one pellicle but rather separate pellicles grown for four, six, or nine days prior to harvesting.

The following points are dedicated to the central claim (and title) of the 2010 study by Kolodkin-Gal et al., that "D-amino acids trigger biofilm disassembly." It stands to reason that, just as growth inhibition by D-Tyr causes biofilm inhibition, growth inhibition also causes biofilm disassembly. Yet, as explained here, this interpretation ignores the biology of *B. subtilis* biofilms.

First, the appearance of the pellicles allegedly disassembled by D-amino acids (Kolodkin-Gal et al., 2010) is surprising. Inspection of the pellicle disassembly images reveals that – despite the broken biofilm pieces – the pellicles retain a wrinkled structure (Kolodkin-Gal et al., 2010). Importantly, *B. subtilis* lacking *tapA* and/or *tasA* do not make wrinkled pellicles, as matrix protein is necessary for the wrinkled pellicle phenotype (Romero et al., 2011). Thus assuming, for the sake of argument, the old paradigm in which D-amino acids lead to the release of TapA and thus TasA from the bacterial cell wall, the pellicle wrinkles ought to have softened or disappeared.

Still, there is a larger issue with the biofilm disassembly results presented by Kolodkin-Gal et al.: the delivery of the D-amino acid treatments.

The *B. subtilis* biofilm matrix forms an impressive liquid- and gas-repellant surface, far surpassing the repellant capabilities of Teflon (Epstein et al., 2011). Non-permeability holds true for biofilms grown on solid medium as well as air-liquid pellicles and is attributed to the hydrophobin BslA (Kobayashi and Iwano, 2012, Hobley et al., 2013). Other groups have demonstrated that *bslA*$^+$ strains of *B. subtilis* repel water droplets as well as droplets of organic solvents, including up to 80% ethanol (Kobayashi and Iwano, 2012, Epstein et al., 2011). Furthermore, these biofilms repel droplets of commercial biocides, including household bleach, disinfectant, and drain cleaner (Epstein et al., 2011). I have independently observed that

B. subtilis biofilms are unaffected by droplets of a concentrated antibiotic (spectinomycin), droplets of a concentrated biofilm-inhibitor (Proteinase K), and droplets of D-amino acids (Fig. B2). I did observe that 10 μL of 1 M HCl penetrated the pellicle at the spot where it was applied; however, this treatment did no further visible damage to the pellicle's integrity (Fig. B2). In fact I was not able to reproduce the pellicle fissures presented by Kolodkin-Gal et al. by any droplet-based treatment, and instead resorted to mechanical disruption of the pellicle (e.g., shaking or cutting) as a positive control for biofilm disassembly (Fig. B2).

To conclude, the hydrophobic, not-wetting nature of the *B. subtilis* biofilm suggests that a 10 μL droplet of D-amino acids could not permeate through the protective BslA layer, let alone reach cells to inhibit biofilm or growth. In agreement with this suggestion, applying D-Tyr to pellicles at the same concentration and volume used previously to disperse biofilms (Kolodkin-Gal et al., 2010) had no effect on pellicle stability (Fig. B2). It remains an open question as to how the original biofilm disassembly results were obtained.

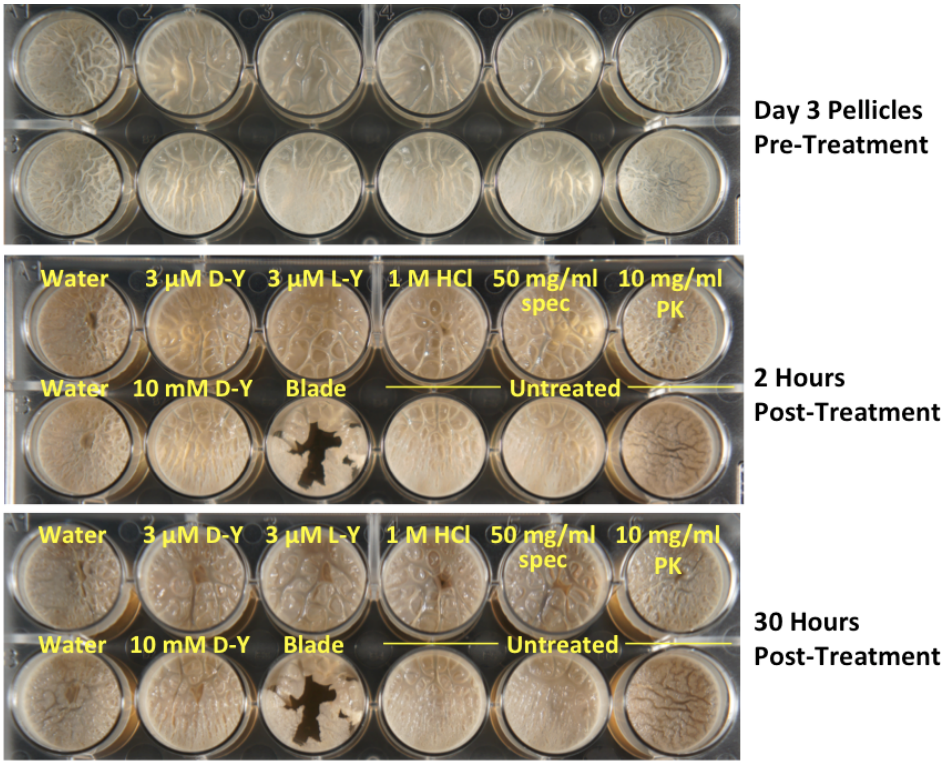

Figure B2. D-Tyr does not induce biofilm disassembly. Day 3 pellicles were treated by applying a 10 µL droplet containing either D-Tyr, L-Tyr, HCl, spectinomycin (spec), Proteinase K (PK) or water. Three pellicles were left untreated as negative controls and one pellicle was cut with a razor blade to represent biofilm dispersal by mechanical disruption. After treatment, the plates were incubated at room temperature and photographed every day for 5 days. No substantial changes in biofilm integrity for any of the treated or untreated samples were visible between 30 hours post-treatment and 5 days post-treatment.

Appendix C

D-amino acids do not inhibit biofilm formation by *Staphylococcus aureus* or *Pseudomonas aeruginosa*

In 2010, Kolodkin-Gal et al. demonstrated that the submerged biofilms produced by *S. aureus* or *P. aeruginosa* are inhibited or weakened in the presence of D-Tyr or D-LMWY (Kolodkin-Gal et al., 2010). A follow-up publication by Hochbaum et al. expanded upon these findings and determined that an equimolar mixture of D-Tyr, D-Pro, and D-Phe (more so than D-LMWY) is a potent inhibitor of *S. aureus* biofilms (Hochbaum et al., 2011).

At the time these papers were published, the general assumption in the field of *S. aureus* biofilms was that these Gram-positive pathogens build biofilm matrix in a manner comparable to that used by the Gram-positive model organism *B. subtilis*. While the authors accepted that *S. aureus* lacks a TapA-like protein, they contended that D-amino acids trigger the release of one or more PG-linked cell-cell adhesion proteins (Hochbaum et al., 2011). We now know that, far from requiring cell wall-anchored adhesion proteins for biofilm formation, *S. aureus* biofilms comprise a net of aggregated cytoplasmic proteins (Foulston et al., 2014). It is possible that these proteins are anchored by transmembrane or PG-associated proteins, but no strong evidence exists for this hypothesis. Surprisingly, Hochbaum et al. did not address whether D-Ala, which happens to be abundantly produced by *S. aureus*, counteracts NCDAA-mediated biofilm inhibition or disassembly. Still, it appears unlikely – given the current understanding of *S. aureus* biofilm formation – that NCDAAs could inhibit or disassemble biofilms by a mechanism analogous to what was claimed to occur in *B. subtilis*.

To resolve whether D-Tyr or an equimolar mixture of D-YPF inhibits *S. aureus* biofilm, I tested the published biofilm-inhibitory concentrations (D-Tyr at 500 µM or D-YPF at 100 µM each) against two strains of *S. aureus*. The first strain was SC01[1], the strain primarily used by Hochbaum et al. The second strain was HG003, chosen because, unlike SC01, it forms robust submerged biofilms that are resistant to dispersal by standard washing. As shown in Figure C1, neither strain's biofilm formation was affected by D-Tyr or D-YPF[2].

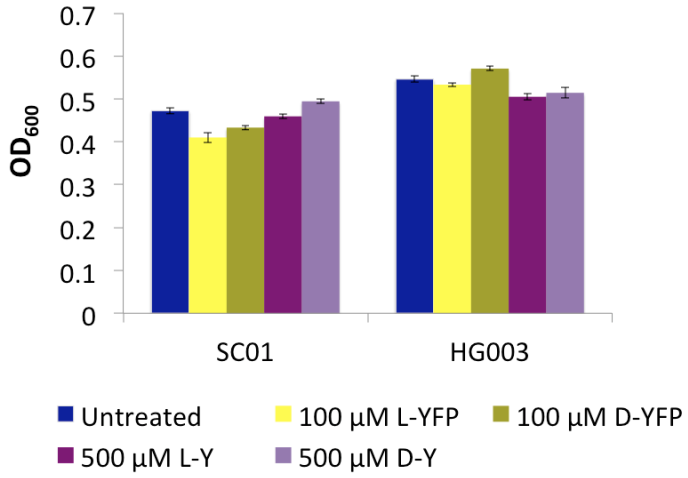

Figure C1. NCDAAs do not inhibit *S. aureus* biofilm formation. *S. aureus* SC01 or HG003 were grown in 96-well-plates in TSB + 0.5% glucose and the indicated treatments. After 24 hours at 25˚C, the optical densities of the supernatant, PBS washes, and remaining biofilm biomass were measured at 600 nM. Results shown here represent the average OD_{600} of the biofilm biomass (n = 8), and error bars represent the standard deviation.

[1] Biofilm experiments by Hochbaum et al. were carried out in TSB + 0.5% glucose + 3% NaCl. NaCl inhibits biofilm formation by HG003 and was therefore not used in the experiments shown in Figure C1. I did, however, try to repeat the results of Hochbaum et al. using SC01 in TSB + 0.5% glucose + 3% NaCl. Even under these conditions I did not observe biofilm inhibition by NCDAAs.

[2] Anecdotally, years prior I attempted to repeat these very results. Occasionally a phenotype appearing to be biofilm inhibition occurred in the presence of D-Tyr, but such results were highly variable. It turned out that in all of the cases in which D-Tyr appeared to inhibit biofilm – as evidenced by large clearings of cells from the wells of a 12-well plate – the pH of the medium had mysteriously dropped to about 2. *S. aureus* cannot survive at pH 2, and as such the observed biofilm inhibition was merely a manifestation of growth inhibition. In cases in which D-Tyr was applied and the pH did not drop to 2, but rather to the usual pH 5, biofilm formation was robust. I was not able to determine the cause of the drastic pH drop.

Similarly to *S. aureus* SC01 and HG003, *P. aeruginosa* PA14 does not require protein attachment factors for biofilm formation to occur. In fact, PA14 biofilms are insensitive to treatment with Proteinase K[3]. Therefore, extending conclusions about NCDAA-mediated biofilm inhibition from either *B. subtilis* (which requires dedicated cell wall-associated biofilm matrix proteins) or *S. aureus* (which requires aggregated cytoplasmic proteins) to the regulation of the PA14 biofilm matrix seems misguided. In addition, *P. aeruginosa* can incorporate NCDAAs into two locations of the muropeptide (the fourth and the fifth position, both by different enzymes; Cava et al., 2011), which further complicates the analogy. Just as I did with *S. aureus*, I investigated whether NCDAAs inhibit *P. aeruginosa* PA14 biofilm formation, with a focus on D-Tyr. As shown in Figure C2, even D-Tyr at 1 mM had no effect on PA14 biofilm formation.

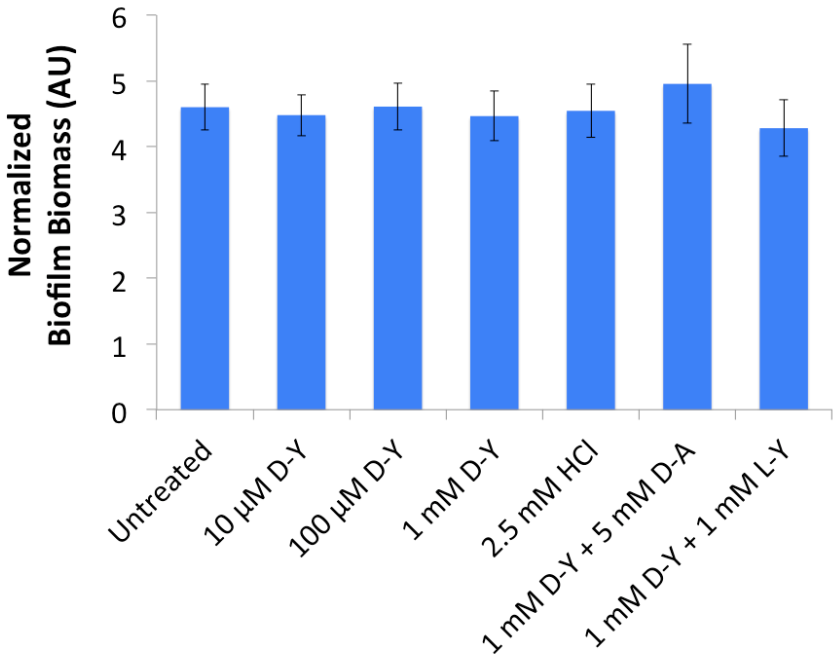

Figure C2. D-Tyr does not inhibit *P. aeruginosa* biofilm formation. PA14 was grown in M6301R in 96-well plates with the indicated treatments for 24 hours at 25˚C. The 2.5 mM HCl treatment was included as a control for the amount of HCl in the 1 mM D-Tyr treatment. Results show the average of four replicates and error bars represent the standard deviation.

[3] See Chapter 5 (Fig. 26).

The lack of NCDAA-induced biofilm inhibition against *S. aureus* and *P. aeruginosa* has a simple explanation. Both species encode and express *dtd*. Consequently, *S. aureus* and *P. aeruginosa* can protect themselves from tRNA misacylation events in the presence of NCDAAs, just as *dtd*$^{+}$ strains of *Bacillus* do (Chapter 3, Fig. 19). Thus the diverse bacteria *B. subtilis*, *S. aureus*, and *P. aeruginosa* do share a common mechanism related to D-amino acids, but it is one mediated by a D-aminoacyl tRNA deacylase, and not one relevant to biofilm.